Dissertation
submitted to the
Combined Faculties for the Natural Sciences and for Mathematics
of the Ruperto-Carola University of Heidelberg, Germany
for the degree of
Doctor of Natural Sciences

presented by

Diplom-Physicist	Carsten Krauss
Born in:	Mannheim

Oral examination: May 22th, 2002

Investigations on the Operational Behavior of the GEM MSGC Inner Tracking System and Study on the Reconstruction of χ_c Events in the HERA-B Detector

Referees: Prof. Dr. Franz Eisele
Prof. Dr. Karl-Tasso Knöpfle

Zusammenfassung

In dieser Arbeit wird über den Betrieb des inneren Spurkammersystems von HERA-B berichtet. Im Jahr 2000 wurde dieses große Spursystem aus GEM MSGC Detektoren in Betrieb genommen. Das Betriebsverhalten der empfindlichen Kammern unter schwierigen Umgebungsbedingungen im hadronischen Teilchenstrahl von HERA-B wurde über einen großen Zeitraum hinweg untersucht. Während des Strahlbetriebes im Jahr 2000 wurden stabile Betriebsparameter gefunden und eine Vorgehensweise zur Gewöhnung der Kammern an den Betrieb im Teilchenstrahl entwickelt und umgesetzt.
Im zweiten Teil der Arbeit wird eine Studie zur Rekonstruktion von χ_c-Ereignissen vorgestellt. Es wurden Daten benutzt, die im Jahr 2000 von HERA-B aufgezeichnet wurden. Das χ_c-Signal wurde beobachtet, sowohl in Daten aus Proton-Kohlenstoff Wechselwirkungen als auch in Proton-Titan Ereignissen.

Abstract

This thesis reports about the operation of the inner tracking system of HERA-B. In the year 2000 this large system of GEM MSGC detectors was commissioned. The operational behavior of the delicate chambers in the difficult environmental conditions caused by the hadronic particle beam of HERA-B was studied over a long period of time. During the operation period in 2000 stable operational conditions were established and a procedure was developed and implemented to condition the chambers to the operation in the particle beam.
In the second part of this thesis, a study to reconstruct χ_c events is presented. Data taken by HERA-B in 2000 was used. The χ_c signal was established in data taken from proton-carbon and proton-titanium interactions.

Contents

Chapter 1

Introduction

The hadronic *b-factory* experiment HERA-B was first proposed in 1992 [1]. HERA-B was supposed to be the first experiment to measure directly the $\sin 2\beta$ parameter, which is a measure for the strength of the CP violation in the system of neutral B mesons. This parameter was only weakly constrained by other measurements. It is one of the missing parameters of the standard model of high energy physics.

The HERA-B detector was therefore optimized and designed to measure decays of $B^0 \to J/\psi\, K_S$, which allow a relatively simple extraction of the $\sin 2\beta$ value. To acquire enough data to measure $\sin 2\beta$ with good accuracy, a few thousand *golden decays* $B^0 \to J/\psi\, K_S$ have to be reconstructed. This decay channel has a very small branching ratio, therefore a large number of B^0-particles have to be produced in the experiment. To achieve this, a high interaction rate is necessary which results in a high particle flux in the detector components of the experiment.

Tolerating very high particle rates is difficult for all particle detectors. Gaseous detectors in particular face severe aging and stability problems under such conditions. In the course of the research and development program for HERA-B, serious problems were discovered in hadronic environments at high particle fluxes. These problems repeatedly enforced a redesign of detectors and caused severe delays. In micro pattern gas detectors severe gas aging and sparking problems were found, since 1994, the time of the proposal [2]. Other collaborations have in the meantime even abandoned these type of detectors because of the observed problems.

The combination of the requirements of operation in high Yet in the course of the work presented here a safe and reliable operation of HERA-B's inner tracker, which is built of micro-strip gas chambers, could be established.

This thesis reports on the commissioning of the inner part of the HERA-B tracking system, which was particularly impeded by the mentioned problems. This system of GEM MSGCs was brought to a stable and reliable operation during the time of the work presented here. The training procedure was developed and implemented for the detector and the operational chamber performance of the complete inner tracker was studied and is described here.

The delays during research and development could at the end not be made up against BaBar [3] and Belle [4] which had in the meantime started operation and have measured the parameter $\sin \beta$ with reasonable accuracy. HERA-B therefore is no longer competitive in CP measurements, so that the original goal of the experiment had to be given up.

The experiment is still very good for a variety of other measurements. The physics program planned for 2002 focuses on the measurement of the B production cross section in nuclei and the charmonium production dependence on the nuclear mass number A.

In the second part of this thesis, a study to reconstruct the χ_c charmonium state is presented. This is done to explore the reach of HERA-B in the field of charmonium production in proton nucleon interactions.

A measurement of the production of charmonia at HERA-B is planned for the running period starting in March 2002.

Chapter 2

Motivation

The HERA-B detector was designed and built to measure the strength of the CP violation in the system of neutral B mesons. This program imposes tough requirements on the detector. This chapter will briefly outline the motivation for the measurement of CP violation – as far as it is necessary to understand the detector design. Finally, as delays have made the experiment not competitive in the field of CP violation in the B-system, the program for 2002 is presented in more detail. A major topic for 2002 is the measurement of charmonium production in nuclear matter, especially the production of χ_c states, which will be discussed.

2.1 Background

The standard model of particle physics is consistent with all important results of the past years' measurements. As new physics will most likely manifest itself experimentally only in small deviations from standard model predictions, it becomes more and more important to determine the parameters of the standard model with high precision. One of the most interesting parameter in this context is the CP-violation in the B-system.

CP violation was first observed in the system of neutral K mesons [5]. The K_L^0 has a CP eigenstate of -1 but it was found that it can also decay in a pair of charged pions with a CP eigenstate of +1, violating CP parity. In the meantime the NA48 and KTeV experiments have shown that the CP violating parameter of the Kaon system $Re(\epsilon'/\epsilon)$ is not consistent with zero [6], [7]. This established CP violation as a property of the weak interaction in the standard model. The CP violation in the K-system leads to very small experimental effects, and the number of independent measurements is small. In the B-system large experimental effects are expected in the standard model; also the number of possible measurements in different decay channels is large.

In the Standard Model the strength of the CP violation in B-decays is given by the area of the unitarity triangle, shown in Fig. 2.1. The aim of the measurement program is to over-constrain the parameters of this triangle. The angles in the triangle are observables which are closely related to the parameters of the CKM[1] matrix. HERA-B was built to determine the first angle of the triangle, by measuring the parameter $\sin 2\beta$.

The measurement is, however, based on a B-decay channel with a very small branching

[1]Cabibbo Kobayashi Maskawa matrix, describing the weak interaction of quarks

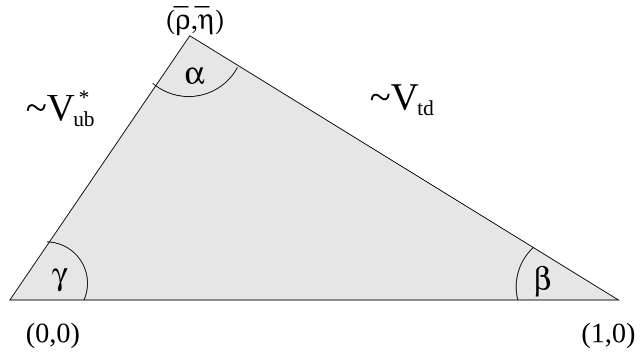

Figure 2.1: The unitarity triangle. The area of the triangle gives the strength of the CP violation.

ratio ($\leq 10^{-4}$). To exploit such a channel more than 10^8 b-pairs have to be produced in a year.

There are two different approaches for *B-factories*: asymmetric electron positron colliders operating at the $\Upsilon(4S)$ resonance and hadronic B production, either in proton–fixed target interactions or in proton (anti-)proton collisions.

The e^+e^- B factory approach was chosen by two groups: The BaBar [8] collaboration at SLAC[2] and the Belle [9] collaboration at KEK[3]. These two experiments were largely able to build and commission their accelerators and detectors on schedule in 1999. The experiments using hadronic b-production (HERA-B, LHC-B [10] and B-TeV [11]) were either planned on a longer schedule (LHC-b, 2006 and B-TeV, 2006+) or were seriously delayed as in the case of HERA-B. The advantages of hadronic b-production are a higher production cross section in comparison to the e^+e^- b-production and the production of B_s^0 and B_d^0 mesons, which open additional channels not available at BaBar and Belle. The disadvantage is the high background in hadronic production, especially when compared to the clean events produced in e^+e^- collisions.

BaBar and Belle were able to present their first measurements of the CP-violation parameter $\sin 2\beta$ in 2000 [3], [4]. Since then both measurements have reached an accuracy level that can not be reached by HERA-B [12], [13].

Because of this HERA-B is no longer competitive in the B-physics sector and focuses on a different physics program for the 2002 running period. This program concentrates on basic measurements in the charm sector, especially the production of charmonium states. In this field HERA-B is able to improve the existing measurements significantly. Some measurements of the 2002 physics program will be unique. The topics of the 2002 running will be:

- Measurement of the b-production cross section in proton–nucleon interactions.

- Measurement of differential charmonium production cross-sections and charmonium ratios as a function of the target material mass.

[2]Stanford Linear Accelerator Center, Stanford, USA
[3]High Energy Accelerator Research Organization, Tsukuba, Japan

In addition to these baseline measurements that are discussed in section 2.3, additional options are studied for a possible future physics program of HERA-B:

- Open charm production.
  For this measurement the trigger system of the experiment has to be upgraded. The possibilities in the charm physics field are still under study and therefore not included in the baseline 2002 physics program.

- Searches for rare charm decays.
  The range in rare decays will be determined by the efficiency of the trigger. As this can only be guessed at this time, the search for rare charm decays is also not part of the 2002 program.

Once the HERA-B detector is well understood, the reach in these physics channels can be explored further.

2.2 Design Objectives of the HERA-B Detector

The original design of HERA-B was optimized for the measurement of the *golden decay* channel of

$$B^0 \text{ or } \bar{B}^0 \rightarrow J/\psi\, K_S.$$

This channel is advantageous for the determination of the CP violation parameter $\sin 2\beta$, because it is only necessary to measure the decay asymmetry between the number of $\bar{B}^0$ and B^0 decaying into the golden channel:

$$\sin 2\beta \propto \frac{N_{\bar{B}^0} - N_{B^0}}{N_{\bar{B}^0} + N_{B^0}}. \tag{2.1}$$

This is possible because this channel has no *penguin pollution* but is dominated by the tree diagram decay (Fig. 2.2).

As the determination of $\sin 2\beta$ was the main objective of the HERA-B experiment, the detector was designed for a maximum performance in this channel.

The J/ψ in the final state of the golden channel decays into two leptons, either a $\mu^+\mu^-$ pair or into a e^+e^- pair (with a branching ratio of 6% each). The lepton-pair has a characteristic signature in the detector. The first level trigger of HERA-B is designed to trigger events containing two lepton tracks with an invariant mass in the range of the J/ψ.

The K_S^0 has a mean lifetime of 89 ps and typically decays into two charged pions with a branching ratio of 68.6% in the magnet area of the detector.

To measure $\sin 2\beta$ according to Eq. 2.1, the identity of the decaying B^0 meson has to be identified. This *tagging* is done by identifying the b-flavor of the other produced b particle by its decay products. This is done by measuring the lepton charge of a semileptonic decay of a K-meson associated with the decay of the b-particle. In order to identify the Kaons efficiently, a particle identification system is needed.

To identify b-particles a detached vertex has to be reconstructed in the event. At HERA-B this was planned to be done on the second trigger level. This secondary vertex

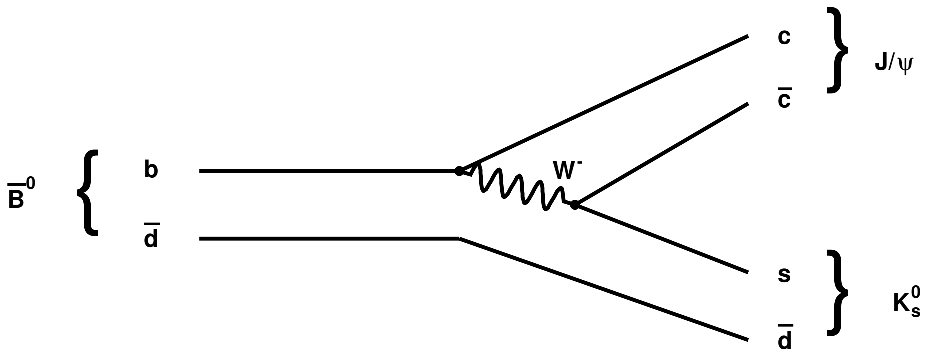

Figure 2.2: Illustration of the tree level Feynman graph of a $\bar{B}^0$ decay in the golden channel.

reconstruction needs a high resolution vertex detector system close to the interaction point.

The basic requirements given by the properties of the golden decay channel are:

- Fast electron and muon track identification for the reconstruction of the J/ψ on the first trigger level.

- Detached vertex reconstruction for b-identification on the second trigger level.

- π - K identification for efficient B tagging.

The B-mesons are produced in proton-nucleon interactions. As the HERA bunch clock is fixed at 10.4 MHz, the only possibility to raise the interaction rate is to allow for more than one interaction per bunch crossing. To separate the vertices of different interactions more than one target wire is used. The baseline design of HERA-B foresaw the use of up to eight target wires at a time with a mean number of five interactions per bunch crossing every 96 ns. This high interaction rate and the resulting high particle rate in the detector had a crucial impact on the development of the detector technologies. All subdetectors had to be tested and often elaborately adapted to the high rate environment.

Table 2.1 shows the number of expected B^0 decays into the golden decay channel. At the time of the proposal slightly less optimistic assumptions about the b-cross section were made, so that a yearly yield of 1000 reconstructed golden decays was estimated.

The sample of fully reconstructed golden B^0 decay events that BaBar has analyzed even before HERA-B starts data taking already exceeds 6300 events [12]. This underlines that HERA-B is no longer competitive in this field.

[4] A typical HERA-B operation year is assumed to have 10^7 s or 2780 h.

Table 2.1: Reconstruction of golden decay events expected in HERA-B

		Events
b-Production, with full interaction rate and for one operation year[4]	$40\,\mathrm{MHz} \cdot 10^7\,\mathrm{s}$ and $\sigma_{b\bar{b}}/\sigma_{inel} = 1.6 \times 10^{-6}$ (based on $\sigma_{b\bar{b}}$ from [14])	6.4×10^8
B^0 or $\bar{B}^0$ formation [56]	$\approx 63\%$	4.0×10^8
BR($B^0 \to J/\psi\, K_S$)	$8.9{\times}10^{-4}$	$3.6{\times}10^5$
BR($J/\psi \to l^+l^-$) and BR($K_S \to \pi^+\pi^-$)	$(6\% + 6\%) \times 69\%$	$30{\times}10^3$
Trigger, reconstruction, and tagging efficiency (from [2])	$\approx$0.09	2700

2.3 2002 Physics Program

In 2002 HERA-B will perform two physics measurements: The b production cross section will be measured to an accuracy of about 30% and the charmonium production process will be studied as a function of the nuclear mass A.

The b production cross section for 920 GeV proton nucleon interactions has not been measured. The existing measurements have been performed with a lower beam energy of 800 GeV and their results are inconsistent. The E771 collaboration has measured $\sigma_{b\bar{b}} = 43^{+27}_{-17}\,(\mathrm{stat})\,^{+7}_{-7}(\mathrm{syst})\,\mathrm{nb/nucleon}$ [15] in proton silicon interactions. The E789 collaboration has found a value of $5.7{\pm}1.5 \pm 1.3\,\mathrm{nb/nucleon}$ [16] in proton gold collisions. HERA-B performed a first measurement in 2001 based on the data taken in 2000 [14]. The result is $\sigma_{b\bar{b}} = 32^{+15}_{-12}(\mathrm{stat}) \pm 8(\mathrm{syst})\,\mathrm{nb/nucleon}$. This measurement is based on about 10 B candidates. The two existing measurements are based on 6 (E789) respectively $\approx$ 20 (E771) B events. In addition to the better statistics that will be available, HERA-B has the unique opportunity to check the result in both leptonic decay channels of the $B \to J/\psi X \to l^+l^-X$ decay. This enables a consistency check within the experiment. HERA-B can achieve a 30% precision in 20002, which will clarify the experimental situation and contribute to the understanding of hadronic heavy quark production which is limited at present.

The main interest in the measurement of charmonium production in nuclei is driven by heavy ion physics. In heavy ion collisions carried out at the RHIC[5] at the BNL[6] or the SPS[7] at CERN[8] suppression of charmonium production is of major interest. A suppression of J/ψ states is used as signature for the phase transition from normal nuclear matter to quark-gluon plasma. Such a suppression has been observed at NA50 [17] at the SPS, but the interpretation is difficult because of the poor understanding of J/ψ production in nuclear matter. In order to interpret the J/ψ rates measured in these experiments correctly, the charmonium (J/ψ, ψ', and χ_c) production cross sections measured at HERA-B are helpful as reference input. It is also very important to measure the fraction of J/ψs produced in feed-down reactions from heavier charmonium states such as the χ_c or the ψ'. At HERA-B the production of charmonium in various nuclear materials and in a large

[5] Relativistic Heavy Ion Collider
[6] Brookhaven National Laboratory
[7] Super Proton Synchrotron
[8] European Organization for Nuclear Research, Geneva

region of phase space can be measured as well as the production ratios between different charmonium states such as the χ_c, the ψ' and, the J/ψ.

These measurements will be unique as HERA-B is the only fixed target experiment capable of measuring χ_c production because it is an open spectrometer. There are also options to study open charm production so that the full range of $c\bar{c}$ production can be covered.

The kinematic reach of HERA-B is also unique as previous experiments have only covered the positive x_F region.

2.3.1 Event Kinematics

The event kinematics in fixed target collisions can be described by two variables: Feynman x_F and the transverse momentum p_t. They are given by:

$$x_F \approx \frac{2p_L}{\sqrt{s}} \quad \text{and}$$
$$p_t = \sqrt{p_x^2 + p_y^2}.$$

The center of mass energy $\sqrt{s}$ at HERA-B is 41.6 GeV for a proton beam energy of 920 GeV. p_L is the longitudinal component of the momentum in the center of mass system. The p_x and p_y are the momentum components in x and y direction, where the z axis defines the direction of motion of the incoming particle. The complete physical region is then covered by

$$-1 \leq x_F \leq 1 \quad \text{and}$$
$$0 < p_t < p_{t,max}\sqrt{1 - x_F^2}.$$

The maximum reachable p_t for heavy quark production is approximately given by

$$p_{\mathrm{t,\ max}} \approx \frac{s - m_{q\bar{q}}^2}{2\sqrt{s}}.$$

Here $m_{q\bar{q}}$ is the mass of the heavy quark final state. Fig. 2.3 shows the kinematic plane for χ_{c2} production with $m_{\chi_{c2}} = 3.56$ GeV. Most events are produced with a p_t smaller than 3 GeV. The used 2000 Monte Carlo sample is described in section 6.2.1.

2.3.2 Charmonium Production in Nuclear Matter

In a proton nucleus interaction, the production cross section is typically factorized into the proton–nucleon cross section σ_{pN} and the nuclear mass dependent term A^α:

$$\sigma_{pA} = \sigma_{pN}\, A^\alpha$$

A is the number of nucleons in the target material and α a correction factor describing the magnitude of the nuclear suppression. If all nuclei contributed equally to the cross

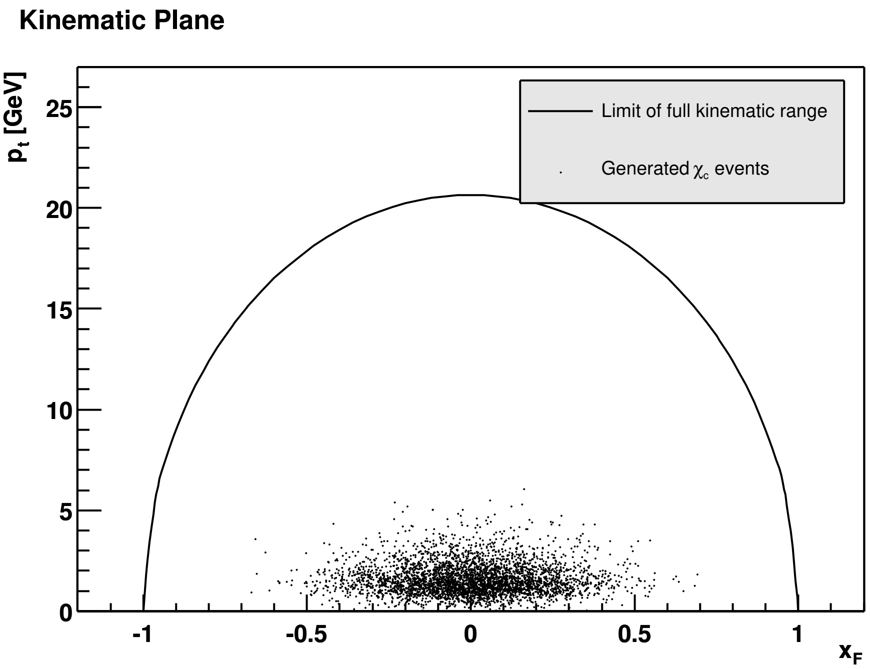

Figure 2.3: Kinematic range of the χ_{c2} production in proton nucleus interactions at HERA-B with a center of mass energy of 41.6 GeV.

section α would be 1. Measurements at E866 have found α to be a function of x_F with values of α between 0.7 and 0.97 [18], as shown in Fig. 2.4. The x_F region covered by E866 is -0.1 $< x_F <$ 0.6. HERA-B covers a region of $-0.4 < x_F < 0.25$.

The goal of the measurement is to determine the A dependence – or the α parameter – for J/ψ, ψ', and χ_c production as a function of x_F.

Theory offers a number of models for the description of hadronic charmonium production and formation in nuclear matter. These theories are not results of calculations from first principle, because all interactions in the models apart from the hard production sub-process are not in the regime of perturbative QCD.

Therefore various models have been introduced to describe the observed properties quantitatively. These models are based on assumptions about the color state of the produced $c\bar{c}$ pair, its propagation in the nuclear matter, or the hadronization.

The production is described best by the color octet model (COM). This model is based on a non-relativistic QCD expansion in the relative velocity of the $c\bar{c}$ pair. It predicts a ratio between the production rates of charmonium states that is almost independent of x_F.

The passage of a $c\bar{c}$ pair through nuclear matter and its absorption in nuclear matter are described by other models. The nuclear absorption model describes the absorption depending on the formation time of the charmonium state and the length of the path inside the nucleus. In this model the nuclear suppression α is therefore depending on x_F and differs for the charmonium states.

Several other models have been suggested. They predict interactions with co-moving particles or multiple scattering and energy loss inside the nucleus. The models predict

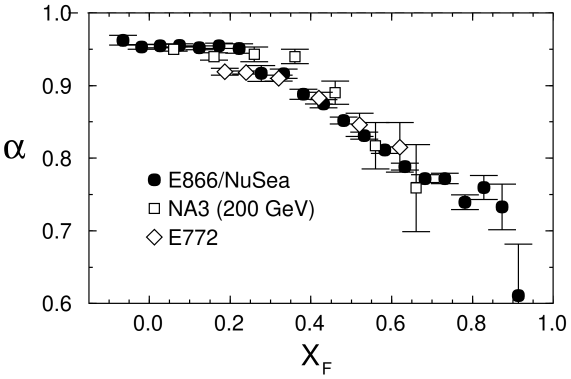

Figure 2.4: Experimental x_F dependence of J/ψ production measured in 800 GeV proton nucleon (Be, Fe and W) collisions [18]. This was only measured for J/ψ and ψ' but not for χ_c.

changes in the charmonium rates or the production threshold.

All models predict effects in the charmonium cross section, that could be visible for HERA-B in 2002. For further details on nuclear suppression, refer to [19] and the references therein.

The parameter $R_{\chi_c} = N(\chi_c)/N(J/\psi)$ is one of the observables that can be measured at HERA-B. A first measurement was performed using data taken in 2000 [20]. The x_F dependence of this parameter can be determined with the data that will be acquired in 2002 and 2003. The NRQCD prediction for R_{χ_c} is 0.3 which is favored by most of the existing measurements including the measurement at HERA-B. The value of this parameter and – even more – its dependence on x_F can add valuable understanding in the field of nuclear interactions.

A key feature of HERA-B for this measurement is the range in negative x_F which was not accessible for previous experiments. Some of the predictions made by the theoretical models differ only at negative x_F.

The knowledge of R_{χ_c} is of great importance for heavy ion physics. In these experiments the reconstruction of χ_cs is not possible which is due to the very high occupancy. The experimental task in heavy ion detectors is to measure the suppression of the J/ψ. It is, however, not possible for them to distinguish prompt J/ψ from feed-down of heavier charmonium states such as the χ_c. The value of R_{χ_c} measured at HERA-B is therefore an important input for the interpretation of heavy ion collisions.

In summary the A dependence of charmonium production can be measured at HERA-B in 2002. This measurement will be a valuable input for heavy quark experiments. It might even be possible to disentangle the production and absorption models of charmonium in nuclear matter with the new data.

Chapter 3

HERA and HERA-B

3.1 HERA – "Hadron-Elektron-Ring-Anlage"

HERA at DESY is the only existing high energy physics accelerator to collide electrons and protons. It accelerates positrons or electrons to 27.5 GeV and protons to 920 GeV, which are collided at two interaction zones in the north and south of the rings (see Fig. 3.1). In the east of HERA HERMES, a fixed target experiment using polarized positrons is located. Starting 1994, the west hall was prepared for the latest HERA high energy physics experiment, HERA-B.

Beginning in September 2000, HERA was upgraded to deliver higher luminosity for the two collider experiments. This upgrade took until the end of 2001, since then the machine is being re-commissioned. HERA will recommence regular luminosity operation in April 2002[1].

3.2 HERA-B

This section introduces the detector of the HERA-B experiment. HERA-B is a fixed target detector which uses interactions of the beam tails around the proton beam of HERA with target wires. The HERA electron ring passes through the detector without being used.

The origin of the HERA-B coordinate system is at the interaction point. The +x direction points to the inside of the HERA storage rings, the +y direction points upwards, and +z is the direction of the proton beam (see Fig. 3.2).

3.2.1 The Sub-Systems

The detector is built out of seven major sub-systems. These will be briefly introduced in the following:

- Target
  The target consists of eight wires made of different materials. In 2000 wires of carbon, titanium, aluminum and tungsten were used. In 2002 targets of carbon, titanium, aluminum, palladium and tungsten will be available. The choice of target

[1] Status of March 2002

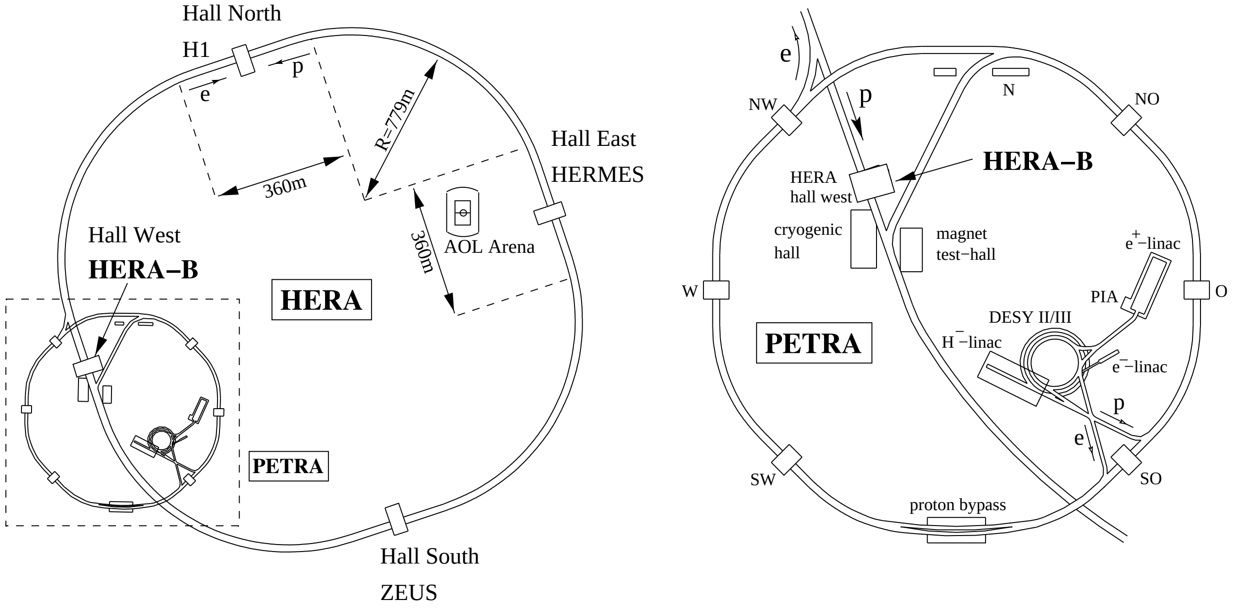

Figure 3.1: Schematic layout of the DESY accelerators. The HERA-B detector is located on the DESY site, which is enclosed by the PETRA ring.

materials is optimized for the measurement of the dependence of proton nucleus cross sections on the nuclear mass A. The metallic wires in 2000 were typically 500μm $\times$ 50μm wide. The new setup in 2002 will have 50μm diameter round wires for materials with a high nuclear mass and ribbons of $50 - 100 \times 500\mu$m for carbon and aluminum. The wires are positioned in two stations around the central beam position, inside and outside of the ring (*inner* and *outer* wires) and *above* and *below* the beam.

The wires are mounted on movable forks. These forks can be individually controlled to select a specific target configuration. The actuators are very fast to allow the wires to follow the movement of the proton beam. The beam itself moves because of fluctuations in the fields of the magnets of the storage ring and because of seismic movements. The wire has to follow these movements to keep the interaction rate stable and at the same time not to interfere with the operation of the other experiments at HERA.

The interaction rate generated by the target wires can never be constant but it can be controlled by the steering logic so that the rate average is kept at the set level. By positioning the wire closer to the beam core the interaction rate can be increased while a position further away yields a lower rate. It is possible to use target configurations of one or more wires. In a multi-wire configuration the contribution to the overall rate by an individual wire is measured with charge integrators which are connected to all wires. These charge integrators are very sensitive charge detectors which, by measuring beam induced delta-electrons, allow a uniform distribution of the interaction rate to all wires. It was shown that a stable multi-wire operation is possible [22].

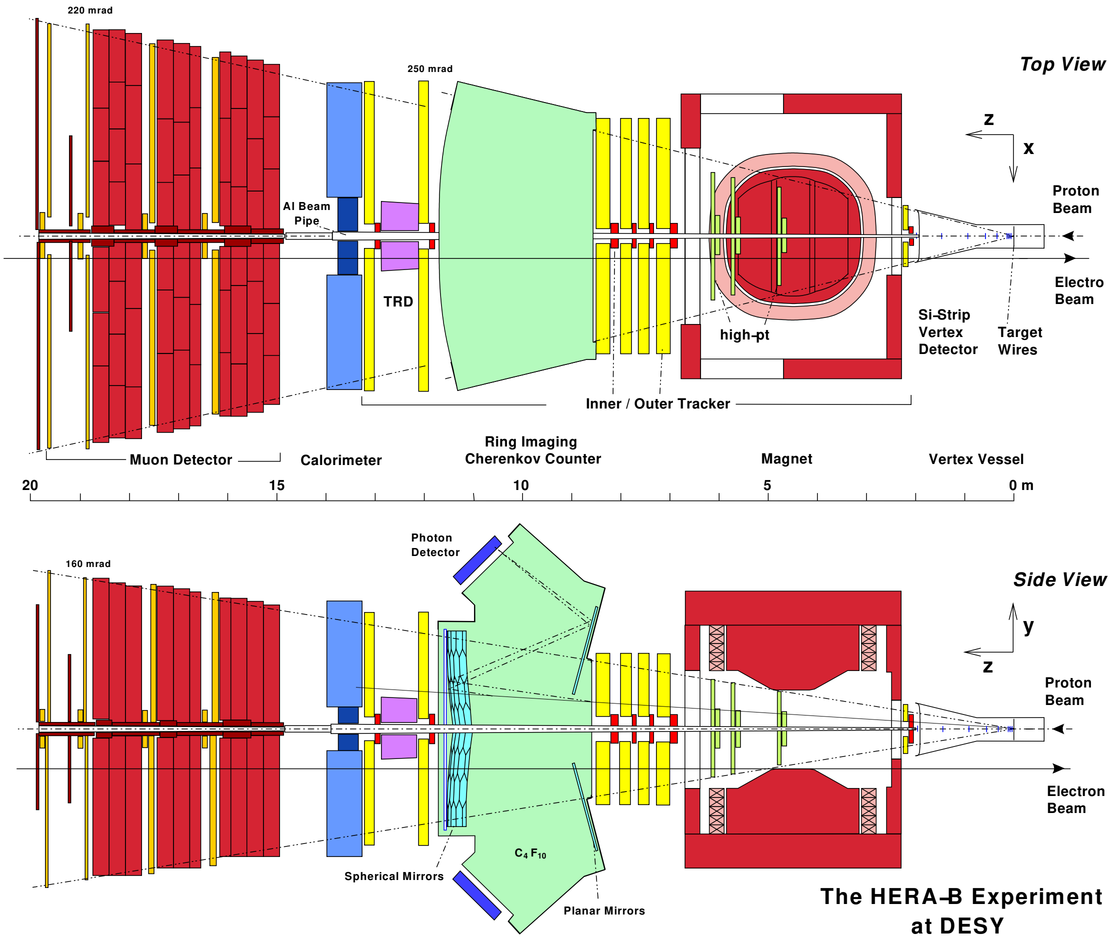

Figure 3.2: Top and side view of the HERA-B detector in the configuration of 2002 [21].

In 2000 only the wires at the inner and above positions could reliably be used. The other wires showed a large fraction of interactions outside the proton bunches. This problem is known as *coasting beam*. Such events cannot be correctly reconstructed, because the readout electronics of the detector relies on a very narrow window in time for the interaction. As it is not known how the fraction of coasting beam protons will change after the upgrade of HERA, carbon wires were placed in three of the four wire positions as reference. The other materials were placed such that even if only the inner position is usable in 2002 the full range of A can be covered; the lightest material Carbon is in the "inner II" position while Tungsten is mounted as "inner I" wire. The materials with intermediate A might only be usable under good beam conditions.

The target system has a good rate stability of 6% to 14%, depending on the time of the day. During night a good rate stability can be achieved, while the seismic activity of a work day limits the rate stability at day time to 14% [22].

- Vertex detector, VDS
  The vertex detector of HERA-B has 8 stations of silicon counters. The side view of the setup can be seen in Fig. 3.3. The first seven detector stations are mounted inside the same vacuum vessel as the target wires (see Fig. 3.3 on the right). To keep the vacuum needed for the proton machine, the vertex detector modules are enclosed in thin-walled aluminum caps which hold a secondary vacuum. The modules are mounted on Roman pots, so that the x and y positions of the detectors can be controlled by actuators from outside the vessel. Station 8 is fixed at the exit window of the vacuum vessel.

  During injection of protons into the storage ring the aperture needed for the beam is much larger than under luminosity conditions, so the vertex detector modules are retracted in this phase of operation.

  The detectors are expected to have a lifetime of less than one year under the full radiation load of $3 \times 10^7 s^{-1}\mathrm{cm}^{-1}$ originally proposed for HERA-B. At a default interaction rate of 5 MHz planned for 2002 this time increases to eight years.

  The detectors are read out with HELIX128[2] chips. The hit-preparation for the complete system is done with a center-of gravity method.

- Main Tracking System
  The purpose of the main tracking system is the determination of the momentum of charged particle tracks and the propagation of tracks from the vertex detector region into the particle identification region. To keep the hit occupancies in the tracking system below 5%, the main tracking system of HERA-B is divided into two parts: The inner tracker and the outer tracker which both use gaseous drift chambers. The inner tracker (ITR) covers the region 5-30 cm from the beam-pipe. This area has the highest track density, the inner tracker therefore is a high resolution device which was designed to withstand a high particle flux of up to $10^7\mathrm{s}^{-1}\mathrm{cm}^{-2}$ corresponding to radiation doses of up to 1 Mrad/y.

[2]developed by the ASIC lab in Heidelberg for the HERA-B VDS and inner tracking detectors. [53]

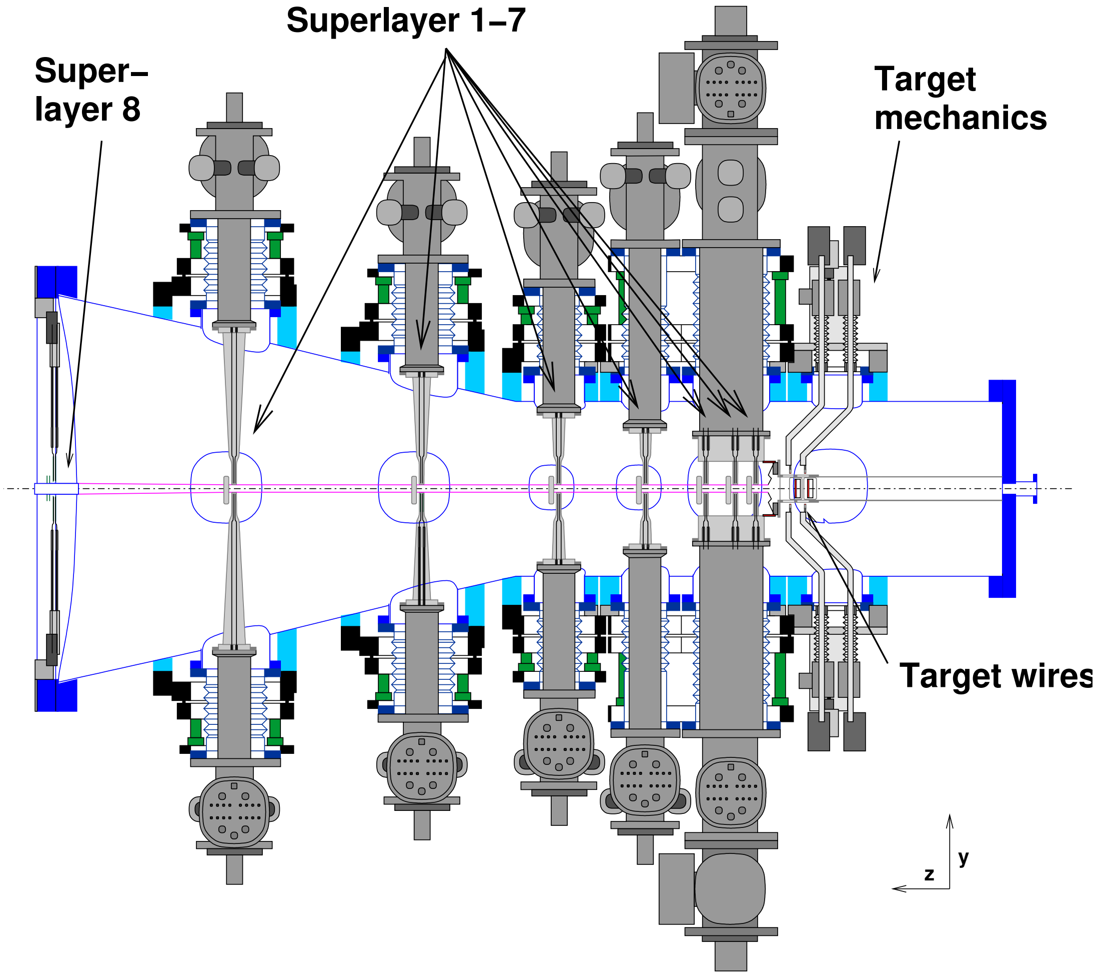

Figure 3.3: Side view of the vertex detector vessel. On the right side the target mechanics is visible.

The outer tracker (OTR) covers a large area, the region starting 20 cm away from the beam-pipe and covering the region up to 6m away from the beam-pipe. In the innermost sections of the outer tracker the particle flux reaches a level of up to $10^5 s^{-1} cm^{-2}$ [35].

The inner tracker which is the main subject of this thesis, is covered in Chapter 4.

- Outer tracker, OTR
  The outer tracker covers an area of 1000 m^2. It is built of honeycomb drift chambers with a cell size of 5mm in the inner region and 10mm in the outer region. The chamber modules are arranged in three angles of 0°, +5° and -5°. Zero degree wires in all HERA-B components are oriented parallel to the y coordinate. The tilted stereo chambers are needed to resolve the y coordinate. The OTR honeycomb chambers are used with a gas mixture of 65% Ar, 30% CF_4 and 5% CO_2. A schematic side-view of the setup for a single layer chamber is shown in Fig. 3.4. The active volume is enclosed by folded *Pokalon C*-foil. In the center of the honeycomb cell volume a gold-plated tungsten signal wire is mounted. The modules built for HERA-B are up to 4.5m long. To center the signal wires they are fixed by G10-strips where necessary. The honeycomb chambers of one half-superlayer are mounted inside a common gas tight box.

  The tracking system is divided into three parts, one before and inside the magnet area (MC), the pattern recognition area behind the magnet (PC) and the trigger area between RICH and electromagnetic calorimeter. In the PC and TC regions of the tracking system, the outer tracker delivers fast digital wire signals for the first level track trigger in addition to the analog drift time information available in the second level trigger and for the full reconstruction of tracks. The wire signal from the outer tracker chambers is pre-amplified and discriminated using the ASD8 chip. These chips are used in outer tracker, muon system, high-pt pretrigger system, and RICH detectors of HERA-B.

  The frames of the outer tracker stations also serve as support for the inner tracker stations.

- Ring imaging Cherenkov counter (RICH)
  A Cherenkov detector is used for particle identification, mainly the discrimination of Kaons from pions. The detection principle uses the emission of a cone of Cherenkov photons caused by fast particles traversing a medium. The HERA-B RICH is filled with C_4F_{10} at ambient pressure. In this gas the Cherenkov momentum threshold is 2.6 GeV for pions, 9.0 GeV for Kaons and 17.2 GeV for protons. The emitted Cherenkov light is focused into an array of photo-multipliers. The Cherenkov photons from one particle form the image of a ring on the plane of photomultipliers.

  Rings in the RICH detector are reconstructed using seeds from the main tracker. The reconstruction program searches for photon hits on a cone around the track direction. If photons are found, particle identification likelihoods are assigned to the track according to ring radius and momentum of the particle.

- Electromagnetic calorimeter (ECAL)
  The calorimeter is designed to measure the energy of electrons and photons. It is a

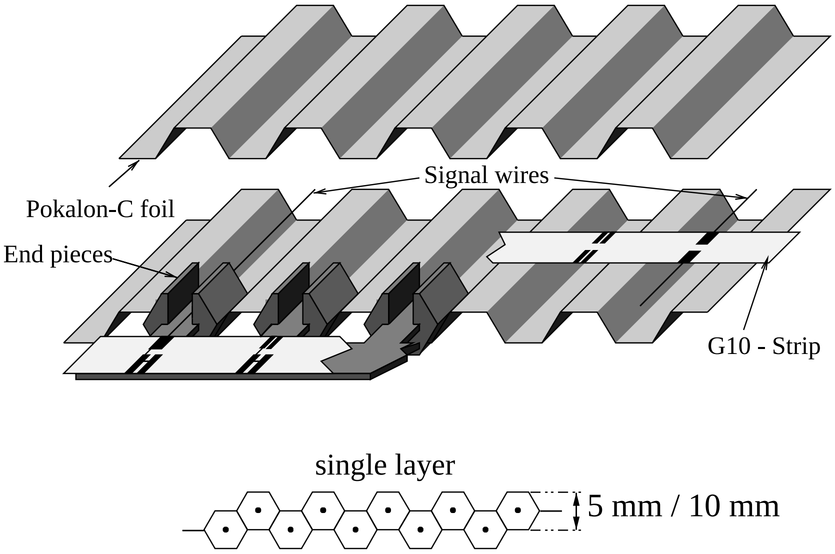

Figure 3.4: Schematic picture of the outer tracker honeycomb chambers.

sampling calorimeter made of scintillating plastic material and absorbers arranged in a 'shashlik' configuration. The layout of an inner part module is shown in Fig. 3.5. Wave-length shifter fibers are inserted in the absorbing and scintillating material. The light output of the optical fibers is collected by photomultipliers.

The ECAL is divided into three parts, the inner with the highest granularity ($2.23\times 2.23\,\mathrm{cm}^2$) and a tungsten alloy as absorber, the middle part with lead absorber and a granularity of $5.8\times5.8\,\mathrm{cm}^2$, and the outer part with a granularity of $11.2\times11.2\,\mathrm{cm}^2$ and a lead absorber. The thickness of the calorimeter varies between 20 and 22 radiation lengths. The energy resolution of the inner part of the ECAL was $\delta E/E = 23\%/\sqrt{E} \oplus 1.7\%$ during 2000. A spatial resolution of $\sim 0.2\,\mathrm{cm}$ was measured [25] in the same region .

The ECAL is also used to generate fast pretrigger signals for the electron channel of the first level trigger.

- Muon system

  The Muon system is divided into four stations (MU1-MU4). In front of these stations steel and concrete absorbers are placed to suppress hadrons. MU1 and MU2 are equipped with tube chambers in three stereo angles (0°, +20°, -20°). The last two stations consist of tube chambers with an additional pad readout. These pads collect the charge influenced by signals in the tube wires. The pads are segmented in x and y direction.

  Pad signal coincidences of MU3 and MU4 which point back to the interaction region are used for the pre-trigger system as muon track seeds in the first level trigger.

  In the region around the beam-pipe, a system of gas pixel detectors is used both for analog and trigger information.

In addition to these core detector systems HERA-B has two more sub-detectors: The high-pt pretrigger system and a transition radiation detector, which were only partly

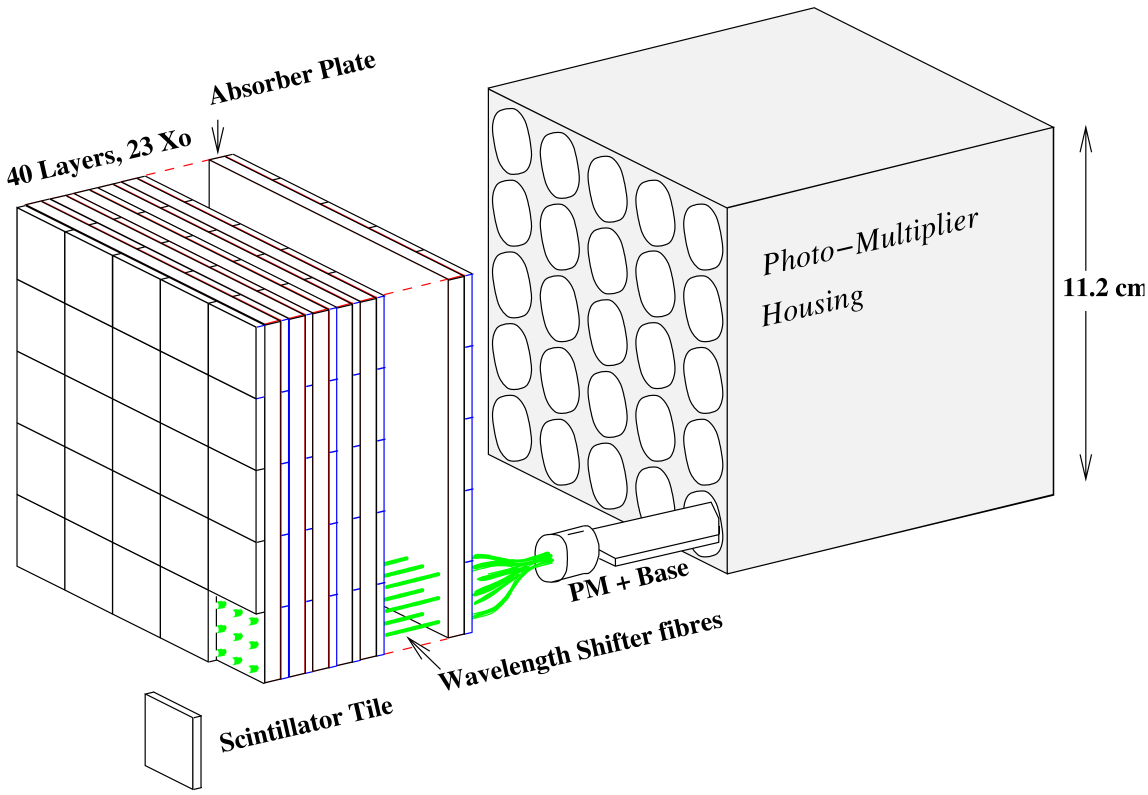

Figure 3.5: Sketch of the layout of an ECAL inner module. Taken from [24]

installed in 2000 and which did therefore not play any role so far.

3.2.2 Track Reconstruction

The track reconstruction program for the main tracker is RANGER [26] which is a track finding and reconstruction program using a Kalman filtering technique. It was designed for very high occupancy events and requires a high efficiency of the tracking detectors. Since the detector efficiency turned out to be lower than anticipated, the tracking software was reviewed and parts of it were replaced by a new pattern recognition program [27]. The track finding efficiency for Monte Carlo tracks coming from J/ψ decays now is about 97% in the main tracker with a detector modeled after the real detector in 2000 [28].

The precision of tracks measured in a detector system is always limited by the amount of multiple scattering in the material of the setup. A detector can therefore never be *optimal*, it can only be optimized for the purpose of the measurement. The measurement program for HERA-B changed in 2001, so the optimization of the tracking system had to be reviewed.

It turned out, that significantly more material than anticipated was used for the construction of the tracking system. This led to considerable degradation of the energy resolution of electrons and photons and to a loss in photon detection efficiency caused by more conversions. The magnet part of the tracking system is only needed for the reconstruction of K_S^0 and to resolve ambiguities in very high multiplicity events. Both features of the tracking system will not be needed for the 2002 physics program. It was therefore decided to remove the tracking stations inside the magnet to improve the detection of electrons and photons, which is essential for the 2002 physics program.

3.2.3 First Level Trigger

The first level trigger (FLT) is a track trigger that is designed to choose events with a pair of leptons which have a high invariant mass. This can for example be the decay product of a J/ψ. The maximum latency for the trigger decision is $10\,\mu$s. In order to calculate the invariant mass of a particle on the first trigger level, the track parameters of the leptons have to be determined.

The track finding in the FLT starts with a pretrigger seed generated in the ECAL or the muon system. The trigger algorithm then tries to find a track in the trigger stations of the tracking system, using the pretrigger information as starting point. This is shown in Fig. 3.6. The track information is updated if a hit is found and the search continues in a smaller region in the next layer of trigger chambers. The track momentum is estimated in the trigger system by the track's x offset from the target position. In the final stage of the FLT the invariant mass of two FLT-tracks is calculated and a trigger decision is made based on the the p_t and the mass of the track pair.

3.2.4 Second Level Trigger

The second level trigger (SLT) is entirely implemented in software. The program is run on a farm of PCs which are directly connected to the second level buffers of all subsystems (shown for the inner tracker in Fig. 4.15). This very flexible concept was used for various triggering scenarios during the commissioning in 2000.

3.2.5 Status of the Sub-Systems in 2000

The 2000 running period was coinciding with the installation and commissioning of many parts of the HERA-B detector. The performance of the detector was therefore not yet satisfactory in many subsystems. The status is briefly discussed here:

- VDS
  In 2000 the VDS was performing well. The alignment was understood in the course of the running period and the detector modules were generally working satisfactory. The signal to noise ratio of the system reaches levels between 20 and 25 on the n-side. The vertex impact parameter resolution for muons is $73\,\mu$m. The alignment constants for the system are known to a precision of 2-7μm in transverse direction and 50-250μm in longitudinal direction [29]. Aging effects were not seen.

- ITR
  The inner tracker was not fully installed in 2000. Many stations were installed in the course of the year, they were then trained to the beam conditions. The chambers were brought to a stable operation mode but the full reconstruction and alignment only became available after the end of the running period. The efficiency of many chambers could not be measured and adjusted during the running, which resulted

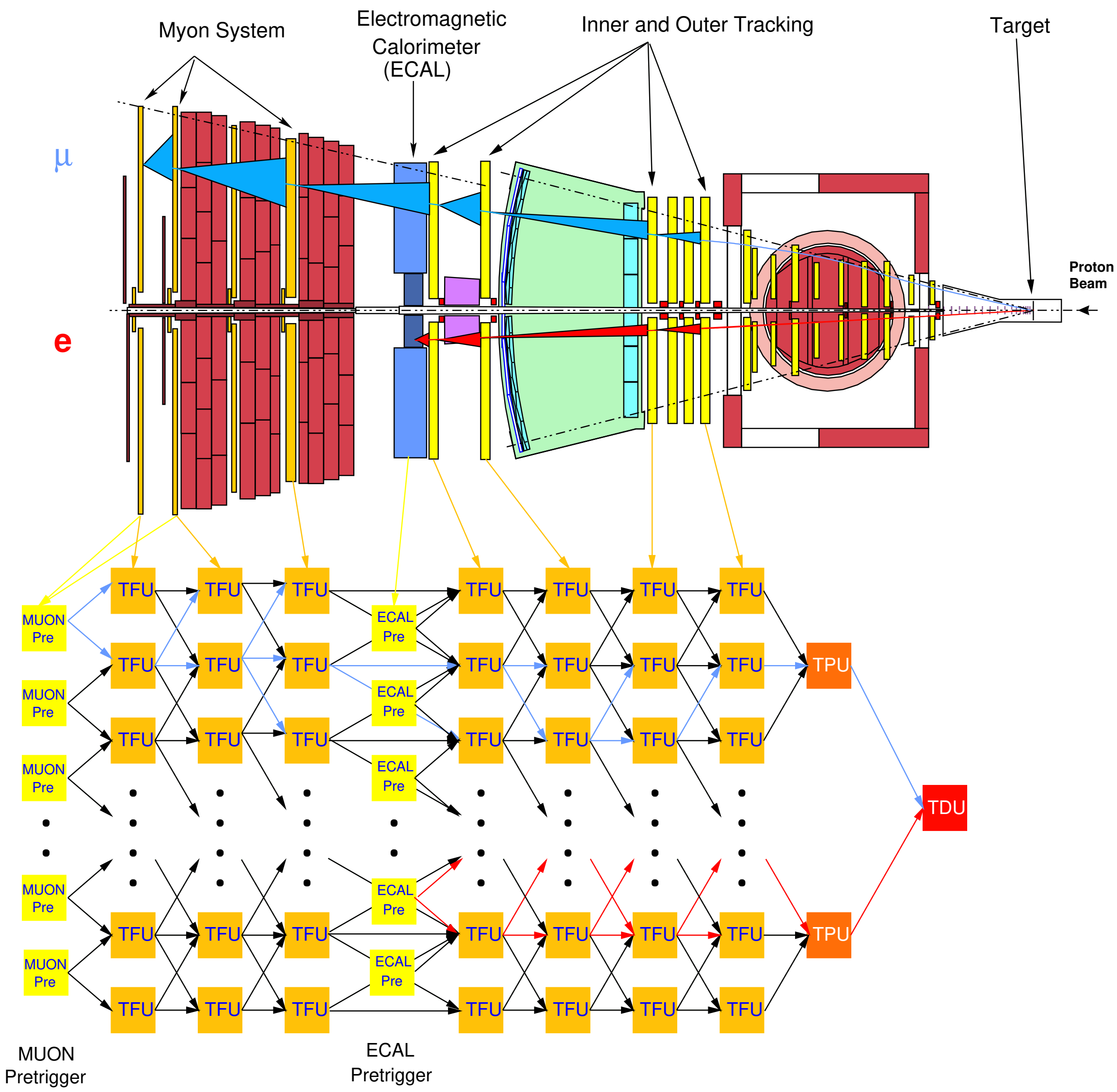

Figure 3.6: Schematic illustration of the first level trigger track reconstruction algorithm.

in a low overall efficiency of the system in the 2000 data. The data taking was additionally hindered by problems with auxiliary systems such as the low voltage or the readout system. The ITR was not contributing to the FLT in 2000.

- OTR
  In the outer tracker the installation was finished earlier than that of the inner tracker, but it became obvious soon that the high voltage stability was insufficient. This resulted in a loss of large parts of the acceptance, especially for the trigger. The system developed high voltage shorts, which in the meantime could be explained by the faulty mounting of some components of the HV system. These were repaired in the meantime. The working chambers showed reasonable hit efficiencies between 85% and 95%. The trigger chambers in addition had a problem with electronic noise. This was improved by changes in the handling of the electronic signals for

the trigger at the front-end.

- RICH
  The RICH system was already completed in 1999. Its performance was mainly depending on the performance of the tracking system because track seeds are needed for the reconstruction of Cherenkov rings.

- ECAL
  During the 2000 running period not all parts of the detector were equipped with readout and pre-trigger electronics. The system was also limited in energy resolution by electronic noise and pickup. These problems were solved during the shutdown in 2001.

- Muon system
  In the running period in 2000 the pad signal efficiency was below 70% in some areas of the muon system. This was caused by noise in the readout and some dead areas in the pad system. The low pad efficiency, together with the pixel-system not in operation lowered the efficiency of muon detection especially in the trigger in 2000.

  During the shutdown in 2001 the grounding schemes of the chambers and the electronics were improved, and damaged chambers were repaired during the shutdown. Therefore an average efficiency of $\geq 90\%$ for the pre-trigger chambers is expected in 2002.

- FLT
  The commissioning of the FLT depends heavily on a working tracking detector. The inner tracker was not connected to the FLT in 2000 at all, and the outer tracker had many inefficient regions. In addition to that problems in the optical signal transmission between the detector front-ends and the FLT electronics were discovered in 2000. This caused even larger areas not to contribute to the trigger. The pair trigger mode of the FLT therefore was never operated successfully in 2000.

  During the shutdown a major effort was undertaken to solve the transmission problems. At the same time the understanding of the trigger system has advanced and confidence has been gained that the default 2002 trigger scenario of one track found in the FLT and one in the SLT will be operated successfully.

Chapter 4

The Inner Tracker

The inner tracking detector is technically very interesting. Several theses, notes and papers [30, 31, 32, 33, 34, 35, 36] have been written about the construction, testing and commissioning of this sub-detector. As the commissioning of the inner tracker was a major part of the work presented here, the inner tracker is introduced in some detail.

The inner tracker was developed by the Universities of Zürich, Siegen and Heidelberg. The micro strip gas chamber (MSGC), which is the basis of the inner tracker chamber technology, was introduced by A. Oed [37] only in 1988. It had to be modified and refined to be able to withstand the harsh conditions of up to 10^7 particles $\mathrm{cm}^{-2}\mathrm{s}^{-1}$ in the HERA-B experiment. The resulting technology of GEM MSGC detectors was the first micro pattern gas detector which has been proven to work in a high rate experiment with highly ionizing particles (HIPs).

4.1 The GEM MSGC Chamber

The micro strip gas chamber alone – with a gas amplification of 6.000 and long strips – can not survive for even a short time in the radiation conditions present at HERA-B. This was discovered in 1996 during test-beam measurements in a π/p beam at PSI[1] [38]. During the research and development phase of the sub-detector, the MSGC technology was combined with the gas electron multiplier (GEM) suggested by F. Sauli [39]. The additional gas amplification at the GEM enables stable operation of the chambers with sufficient total gas gain. The schematic setup of the chamber as used in the inner tracker of HERA-B is shown in Fig. 4.1.

The GEM MSGC has a two stage gas amplification. The first amplification factor of $\approx$35 is reached at the GEM foil. This is a 50 μm Kapton foil with a 7μm copper layer on both sides. The gas amplification takes place in the holes etched into the foil. During operation a voltage difference of 420-460 V is applied to the two sides of the GEM. The holes have a typical diameter of 55 μm at the narrowest point and a pitch of 140 μm. The inner tracker GEM foils were produced at the CERN workshop [40] with a photo-lithographic method.

The signal is further amplified by a factor of $\approx$250 at the MSGC wafer. This wafer is made of 400 μm thick DESAG AF45 glass which is coated with an 80nm layer of

[1] Paul Scherrer Institute, Villingen, Switzerland

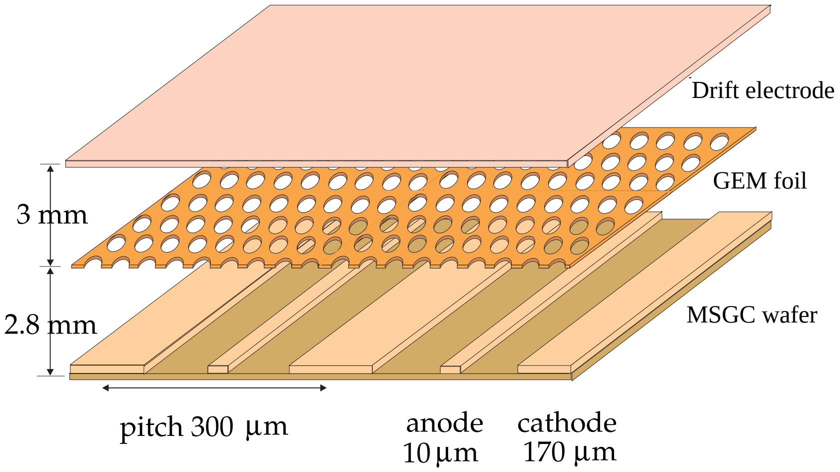

Figure 4.1: Schematic view of the GEM MSGC used for the inner tracker.

amorphous carbon ("diamond-like coating"). This coating is applied in a CVD (chemical vapor deposition) process [41] to get a surface with a defined resistivity. The structure of strip electrodes is applied on top of this layer with a photo-lithographic process. The strips consist of gold with a thickness of $0.5\,\mu$m, the anode strips are $10\,\mu$m wide while the cathode strips have a width of $170\,\mu$m. The pitch of the strips is $300\,\mu$m. One chamber has, depending on the type of the chamber (see Table 4.1), up to 756 anode strips which are connected to analog readout electronics.

The GEM foil is stretched and glued to a hollow frame which takes the force of the foil and distributes the counting gas within the chamber. The top of the chamber is covered by a G10 plate with a thickness of $300\,\mu$m, which also holds the drift electrode. The geometry of the chambers differs from region to region, in Table 4.1 the different sizes of the chamber types are presented. All three types have a recess of different radius to adjust to the 10 mrad inner acceptance line of the beam-pipe. The type III chambers used behind the RICH in addition have a larger overall size to allow the outer tracker to start at a slightly larger radius, so that the OTR occupancy is kept at a low level. To keep the changes in the design of the readout system for the type III chambers as limited as possible the pitch of these chambers was adjusted to $350\,\mu$m, so that not more than 756 readout strips are in one chamber.

The counting gas used for the inner tracker GEM MSGCs is Ar/CO_2 with a composition of 70% Argon and 30% CO_2.

The addition of the GEM to the micro strip gas chamber enabled stable operation with the necessary gas gain in the hadronic environment of HERA-B. The GEM however introduced a lot of unwanted new operational problems such as GEM sparks, multiple electrode sparks, and large variations of gas gain because of variations in the geometrical properties of the GEM. Difficulties in the operation of GEM MSGCs resulting from the hadronic environment at HERA-B are reported in Section 4.3, the performance in 2000 is presented in Chapter 5.

An in depth description of the functionality of GEM MSGCs can be found in [33]. The production of the inner tracker chambers is described in [34].

Table 4.1: Dimensions of the inner tracker chambers in the different regions of the HERA-B detector. Type I and type II detectors only differ in the size of the beam-pipe recess. All sizes are outside dimensions [34], [31].

Type	Size	used in Super-layer	Readout pitch	Beampipe recess size	Number of anode strips
I	25 cm × 23 cm	MS01–MS05	300 μm	5.5 cm	752
II	25 cm × 23 cm	MS06–MS13	300 μm	8 cm	752
III	27.5 cm × 27 cm	MS14, MS15	350 μm	12.5 cm	756

4.2 The Inner Tracker System

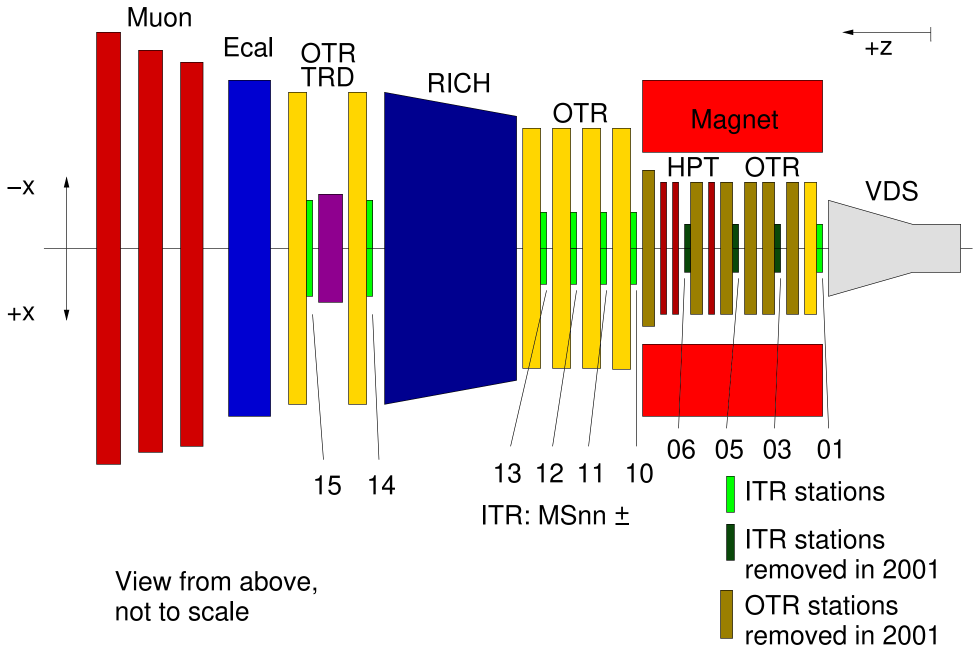

Figure 4.2: Schematic overview of the HERA-B experiment. The inner tracker stations which were installed in 2000 are indicated.

This section introduces the layout of the inner tracker (ITR) system. The inner tracker is divided into ten *stations* along the beam-pipe. These stations consist of 8 to 32 chambers. Four chambers form a complete layer. A layer is arranged around the beam pipe and covers an area of $\approx 48 \times 44$ cm^2 with a recess at the center of the active area. The arrangement of the four chambers is shown in Fig. 4.3. Because of the overlap the chambers of one layer are not mounted at the same z-position.

Every station is mounted to the frame of an outer tracker station. In Table 4.2 the correlation between ITR and OTR names and the number of inner tracker chambers per station can be seen. A *superlayer* denominates one of the stations while a *half station* like MS10- only refers to one half of the superlayer, in this case the -x side. The half stations are often referred to, because half-stations can be moved out of the beam position in

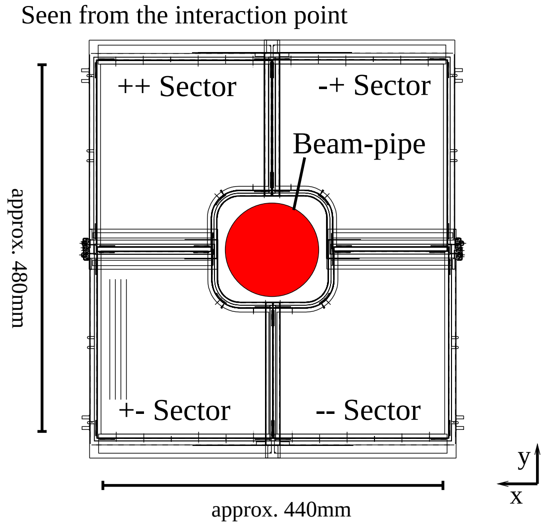

Figure 4.3: Front view of the layout of an inner tracker layer of four chambers. The readout strips are arranged vertically in the chambers. Some layers are rotated by $\pm 5°$ to resolve the y coordinate. The -x and +x chambers are mounted on individual structures that can be removed to perform maintenance work.

order to access the chambers during breaks in the HERA operation for maintenance and installation work.

The naming convention of the inner tracker uses five characters to identify each chamber. The first two characters are the number of the superlayer (01 to 15). The next character behind the superlayer number is a -(x) or +(x) indicating the position in x-direction (e. g. 10-). The following character is again a minus or plus to indicate if the chamber is above (+) or below (-) the beam pipe in y-direction. The last digit of the chamber name is the number of the layer inside the superlayer. For example the first chamber in the superlayer 10 which has its active volume in the +x direction and below the beam pipe (-y) is (MS)10+-1. The superlayer 10 has 32 chambers in four quadrants (++, +-, -+, - -), that means this superlayer has eight layers.

The regions of the tracking system are referred to by the names of the outer tracker stations (see table 4.2). Therefore the magnet region is called MC (magnet chambers), the PC region refers to the *pattern recognition* area, and the *trigger* area stations are in the TC region.

4.3 Problems of Gaseous Detectors in Hadronic Environment

In a high rate hadronic environment like in HERA-B the operation of gaseous detectors is difficult. Micro pattern detectors were originally planned to be used for tracking in all new high rate experiments such as HERA-B and the LHC experiments. While they fulfill the basic requirements, several operational problems remain.

In GEM MSGCs the following operational problems can be seen:

Table 4.2: Naming convention of the HERA-B main tracker and chamber configuration of the ITR. Double layers of inner tracker chambers, which are contributing to the first level trigger are shown connected by a slash. MS03, MS05, and MS06 are removed for the running in 2002.

OTR station	ITR station	number of ITR chambers	ITR stereo views	contribution to FLT by ITR and OTR
MC1	MS01	16	0°, -5°, 0°, +5°	no
MC2	-	-		no
MC3	MS03	8	0°, -5°	no
MC4	-	-		no
MC5	MS05	8	0°, +5°	no
MC6	MS06	8	0°, -5°	no
MC8	-	-		no
PC1	MS10	32	0°/0°, -5°/-5°, 0°, +5°/+5°, 0°	yes
PC2	MS11	16	0°, -5°, 0°, +5°	no
PC3	MS12	16	0°, -5°, 0°, +5°	no
PC4	MS13	32	0°/0°, -5°/-5°, 0°, +5°/+5°, 0°	yes
TC1	MS14	24	0°/0°, -5°/-5°, +5°/+5°	yes
TC2	MS15	24	0°/0°, -5°/-5°, +5°/+5°	yes

- Discharges between the anodes and the cathodes of the MSGC.
  These discharges can cause permanent damage to the structure of the wafer. In a coated MSGC, like the one used for the inner tracker, a single discharge does not result in a cut of an anode. Frequent discharges on a strip, however, cause permanent damage. This damage is either a cut in the anode or a short between the anode and the adjacent cathode strip. Discharges can not be directly detected in inner tracker chambers, it is only possible to detect shorts. The observation of anode-cathode shorts is discussed in Section 5.4.

- Discharges in the GEM.
  The two copper layers on the GEM foils are only separated by 50μm Kapton. In this small distance a large gas amplification takes place and any dust particle can cause a discharge in this region. If a discharge within the GEM foil takes place, the resulting voltage drop between the sides can be detected. The occurrence of these GEM sparks is the subject of section 5.2.

- GEM shorts.
  At dust on the GEM or weak points caused by production defects repetitive GEM discharges can produce a short between the two sides of the GEM. If a GEM is shorted the complete chamber is unusable.

  A short under these circumstances means a conductive connection between the two sides of the GEM with a resistance of 1-100 MΩ. The observations of GEM shorts in 2000 are presented in 5.3.

- Aging.
  The performance of all gaseous detectors deteriorates with operation time. In the harsh environment of HERA-B aging effects are so serious that a lot of work was invested to study them during the research and development phase [33].

  Two effects were observed: Gas aging and diamond aging.

  Gas aging means the deposition of material on the anodes, causing the detector signals to deteriorate. It was discovered only during the illumination of large areas, both with x-rays and with pions/protons at PSI. However, this problem was only seen with DME[2], the quenching gas which best protects against discharges. To avoid this problem the gas mixture for the inner tracker was changed from Ar:DME (50%:50%) to Ar:CO_2 (70%:30%). This mixture of gases is the only choice for long term MSGC operation under HERA-B conditions.

  Diamond aging was observed when a large area of the chamber was irradiated with a very intense X-ray source. It was observed that the diamond-like coating was partly removed in the area close to the anodes. Such a change in the wafer surface causes the gas amplification to become inhomogeneous. This was observed after an exposure equivalent to about three years of HERA-B operation. After an irradiation time corresponding to about five years of HERA-B operation the gas amplification again becomes stable and is then four times higher than at the beginning. It is however not clear if these results obtained in the laboratory can be transferred to the hadronic beam present at the experiment.

4.4 The Setup of the Inner Tracker

4.4.1 High Voltage System

The High Voltage System of the HERA-B inner tracker was developed with the objective to control and monitor the high number of 736 high voltage channels with an affordable system. A commercial solution with full monitoring was not available at the time, and the price and time for a development by a commercial supplier was too high. The high voltage distribution system was therefore built partly with off the shelf components and partly with custom-made modules developed in the electronics workshop in Heidelberg.

Fig. 4.4 shows the layout of the inner tracker high voltage system with all components for a single chamber. The components are:

- The High Voltage Power Supply
  The C.A.E.N.[3] SY527 is a modular power supply equipped with two different types of modules for the inner tracker. One Type (A734N) is used to generate the cathode voltage; the other type (A732N) is used for the drift voltage. The modules for the cathode voltage have a maximum current of 2.7 mA. The cathode voltage for the inner tracker is typically set to 510 V[4].

[2]dimethyl-ether

[3]Costruzioni Apparecchiature Elettroniche Nucleari spa., Viareggio, Italy

[4]All voltages in the inner tracker high voltage system are negative. The values mentioned here are stated without the sign for simplicity.

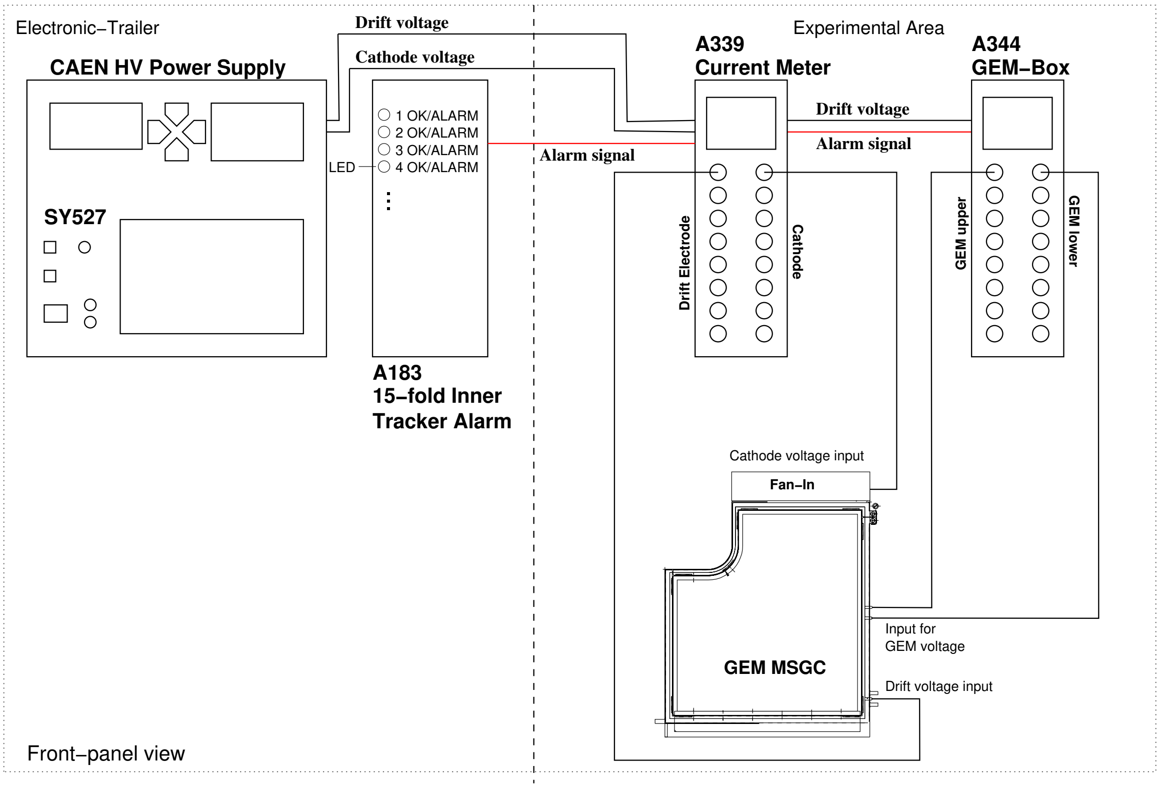

Figure 4.4: Layout of the inner tracker high voltage system. Shown is the distribution for a single chamber. Taken from [42]

The module for the drift voltage has a maximum output voltage of 6 kV at a maximal current of 1 mA. For the inner tracker the voltage is set to 2,500 V.

The high voltage power supply can be remote controlled by a VME module via a serial link. The high voltage power supply and the VME crate are located in the electronics trailer. In this VME crate all components of the inner tracker slow control are assembled. All processes of the slow control system for the inner tracker are run on the CPU in this crate (see Section 4.4.4).

- High Voltage 8-channel Current Meter A339 (*HV Box*)
  The A339 [44] as well as the other NIM units A344 and A183, introduced below, were developed and built for the inner tracker by the electronics workshop in Heidelberg.

  The drift and cathode voltages from the power supply are distributed by the HV box to eight chambers. The drift voltage is also passed on to the GEM voltage distribution. All 16 currents at the outputs are measured in the high voltage box. If the set current limits are exceeded (alarm state) its two high voltage relays open, to disconnect all connected chambers from high voltage. The high voltage line to the GEM box is also switched off in this case. The HV box also has an alarm input, if a signal is applied by the GEM box the high voltage relays open.

  The HV box communicates with a CAN bus interface which is used by the slow control system to read drift and cathode currents and to set current limits.

In case of an alarm a NIM signal is generated at the alarm output, which is sent to the A183 alarm box.

The High voltage box is micro processor controlled. The processor can be fully re-programmed to add additional features in situ. This was done in 2000 to add the alarm input feature, to enable the HV box to react on GEM box alarms.

- GEM Voltage Distribution Box A344 (*GEM box*)

  For the inner tracker chambers the GEM voltage is not fixed by a simple voltage divider. Instead the voltage is derived by a variable resistance voltage divider. This enables the user to set individual voltages at each of the eight GEMs controlled by one GEM box [45].

  The other task for this unit is to detect and to react to GEM sparks. A GEM discharge, called GEM spark results in a characteristic voltage drop at the output of the GEM box. The output voltage is constantly monitored in the box. If a drop below a set threshold is detected, the variable resistor chain for the affected channel is set to the minimal possible setting to stop the discharge.

  If the GEM discharge does not stop within one minute and the GEM voltage stays below a selected value, the GEM box issues an alarm signal to the high voltage box, to switch the high voltage off.

  The GEM box also has a CAN bus interface. The slow control uses this interface to set the GEM voltages and spark detection thresholds and to read the number of detected GEM sparks or GEM alarms and the measured GEM voltage for each channel.

  In total the inner tracker uses 26 pairs of high voltage boxes for the complete system. They are located in NIM crates in the experimental area.

- Inner Tracker Alarm Unit (A183)
  In these boxes the alarm signals generated in the HV boxes are collected. They are used to generate a single alarm signal by calculating a logic OR of up to 30 input signals. The output alarm signal is sent to the control room to bring it to the immediate attention of the shift crew.

  The inner tracker uses two of these modules which are located in a NIM crate in the electronics trailer. This part of the high voltage system was not used in 2000.

In Fig. 4.5 the electrical layout of the high voltage supply for a single chamber is shown. The high voltage power supply also measures the voltage and the current, but this is a sum for eight chambers connected to a pair of high voltage current meter and GEM box. It provides therefore no information about the behavior of an individual chamber.

4.4.2 Gas System

For the operation of a gaseous detector at large particle rates a constant exchange and control of the counting gas is crucial. For the inner tracker the composition of the gas

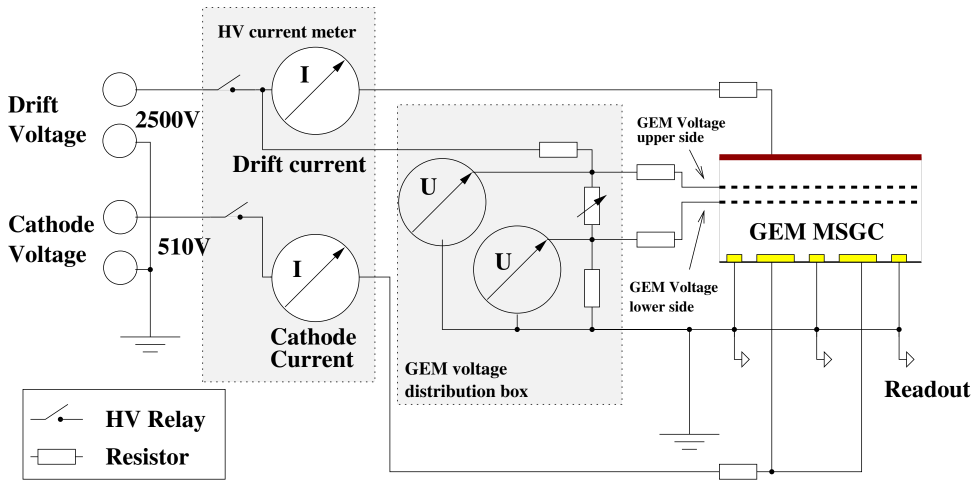

Figure 4.5: Electric scheme of the high voltage supply for one chamber. The system is distributed into two hardware units (The HV box and the GEM box).

mixture has to be very well controlled. Even more critical is the control of the detector gas pressure relative to ambient pressure. The wafer of the MSGC is only 400 μm thick, the pressure difference therefore has to be controlled to an accuracy of about 10 μbar, avoiding pressure differences above 3 mbar [46].

This is achieved by a sophisticated gas distribution system. The gas is distributed in an open loop system. The gas returning from the experiment is pumped from the experimental hall and released to the atmosphere.

The schematic layout of one group of the gas system is shown in Fig. 4.6. The full distribution system consists of four such groups, of which three are identical. In the fourth group, which supplies gas for the magnet chambers, the distribution for the +x and the -x stations is combined and therefore different in setup.

The parameter controlled by the system is the chamber pressure. This value has to be kept stable to protect the chamber and at the same time guarantee a constant gas flow. The active steering of the pressure is done with a mass flow controller (MFC). The valve of the MFC sets the flow in the system according to the input signal voltage. The signal is provided by a PID controller[5] which receives its input signal from one of the pressure sensors at the station.

The gas system has some redundancy and safety measures. This ensures a safe switching off of the system even in case of failure of a PID controller or a pressure sensor. The system is controlled by a Siemens S7 PLC[6]. The PLC also slowly starts the gas system at the beginning of the operation and selects the desired gas flow through the system. It is also used to transmit the parameters of the gas system, so that they can be stored in the HERA-B slow control database.

Because of the aging problems inherent to GEM MSGC detectors, the gas system has

[5]A PID controller is a unit that controls a value by reacting on **p**roportional, **i**ntegrated and **d**ifferential changes in the input property (in this case the chamber pressure). In the inner tracker gas system the Commander100 from ABB Kent-Taylor is used. This PID controller is fully user programmable.

[6]programmable logic controller

to provide extremely clean gas. In order to prevent even the tiniest pollution in the system, materials were only used after their out-gassing properties had been intensively studied. This results in a short list of allowed materials which can be used in the components that have contact to the counting gas. The distribution and mixing systems were built using only high-grade stainless steel components. The parts of the gas system placed in the acceptance region of the experiment are kept as low in material budget as possible with the available materials. These parts are either equipped with thin stainless steel components or are produced from Peek, one of the few qualified plastic materials. The connections of the steel capillaries with the Peek distribution system use seals with Kalrez[7] O-rings. The gas distribution for one chamber is schematically shown in Fig. 4.7. The panel at the bottom of the Figure is mounted to the outer tracker frame. This part of the distribution is outside of the acceptance region and it is equipped with thick-walled tubes.

The gas supply is provided by a mixing system. This system was also specifically built for the inner tracker. It can produce mixtures of gases with two components containing a CO_2 fraction of up to 30%.

The gas system parameters can be inspected online by a graphical tool based on the Siemens software ProTool. This tool enables the gas technicians to handle the day-to-day operation of the system [47].

4.4.3 Low Voltage System

The inner tracker front end electronics need a stable low voltage supply. For the supply of low voltages and high, strongly varying currents the regulation is usually placed as close to the consumer as possible. In case of the inner tracker front-end this was not possible, because no radiation-hard regulator components existed. In addition no thick, low-resistance cables were allowed within the detector acceptance. The low voltage therefore has to be supplied over cables of up to 20 m length and the voltages at the front end have to be controlled actively via sense lines of the same length.

This seems to be trivial, but the operation of this system in the environment of the west hall experimental area caused extensive problems in 2000.

The low voltage system for the inner tracker front end electronics was developed by a commercial supplier[8]. Each half-station of the inner tracker has its own low voltage power supply. The front-end electronics needs voltages of +5, +3, +2, -2 and, -5 V. These voltages have to be supplied with a low ripple and high currents of up to 40 A (peak current at -2 V). The units are located in the experimental area so they have to be equipped with a remote control.

The PL500 power supplies have exactly the technical properties needed for the operation of the inner tracker electronics. However, during the operation in 2000 the power supply units frequently failed. They either switched off regularly for no apparent reason or fuses blasted. In a few incidents the power supply even suffered from internal discharges destroying it. Only after the end of the 2000 running period the reason for the failures was found. The AC input voltage in the west hall of HERA is polluted with strong harmonics,

[7]A product of Dupont Dow elastomers, Kalrez Parts Marketing Division, Newark, USA

[8]Plein&Baus Elektronik, Müllersbaum

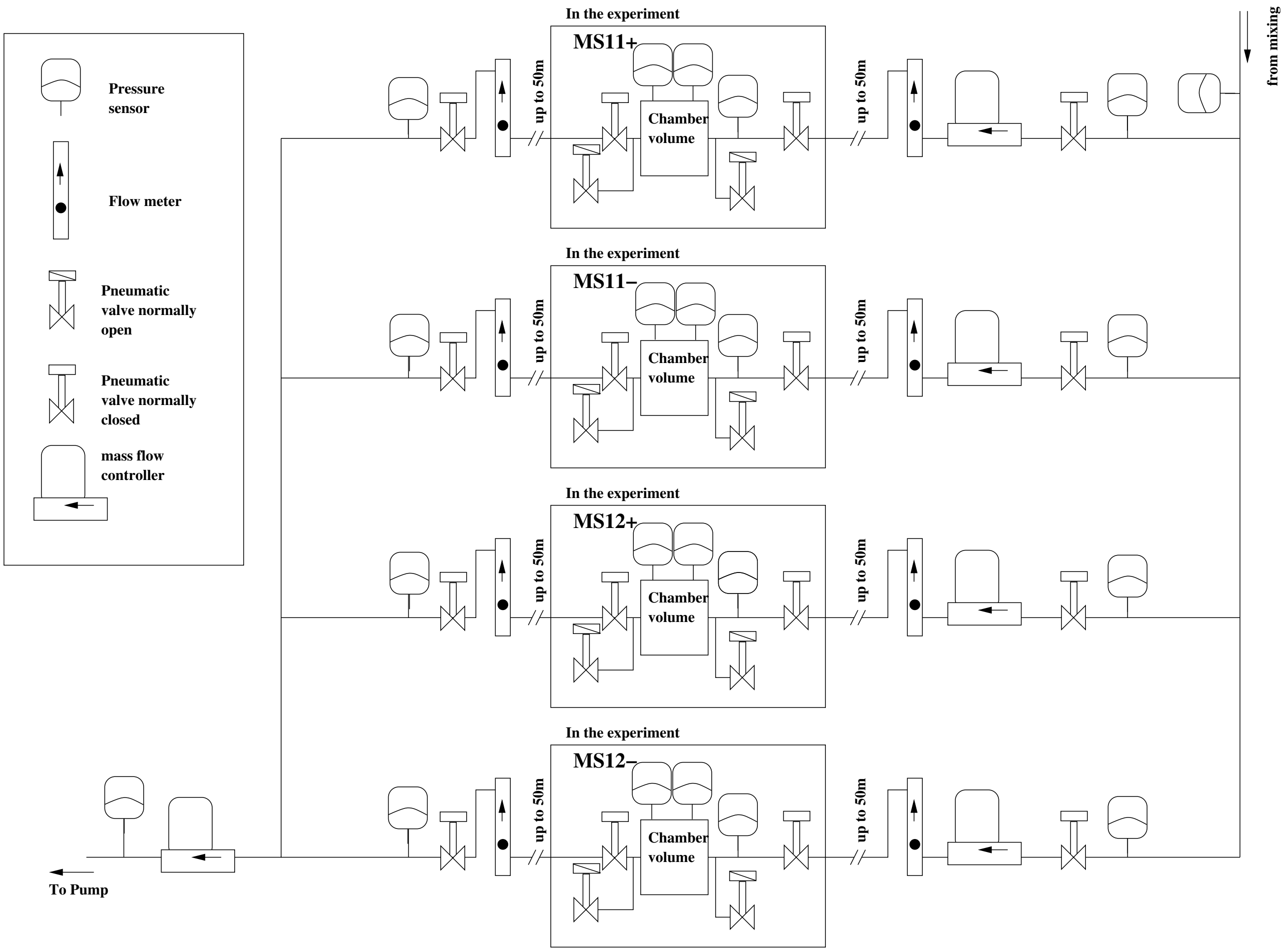

Figure 4.6: Schematic view of one out of four groups of the gas distribution system.

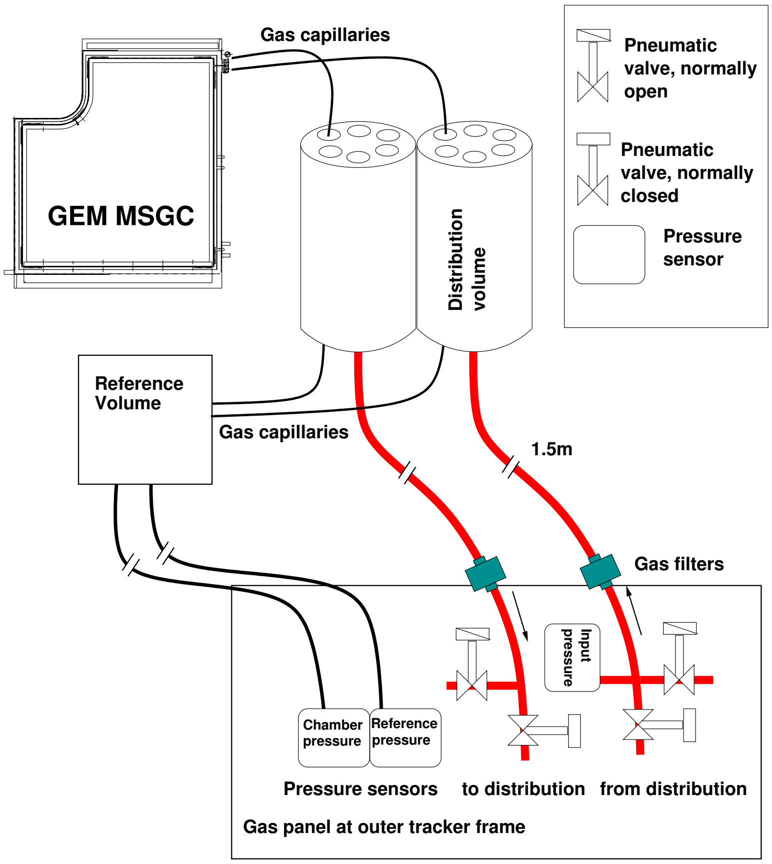

Figure 4.7: Schematic view of the gas distribution at the stations. The gas pipes in the active volume of the experiment are made of stainless steel tubes with 1 mm wall thickness.

which put a strain on the input stage of the switch-mode power supplies that it can not tolerate for a long time [48, 49].

Some other production related problems were also seen in 2000. In the mean time all power supplies were repaired and upgraded. In the west hall a two stage filter has been added to the AC input line. A commercial AC filter was introduced to the AC distribution of the experimental area and individual filters made of ferrite rings were added to each PL500. Fig. 4.8 shows the positioning of the ferrite filters in low voltage system.

With these improvements in the low voltage system no problems were observed since October 2001.

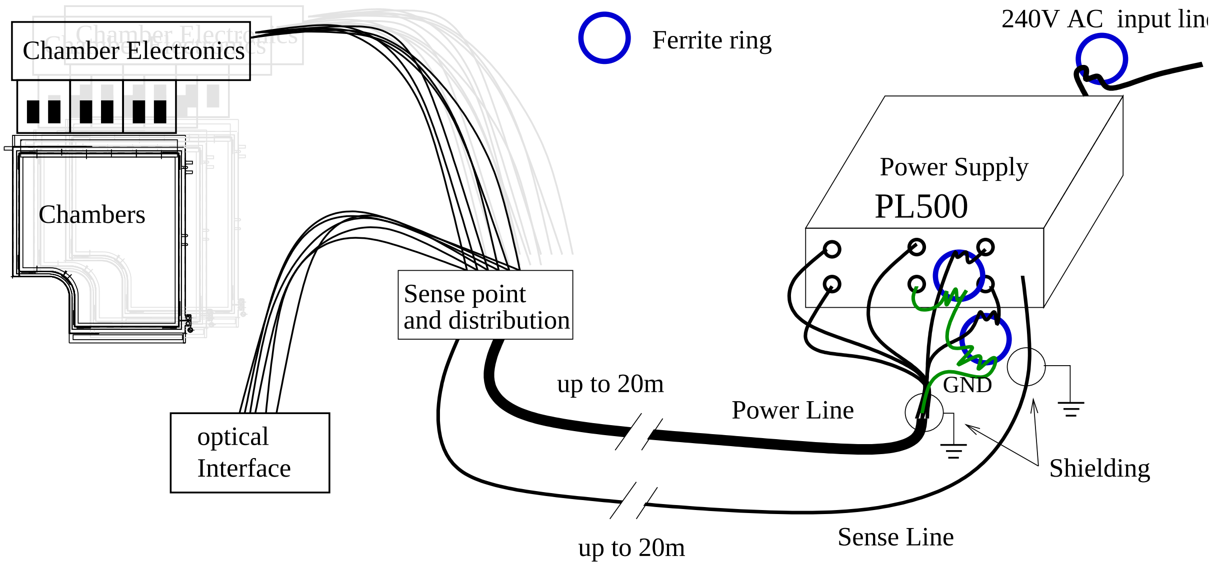

Figure 4.8: Scheme of the low voltage distribution in a station. The changes introduced in 2001 are indicated by the ferrite rings at the low voltage output (+2 and -2 V) and at the AC input on the back side of the PL500 power supply.

4.4.4 Slow Control System of the Inner Tracker

The slow control system is crucial for the safe operation of the inner tracker. The slow control system of HERA-B uses a common library and user interface, so that the underlying structures are identical for all HERA-B subsystems and the users have to get used to only one interface. This common structure (SPC, sub-system parameter control [50]) provides an interface to the slow control database, by which all status information gathered in the slow control processes can be stored.

The inner tracker slow control processes store information about the performance of the chambers into this database. This information can immediately be displayed in the control room or can be analyzed with off-line analysis tools later.

The slow control software of the inner tracker is divided into five processes. Each of them stores a set of data into the slow control database:

- The High Voltage Process (`spc_it_hv`)
  This process is the main part of the high voltage system steering. It sets the voltages

for all channels and reads the currents from high voltage power supply (C.A.E.N. SY527). The values of the actual voltages and currents are stored to the slow control database.

- The High Voltage Current Monitoring Process (`spc_hvcur`)
  The high voltage current meters (A339) are controlled and read out by this process. The information about drift and cathode currents is stored in the slow control database.

- The GEM Control Process (`spc_gem`)
  The GEM box (A344) is controlled and read out by the GEM control process. The actual GEM voltages and the number of detected GEM sparks are stored in the slow control database.

- The Low Voltage Process (`spc_lv`)
  The low voltage power supplies (PL500) are read out and controlled by this process. The actual voltages and currents are stored in the slow control database.

  The information of these four processes is stored with a frequency of 3 per minute.

- The Gas Monitoring Process (`spc_it_gas`)
  The gas system PLC sends status information on a serial line. This information is decoded in this process and then sent to the slow control database. The information of the gas system is updated in the database once per minute.

4.5 Installation and Commissioning of the ITR in 2000

During the running period in 2000 the inner tracker was step by step installed and commissioned. This section reports on the installation process during the year and the optimization of the operation parameters.

The inner tracker was installed during short breaks in the HERA operation between February and May 2000. During this time the first installed stations of the system were commissioned and the operation procedures were established. The chamber operation in this period was therefore not continuous but interrupted by tests and constant changes in the operational parameters.

In total 150 GEM MSGCs were operated in 2000, positioned in all three regions of the tracking system, in the magnet (MC), the pattern recognition area (PC), and the trigger area (TC). The MC and PC region were fully equipped with four stations in the magnet area consisting of 40 chambers and four stations built of 96 chambers in the PC area. The chambers in the TC region were only used for chamber tests, and had a maximum of 14 out of 48 chambers installed. The sequence of installation and removal of inner tracker half stations is in part shown in Fig. 4.9. Some half stations had to be removed to repair or examine them after some time of operation. The plot shows the number of chambers that were installed and connected to the high voltage system and the number of chambers that were operated with the full high voltage

At the beginning of the year modifications in the high voltage system hardware and software were made, lowering the number of chambers that could be operated at a time. During this time the "training" procedure was established. The chamber training procedure is described in detail in Section 4.6.

With increasing operational experience and when all chambers were fully trained, all installed chambers were operated. After the re-installation of MS13- and MS12+ at the end of May all installed chambers were reliably operated and the status of the MC and PC stations was kept unchanged for the rest of the operation period. In June and the following two months the ratio of operated to installed chambers was always exceeding 95%, even though the training of the half-station MS15- was going on in July.

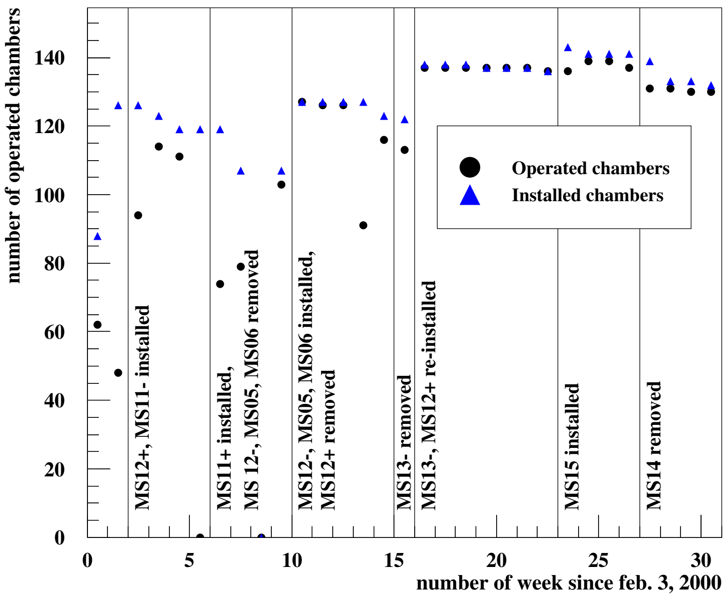

Figure 4.9: Maximum number of chambers that were used at a time. The most important changes in the configuration of the inner tracker are noted in the plot.

The change from commissioning to stable operation is visible in the number of operation hours accumulated in one week, which is shown in Fig. 4.10 a). Before the end of May (week 15 in the Figure), the chambers were operated only occasionally, while later more than 6000 h of operation were regularly achieved in a week. The handling and ease of operation also had a considerable effect on the operation efficiency. The fast switching on procedure and the automation of the GEM voltage ramping (see section 5.1.1) helped to bring up the operation efficiency.

During the complete year 2000 the inner tracker was operated by dedicated shift personnel. After the installation of a full time shift crew for the operation of the inner tracker, an operation efficiency of above 90% was reached, as shown in Fig. 4.10 b).

At the end of the year 2000 run, 56 chambers reached an operation time of more than

[10]Operation time here is always the time when luminosity is declared by HERA, the HERA-B wires produce interactions and the inner tracker high voltage is switched on.

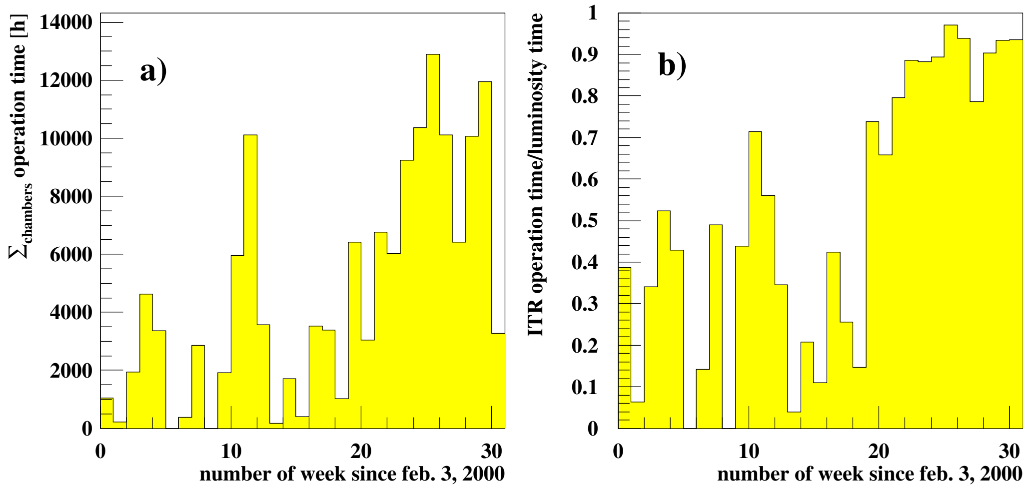

Figure 4.10: Inner Tracker operation in the course of the year 2000. The impact of the full-time shift crew and the improved slow control program can be clearly seen. a) sum of chamber operation hours[10] per week. b) shows the fraction of luminosity time the inner tracker high voltage was on.

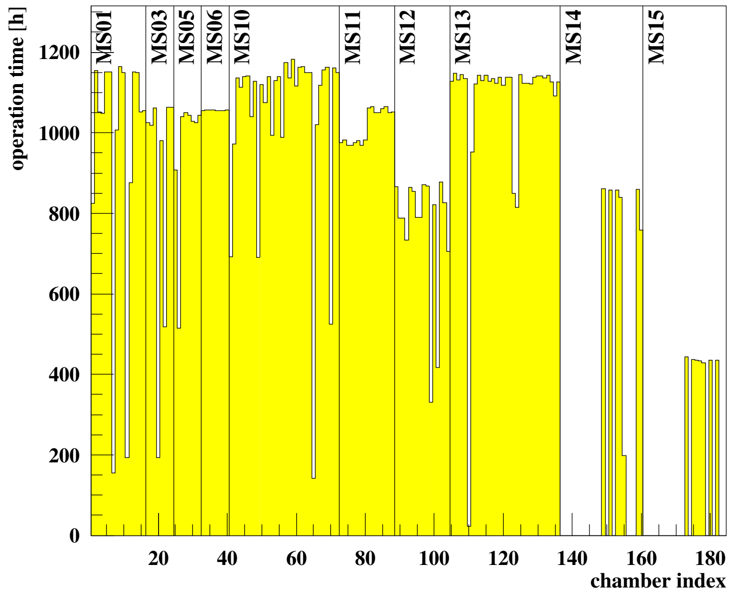

Figure 4.11: Sum of operation hours for each inner tracker chamber. The chambers which were not installed or failed during operation can be easily detected by the shorter operation time accumulated.

1,100 hours each. The operation time collected by all chambers is shown in Figure 4.11. All inner tracker chambers combined have accumulated 162,500 hours of chamber operation.

The inner tracker collected more than one third of a nominal HERA-B operation year (1×10^7 sec) in parallel to the detector commissioning during the 2000 running period.

4.5.1 HV Operation

The initial high voltage settings for the inner tracker GEM MSGCs were found experimentally by determining the chamber behavior both under γ- and π-irradiation. During a PSI test-beam run in 1999 [51] two full size GEM MSGCs were irradiated for one week with the final gas mixture of 70% Ar and 30% CO_2. From the results of these measurements the high voltage settings for the training of new chambers at HERA-B were determined. These settings defined a voltage of 3.2 kV at the drift electrode, 490 V at the cathodes and 390 V GEM voltage[11]. These values were used during the training in 1999 and at the beginning of 2000 (see first row in Table 4.3). The settings were chosen below the final operation point to avoid damage during the first operation.

For the operation of the inner tracker GEM MSGCs the strength of the fields between the drift electrode and the upper side of the GEM, the drift field, was chosen to be equal to the transfer field, the field between the lower side of the GEM and the wafer. While a transfer field that is stronger than the drift field yields a higher GEM transparency for primary electrons, this mode was not chosen to avoid deformations of the GEM by electrostatic force. The ratio between drift and transfer field is defined by the choice of resistors in the GEM voltage distribution boxes.

During operation in an environment with heavily ionizing particles, the GEM MSGCs show four operational problems:

- When the chambers are exposed to a high particle flux and heavily ionizing particles without careful training, it is likely that they develop a serious malfunction or are lost altogether. The most dangerous failure is a short between the two sides of the GEM. A careful training procedure significantly reduces the risk of such a short. Therefore a training procedure is necessary before the chamber can be used with high voltage and full efficiency. The training procedure developed for the inner tracker chambers is discussed in Section 4.6.

- During the operation 41% of the chambers developed one or more shorts between an anode strip and an adjacent cathode strip. Such a short reduces the active area of the chamber by 2% each. As the number of chambers that show this problem is high, this problem is presented in Section 5.4 in detail .

- Another problem that was only seen in hadronic beams is the occurrence of multiple electrode sparks (MES). This is a discharge that develops in the GEM and propagates to the structure of the micro strips, discharging the transfer gap. If such a MES occurs, several anode strips are severely damaged and can develop shorts to their neighboring cathode strips. Fig. 4.12 shows a photograph of the damage done by a MES. Multiple electrode sparks involving more than three groups of 16 strips

[11] Whenever the phrase "GEM voltage" is used here it refers to the difference of the voltages applied to the two metalized sides of the GEM foil.

were observed. If a MES of this extent happens, the chamber becomes unusable. The probability for a MES depends on the strength of the transfer field. Therefore the only possibility to lower the probability of these discharges is to reduce the transfer field by reducing the voltage at the drift electrode.

- The last problem seen during operation of the inner tracker chambers are GEM sparks. A GEM spark is a discharge between the upper and lower side of the GEM. The experience made with these sparks and the protection system installed is described in detail in Section 5.2. These discharges occur unavoidably in intense beams. They are also potentially dangerous, because they can develop into multiple electrode sparks or GEM shorts.

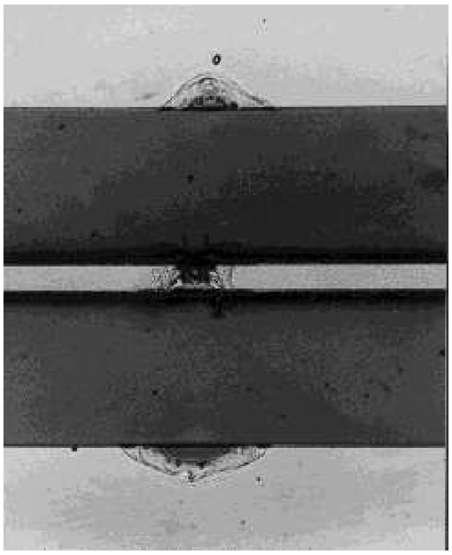

Figure 4.12: Typical damage at a wafer after a multiple electrode spark [33].

When multiple electrode sparks were seen in HERA-B in February 2000, the transfer field strength had to be reduced. The reduction from 3.3 kV/cm to 2.6 kV/cm had the side-effect of lowering the gas amplification in the GEM and at the MSGC for otherwise unchanged GEM and cathode voltages. To reach the same GEM voltage difference as with the old high voltage setting, a change in the resistor network of the GEM box was necessary. This was done starting end of February and operation was resumed with all chambers on April 6th. The changes in the operation voltages resulting from this modification can be found in Tab. 4.3.

Between May and July the cathode and GEM voltages were raised for all trained chambers in order to raise the chamber efficiency. From July on the GEM settings of the chambers were individually adjusted as the final step.

4.5.2 Variations in the GEM

When the hit efficiency was determined for the first chambers, large variations between chambers with identical high voltage settings were observed. These variations in the

Table 4.3: Operational parameters of the inner tracker running in 2000. The changes with respect to the previous settings are marked in bold face. All voltages are negative.

Starting date	Operational Parameters			Time operated
	U_{Drift}	U_{Cath}	U_{GEM}	
February 2, 2000	3200 V	490 V	390 V	147.5 h
February 29, 2000	**2900 V**	490 V	380-400 V	37.25 h
March 17, 2000 (some chambers)	**2400 V**	490 V	400V	178.5 h
April 6, 2000 (all chambers)	**2400 V**	490 V	400V	23.5 h
April 10, 2000	2400 V	490V	**410 V**	142 h
May 5, 2000	2400 V	**500 V**	410 V	85.6 h
June 8, 2000	2400 V	**505 V**	**420 V**	43.6 h
June 16, 2000	2400 V	**510 V**	420 V	186.1 h
July 3, 2000	**2500 V**	510 V	420 V	56.6 h
July 11,2000	2500 V	510 V	**420-460 V**	472.6 h

chamber performance are due to geometrical variations of the GEM hole size. They are assumed to be caused by problems in the alignment of the masks during the production of the foils. The result of these variations can be seen in the schematic cross section of a GEM shown in Fig. 4.13. This change in the geometry of the holes also changes the field in the GEM so that the gas amplification is affected. In chambers which are already in use, this can not be examined because the glass of the wafer is covered with an aluminum foil. In GEM foils not yet used for chamber production it could be verified that a misalignment of the two sides of the GEM is present in some of the GEM foils produced for the inner tracker.

Figure 4.13: Schematic cross section of GEM foils. On the left a GEM which was produced with well aligned masks is shown. The picture on the right shows the result of a bad alignment between the upper and lower mask.

To compensate the effect of these GEM variations, the high voltage at the GEMs had to be increased for some chambers which showed a very low gain at the nominal voltage of 420 V. For one of these chambers the GEM voltage had to be increased up to 460 V to reach an efficiency of 90%. Other chambers showed this efficiency already at a GEM voltage of 390 V. In order to achieve a homogeneous efficiency in all chambers the GEM voltages were individually adjusted for all chambers in 2000. The settings used at the end of the running period are shown in Fig. 4.14. The same adjustment will be repeated for the 2002 data taking period. The implications of the GEM variations for the efficiency are discussed in Section 5.6.

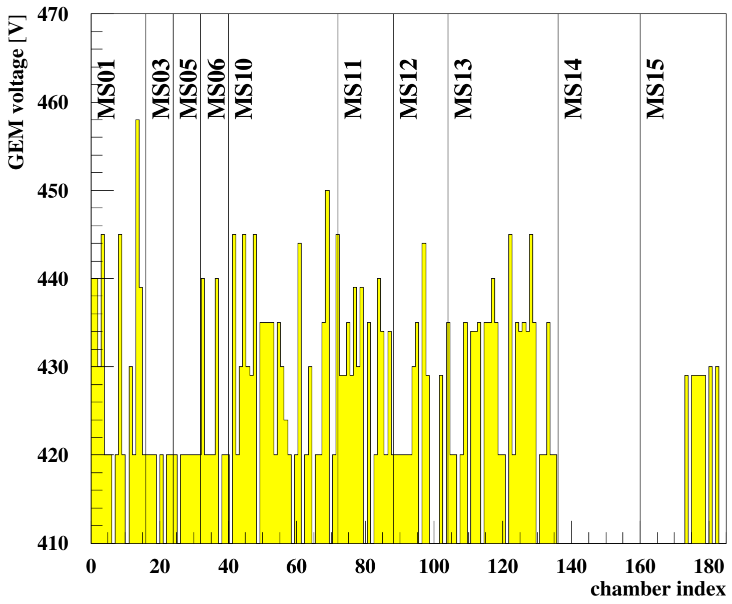

Figure 4.14: Settings of the GEM voltage at the end of the 2000 running period. The chambers are numbered from 1 to 184, number 1 is located in front of the magnet while 184 will be behind the RICH.

4.6 Training of GEM MSGCs in the Hadronic Beam

The GEM MSGCs cannot be operated in the beam at full high voltage from the first day. The chambers have to be carefully "trained" to the beam conditions in a period in which the high voltage is increased step by step. During this period small irregularities coming from the production or dust particles, which have settled on the micro structures, are removed, giving the chamber a better high voltage stability.

The training sequence changed — as did the high voltage settings — many times during the 2000 operation. Therefore Table 4.4 shows the training procedure as it will be used for the chambers in 2002. The training process takes between 150 and 400 operation hours in the beam which is equivalent to 15 – 40 HERA fills, depending on the behavior of the chamber (and the HERA efficiency). Chambers in the stations MS11 and MS12, which were the last to be installed in 2000, took less than three weeks or ≈21 HERA fills to be fully functional.

The decision to continue with the next step in the training procedure is taken based on experience and a stable behavior in the previous step. An unstable behavior is characterized by frequent discharges causing over-currents both in drift electrode and at the cathode. These over-currents cause the high voltage for a group of eight chambers to be switched off. Some chambers also show a high number of GEM sparks (see section 5.2) during the training phase.

Table 4.4: Phases of the training of inner tracker GEM MSGCs. These phases will be used for the inner tracker chambers in 2002.

Step	Drift voltage	Cathode voltage	GEM voltage
1	1200 V	250 V	169 V
2	1800 V	350 V	254 V
3	2000 V	450 V	282 V
4	2000 V	500 V	282 V
5	2250 V	500 V	317 V
6	2500 V	500 V	352 V
7	2500 V	500 V	360 V
8	2500 V	500 V	380 V
9	2500 V	500 V	400 V
10	2500 V	500 V	420 V
11	2500 V	520 V	420 V
12	2500 V	520 V	420-460 V

The chamber training procedure is done for groups of eight chambers which are connected to the same high voltage box pair. A chamber not behaving well can be taken out of its group and is then operated at a constant, lower voltage before the next training step is tried again. By "hospitalizing" problematic chambers, some of these chambers could be brought to stable operation at full high voltage. However, these chambers took up to seven weeks of careful operation before they could be used. Out of the 150 chambers used in 2000 five chambers were successfully treated this way. For another five chambers this treatment was not successful, and these chambers were lost.

When operation of the inner tracker system resumes in 2002, all chambers will be trained again. The reason for the decision to go through the time-consuming procedure again, is that during the upgrade and repair program in 2001 dust particles can have settled or re-arranged within the chambers. These particles have to be removed before a stable operation mode can be reached. In addition many completely new chambers were mounted in the system, they have to be trained as well.

4.7 Readout System

The readout systems of the HERA-B vertex detector and the inner tracker have been developed for the same front end readout chip, the HELIX128. This enabled both groups to develop a common set of electronics for the control and digitization of the analog data stream of both detectors. The functioning of this system and the treatment of raw and digitized data is documented in detail in [52] and [31]. Here only an overview of the system is given and some implications for the chamber operation are discussed.

The readout system of the inner tracker is based on the HELIX128 [53]. This chip has 128 analog inputs and can store the analog signals in an analog pipeline buffer for 128 bunch crossings. In addition to these 128 events up to eight triggered events can be stored while the chip is sending data. This is necessary to avoid dead-time at high trigger rates.

The HELIX chips are controlled by digital control signals. These signals are generated in the electronics trailer and transported to the experiment via optical fibers. At each inner tracker station an interface converts these signals to electrical LVDS signals which are fed to the HELIXes. The analog data from the HELIX chips is converted into analog optical signals which are transmitted to the electronics trailer as shown in the schematic overview of Fig. 4.15.

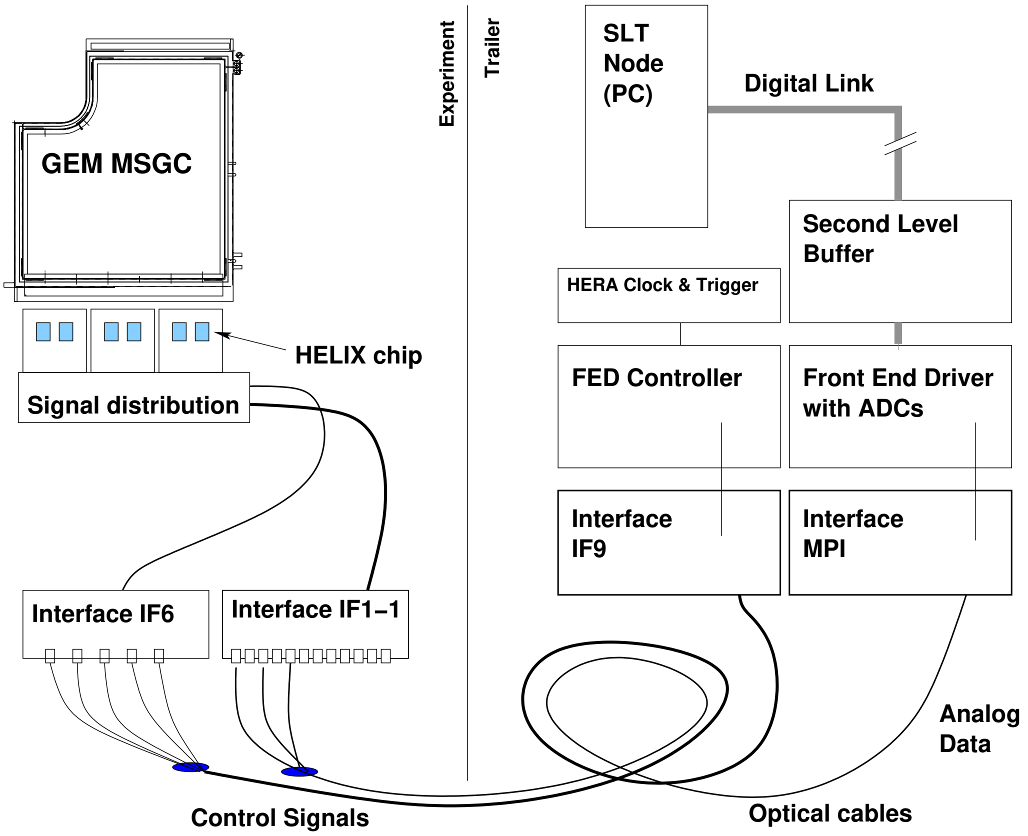

Figure 4.15: Schematic view of the components in the inner tracker readout system.

The data of two HELIX chips is sent consecutively on one optical fiber. These signals are again converted to electric signals in the electronics trailer, digitized by an 8-bit FADC, and stored in second level buffers. The raw data is transferred to the second level trigger farm where hit-finding is performed. Only the hit information, which is reduced by a factor of 10 in size with respect to the raw data, is stored to tape. In total the inner tracker is read out by 960 HELIX chips and the data is digitized by 480 ADCs on 40 ADC boards and transferred to 40 second level buffer boards.

Some parts of the readout system are inner tracker specific. The MSGC signal pulses require a specific pulse shaping to improve the signal to noise ratio and to keep the duration of the pulse below 100 ns. To select an inner tracker specific operation mode the HELIX provides adjustable signal amplification, shaping times and trigger threshold for the trigger output. The values for these chip properties are set via a CAN bus interface using electronics developed by the electronics workshop in Heidelberg for the inner tracker.

The inner tracker uses a mixture of different HELIX chip versions. These versions have different timing behaviors. In order to operate both kinds of chips at the same time careful adjustments in the relative timing of control signals have to be made. The mixing of HELIX chip versions caused a considerable amount of work to understand and adjust the system during 2000. For 2002 the problem will be circumvented by feeding different versions of the HELIX chip with individual control signals.

Chapter 5

Performance of the Inner Tracker

In total 150 inner tracker chambers have been operated in 2000 for 1/3 of a nominal operation year. This amount of time allows to judge on the performance of these chambers under 'real-life' conditions. During this time also valuable experience about the start-up behavior of GEM MSGCs was gained.

This section reports on the operation and performance of the chambers in 2000 and how the GEM MSGCs were trained and switched on.

5.1 Currents in GEM MSGC Detectors

The electric currents in a working chamber are good indicators for their functioning. Therefore a *quick glance* at the currents in the chamber can immediately tell a working chamber from a broken one and allow to get an impression of the gas amplification in the chamber. Fig. 5.1 shows the nomenclature of the currents in a GEM MSGC. The high voltage distribution system measures the currents at the drift electrode and at the cathodes. The current at the lower side of the GEM is very small (usually below 20 nA) while the current at the upper side of the GEM is larger (≈ 100 nA), but still considerably smaller than the currents at the drift electrode. Both currents of the GEM electrodes vary from GEM to GEM reflecting variations of the GEM hole geometry caused by production variations (as described in 4.5.2). Both GEM currents are not measured during operation at HERA-B.

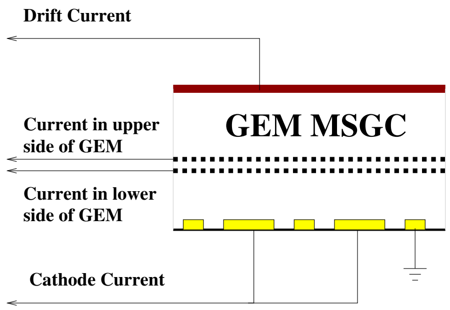

Figure 5.1: Nomenclature of the currents referred to in the text.

The drift current is proportional to the gas amplification in the chamber and the interaction rate at the target wire (the particle density in the chamber). In working chambers the drift current is of the order of 350 nA at an interaction rate of 5 MHz for a chamber in inner tracker station MS13 at typical high voltage settings.

Fig. 5.2 shows the correlation between the drift current and the pulse height of the clusters found in the analog readout for MS13. This correlation can be seen in all stations and shows that chambers with a high pulse height also have a high drift current for otherwise identical high voltage settings.

The average drift current of chambers of a station at identical high voltage settings increases with the z position of the station, because the number of crossing particles increases with rising z, as particle showers develop in the beam-pipe and the material of the detector.

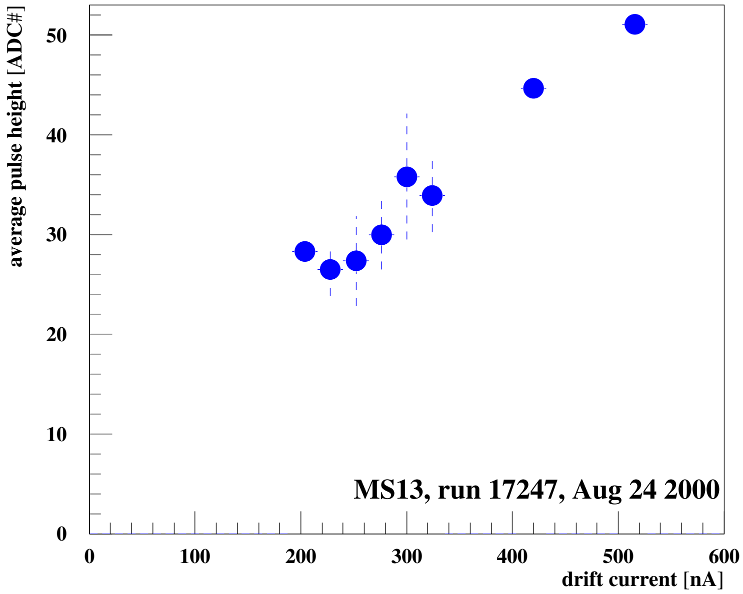

Figure 5.2: Correlation between the drift current in the chamber and the average cluster pulse height for station MS13 (Run 17247). The error bars indicate the spread of values that is observed.

The drift current is the most convenient quantity to determine the functionality of a GEM MSGC, and in fact the individual adjustments of the GEM voltage reported in section 4.5.1 were in large parts done based on the drift current measurements alone. This method is only suitable for coarse adjustments, because the correlation between pulse height and drift current is not strict but can vary up to a factor of two, as visible in the errors of Fig. 5.2.

Fig. 5.3 shows the dependence of the drift current on the interaction rate. The drift current is proportional to the interaction rate in the range between 4 and 20 MHz.

In Fig. 5.4 the drift current dependence on the GEM voltage can be seen for a typical chamber. For this chamber the GEM voltage was raised to 440 V to increase the efficiency. At this GEM voltage the efficiency of the chamber was measured to be 94.5% [54].

The current in the cathodes is dominated by the conductive coating of the MSGC

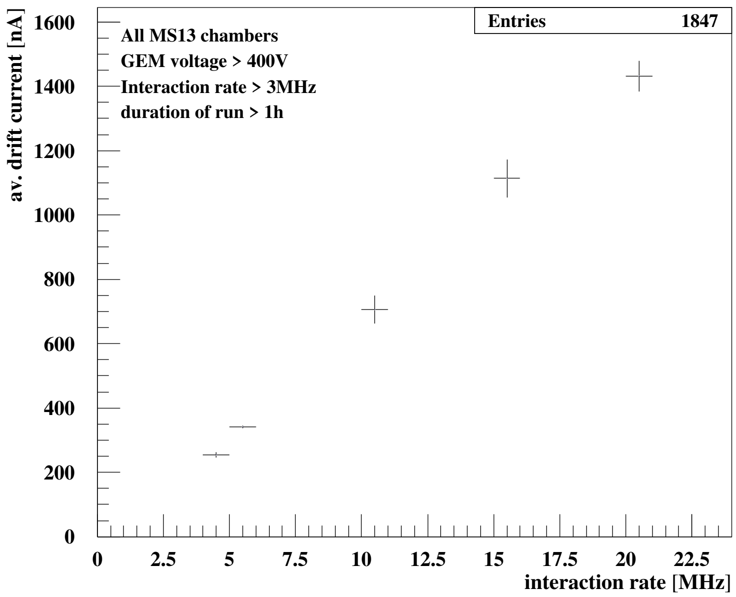

Figure 5.3: Average drift current against the interaction rate. This is an average over all 32 chambers in MS13 area with GEM voltage above 400 V in the runs of July and August 2000. Only runs lasting longer than one hour were taken into account for this plot, to suppress switching-on effects.

wafer. At a cathode voltage of 510 V it has typical values of 3 to 29 μA even without beam. During chamber operation the cathode current increases by 0.3-1.500 μA. Variations in the wafer temperature change the current by 2-3 μA. The change caused by the gas amplification during operation is therefore difficult to observe.

Towards the end of the production of the wafers annealing ("baking") was introduced to get a more uniform behavior of the chambers and to improve the aging properties of the chambers. Wafers which have been baked during production show currents between 3 and 8 μA, while the others have currents in the range between 18 and 29 μA. The surface resistivity of the coated wafers is in the range between $10^{14}\,\Omega/\Box$ for not baked and $10^{15}\,\Omega/\Box$ for baked wafers.

The cathode current changes drastically when a group of cathodes in the chamber develops a short between an anode and a cathode strip on the wafer (*cathode short*). This is discussed in section 5.4.

Fig. 5.5 shows the development of all important chamber properties as a function of time for chamber 13++4, a chamber with typical behavior. Plot 5.5 b) shows that this chamber was built with a baked wafer, the current is below 8 μA. The chamber also did not develop a cathode short during operation. A cathode short would be seen as a sudden increase in the cathode current of $\gtrsim$40 μA.

The drift current of this chamber (Fig. 5.5c) clearly reflects the change in the GEM voltage that was made in the 21st week of the operation. Fig. 5.5 d) shows the average rate of GEM discharges per operation day for each week in 2000.

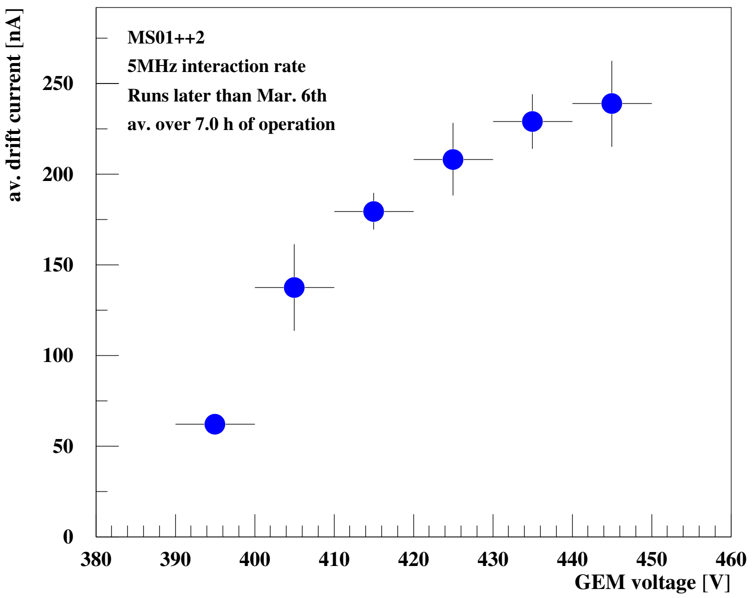

Figure 5.4: Average drift current in chamber MS01++2 as a function of the GEM voltage. Only runs with 5 MHz interaction rate and the reduced drift field (2.6 kV/cm) were used for this plot. This chamber was chosen, because it was operated at many different GEM voltages to reach a high efficiency.

5.1.1 Switching-On Procedure

Already in 1999, when the first GEM MSGCs of the final design were operated in a hadronic environment at PSI and in HERA-B [55] [51], it was established that the high voltage in these chambers has to be switched on in a well defined procedure. The switching-on procedure for the inner tracker chambers is modeled after the sequence of the training procedure that was presented in Section 4.6.

GEM MSGCs need some time to adjust to a new interaction rate, because the GEM polarization is rate dependent. Drastic changes in the interaction rate therefore either have to be avoided or the chambers have to be switched to a safe setting during such changes. In order to lower the time needed for the inner tracker system to be switched on, the system is kept at an intermediate voltage setting with no gas amplification during HERA injection and during the beam finding of the target wire.

It was also observed that the number of discharges in the GEM is lower if the chamber is not ramped from 0 V to the full high voltage but from a standby setting.

The ramping procedure for the inner tracker was developed and rigorously followed to ensure a fast and safe transition to the operational mode of the detector. The switching-on in 1999 was done by hand. During the year 2000 the scheme was step by step automated by the slow control programs. During the first four months of operation only the GEM voltages still had to be set by hand; the other voltages were already automatically controlled [42]. At the end of the running, the complete ramping-scheme was automated.

Fig. 5.6 shows all slow control measurements for one chamber during the automated

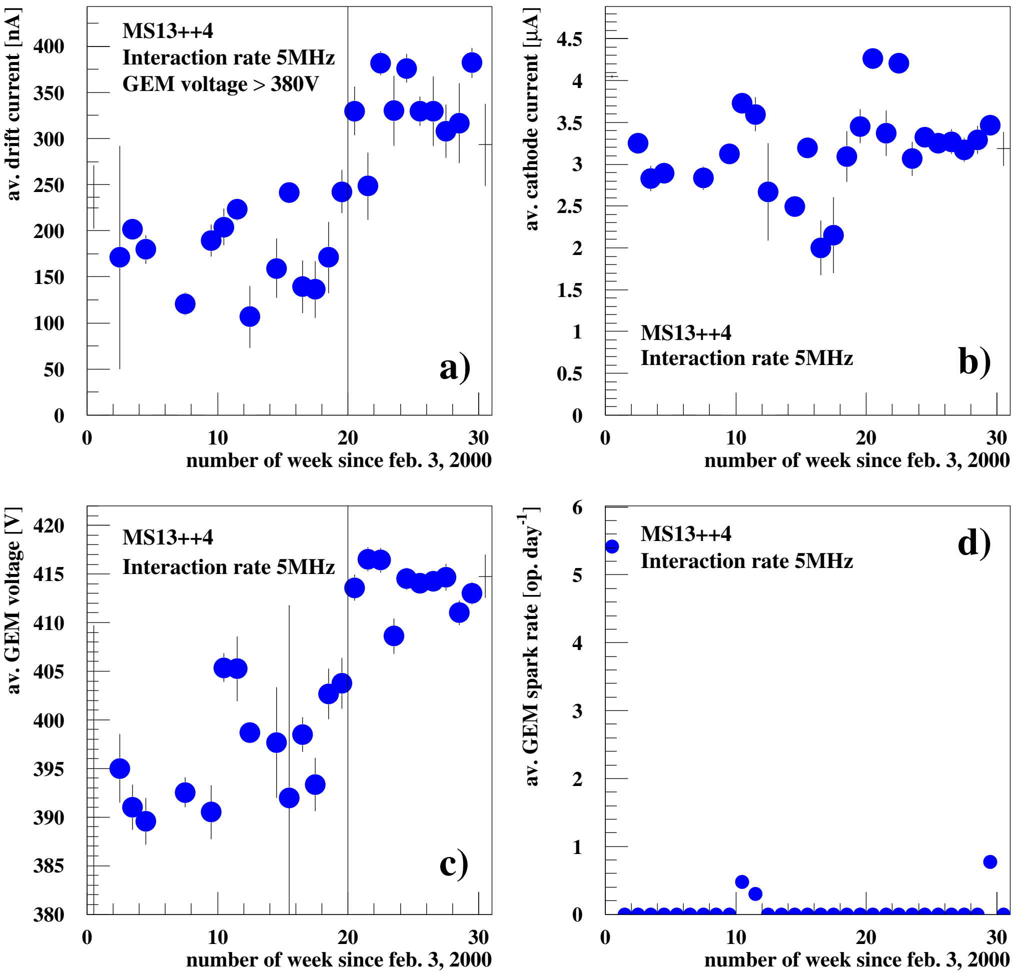

Figure 5.5: Development of a single chamber in time. a) Drift current , b) Cathode current, c) GEM voltage and d) Rate of GEM sparks/day.

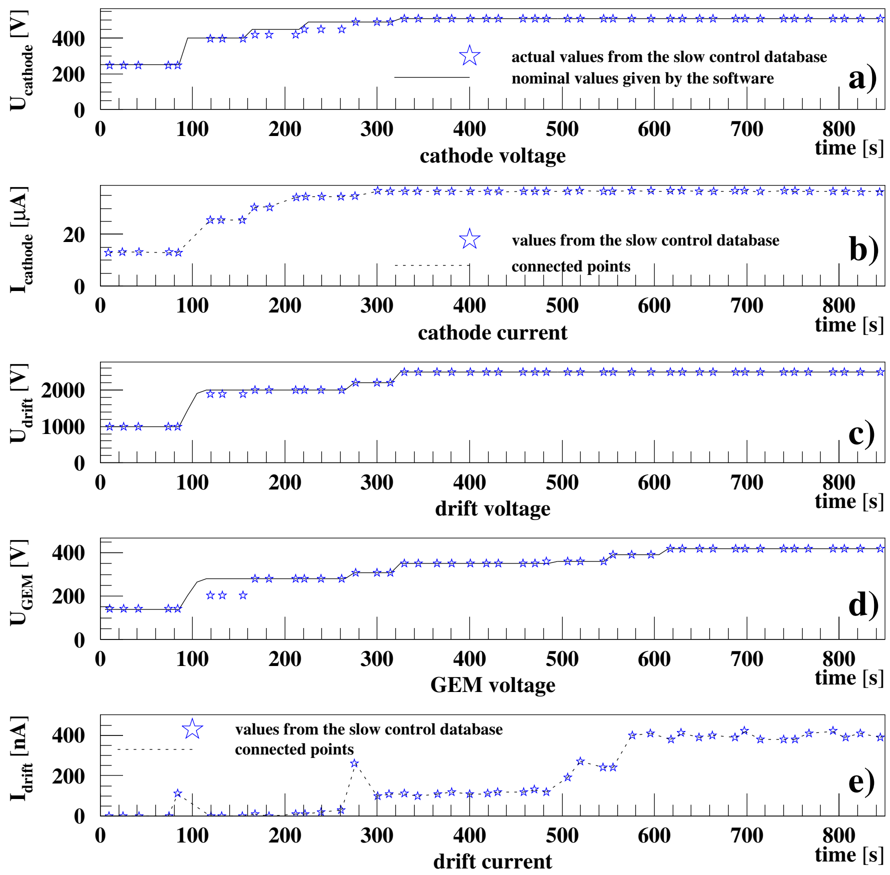

Figure 5.6: The switching-on procedure of one HERA-B inner tracker chamber (MS13-+7) as measured by the inner tracker slow control system. The rise in the drift current in plot e) corresponds to the increase of the GEM voltage at constant interaction rate of 5 MHz.

ramping.

Table 5.1 shows the sequence of voltages applied in the ramping scheme. It starts with the voltages shown in Step I, these are the standby settings. This is also visualized in Fig. 5.6. The inner tracker should only be switched on when a stable interaction rate has been reached at the HERA-B target.

The ramping scheme is realized in ten steps. In the first six steps the GEM voltage is set to minimum and follows the drift voltage. The GEM voltage is fixed to be 7.1 times smaller than the drift voltage in Step I to VI.

In the transition from Step I to Step II both drift and cathode voltage are raised to a level just below the onset of gas amplification. When this level has been reached, the cathode voltage is slowly increased in two steps. In step V the drift voltage is set to 2200 V while the cathode stays at 490 V. The next step takes both the drift and the cathode voltage to their final level of 2500 V and 510 V respectively. The complete ramping of the high voltage at the power supply takes about 200 s. At this stage the high voltage control process sends a message to the GEM control process indicating that the high voltage ramping is finished.

The GEM control program first waits for 60 s to allow the GEM to build up the polarization of the Kapton foil. The GEM voltage is then set to

$$U_{\mathrm{GEM},\,i} = U_{\mathrm{GEM,\,max}} - (10 - i) * 30\,\mathrm{V}$$

for the steps i from VI to X. Each of these steps of 30 V is delayed by 60 s to allow the GEM foil to slowly "settle".

The GEM voltage settings in the GEM MSGCs are individually set to achieve a uniform efficiency. The GEM settings used in 2000 are shown in Fig. 4.14.

Chambers with a low maximal GEM voltage (high intrinsic efficiency) such as the one marked *GEM1* in Table 5.1 have a set GEM voltage that is lower than the minimal voltage in Step VII. This can also be seen for chamber MS13-+7 in Fig. 5.6. This chamber needs only 3 steps in the GEM voltage ramping, so in Step VII the voltage stays unchanged.

Chambers with a higher final GEM voltage (or a low intrinsic efficiency, such as the *GEM2* chamber in Table 5.1) need all four ramping steps of the GEM.

Table 5.1: Steps in the inner tracker switching-on procedure. This example is shown for two chambers with 430 V and 450 V GEM final voltage.

Step	Drift voltage [V]	Cathode voltage [V]	GEM 1 voltage [V]	GEM 2 voltage [V]
I	1000	250	141	
II	2000	400	282	
III	2000	450	282	
IV	2000	490	282	
V	2200	490	311	
VI	2500	510	353	
VII	2500	510	353	360
VIII	2500	510	370	390
IX	2500	510	400	420
X	2500	510	430	450

Fig. 5.6 b) and e) show the development of the currents during the ramping. The cathode current shows a linear current behavior during the ramping. The start of the gas amplification at the anodes can not be seen at the scale of Fig. b).

The drift current shows two peaks at 80 s and 280 s during the ramping of the drift voltage; this is the charging current at the drift electrode. The height of these peaks is determined by the ramping speed which is set to 45 V/s for the drift voltage. The start of the gas amplification in the chamber can be seen after 300 s. After 500 s, when the GEM voltage is ramped, the drift current reaches its final level for the interaction rate of 5 MHz.

5.2 GEM Sparks

In this section the behavior of GEM MSGCs with respect to GEM sparks, discharges between the upper and the lower side of the GEM is explained. When a GEM spark occurs the complete capacitance of the GEM discharges over a spark in the gas volume. The capacitance of the GEMs used in the inner tracker chambers is large, because of the large area covered by the chambers. This large amount of electrical energy stored in the GEM makes a discharge in the GEM potentially dangerous to the chamber.

A single GEM spark in itself is no problem for the operation of a chamber, yet if many such shorts occur at the same place of the foil a permanent short in the GEM can develop. A short in the GEM makes the chamber unusable. It is also possible that other operational problems such as multiple electrode sparks develop from such discharges. It is therefore important to study the occurrence of GEM sparks during the operation.

The occurrence of such a discharge in the GEM is seen as a drop in the difference of the voltage between the upper and lower side of the GEM foil. This voltage difference is monitored in the GEM voltage distribution box ("GEM box"), where the voltage drop below 300 V is detected. If a GEM spark is detected the voltage divider of the GEM box is set to the minimal value of $\sim$353 V for one minute.

At this voltage GEM sparks usually stop and the chamber recovers within one minute. In case the GEM voltage is still below the threshold after 60s because the discharge is continuing, the GEM box sends an alarm signal which immediately switches the high voltage relays off. This switching off is done to prevent the GEM spark to develop into a permanent GEM short.

The numbers presented in this section are based on the count of GEM sparks by the GEM voltage distribution boxes and recorded in the slow control database.

Altogether 6,485 GEM sparks were recorded during the year 2000. In most of the 150 operated chambers only very few sparks were recorded, while in three chambers alone 2,587 sparks were seen. Fig. 5.7 a) shows the distribution of the number of GEM sparks seen in the chambers. The majority of chambers show little or no GEM sparks during $\approx$ 1000 h of operation. A small number of chambers spark comparably often.

For the comparison between chambers it is more useful to calculate the spark rate of the chambers. This rate, whenever mentioned in the text or in the figures, is the number of GEM sparks per 24 hours of target operation. The distribution of spark rates in the inner tracker chambers can be seen in Fig. 5.7 b).

Fig. 5.8 shows the spark rate for each chamber. As in Fig. 4.14 before, the chambers are numbered from 1 to 184. The chambers 133-145 and 159-171 represent the stations MS14+ and MS15+ in the TC region, which were not installed in 2000.

With a total number of 162,479 hours of operation in 2000, the average rate of GEM sparks per operation day is 0.96 sparks/day and chamber.

Only six out of the 150 chambers have a spark rate of more than 6 sparks per 24 operation hours. These are the chambers 01--3, 01--4, 10--1, 11++3, 12--3 and 13++6. Of these six chambers three (01--3, 12--3 and 13++6) were lost for operation during the year, either because of operational instabilities of the GEM, in the drift voltage, or because of too many cathode shorts (16++6). The other three chambers also developed at least one cathode short during the operation. Chamber 01--4 developed three cathode shorts and was therefore close to being a total loss, too (see section 5.4). This suggests that chambers with a very high GEM spark rate also have an increased probability to develop further operational problems. Chambers with a GEM spark rate below 6 per day however do not represent a problem for the operation of the system because we have gained confidence that a large number of GEM sparks is needed to damage a chamber seriously.

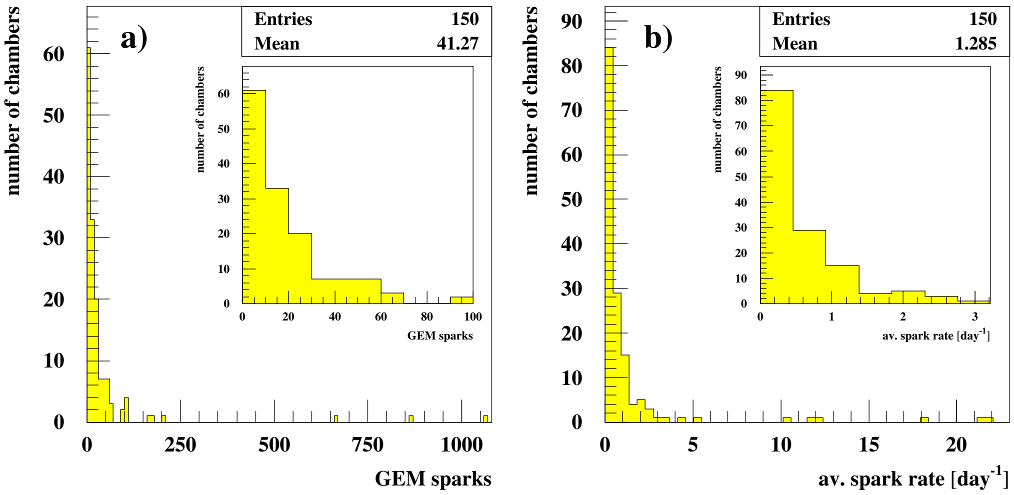

Figure 5.7: GEM spark distribution in the inner tracker. a) Absolute number of GEM sparks during 2000. b) Average spark rate per 24 hours of operation.

When the GEM spark rate during the training phase is shown (Fig. 5.9), a higher number of sparks during the training can clearly be seen. The figure shows that at the end of the chamber conditioning a stable operation mode with an average of less than one spark per day was reached. The error bars in Fig. 5.9 show the error of the mean value for all chambers. The GEM spark rate rises when the GEM voltages are increased to their final levels, this is not significantly visible in the average shown in Fig. 5.9 but can be seen in the behavior of individual chambers during the training process.

An observation made very early during the operation was that a higher number of GEM sparks was seen when the chambers are switched from standby to operational voltages at the beginning of a new fill. This can be seen in Fig. 5.10. The GEM spark rate falls with the duration of the fill. It was also observed that the GEM spark rate is rising at the end of very long runs (>6 h). This can be explained by the decreasing beam quality and a higher background rate produced near the end of the proton beam lifetime.

Also a very distinctive behavior can be seen in the GEM spark rate versus the GEM voltage (Fig. 5.11). The spark rate is below one per day in the GEM voltage range between 380 and 410 V. Above 410 V the spark rate increases exponentially and reaches a level of three per day at 450 V. The higher GEM voltages of 450 V and above were only used for very few chambers with low drift currents and therefore low gas gain. The behavior at higher GEM voltages can be studied further in 2002 when more chambers will be operated at high gas gain.

The interaction rate during the operation in the year 2000 was mainly 5 MHz. There were only brief periods with a higher interaction rate, most of them during *rate-scans*,

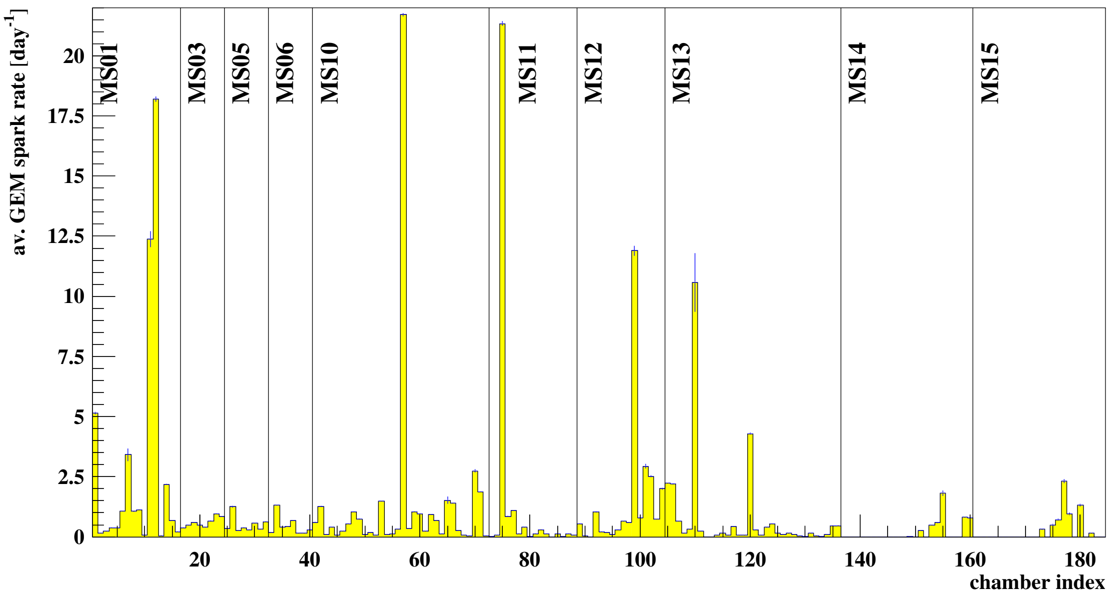

Figure 5.8: Distribution of the GEM sparks in the complete system. The numbering of chambers starts with the magnet chambers and ends in the TC region. The empty bins above chamber number 140 are reserved for the TC chambers that were missing in 2000.

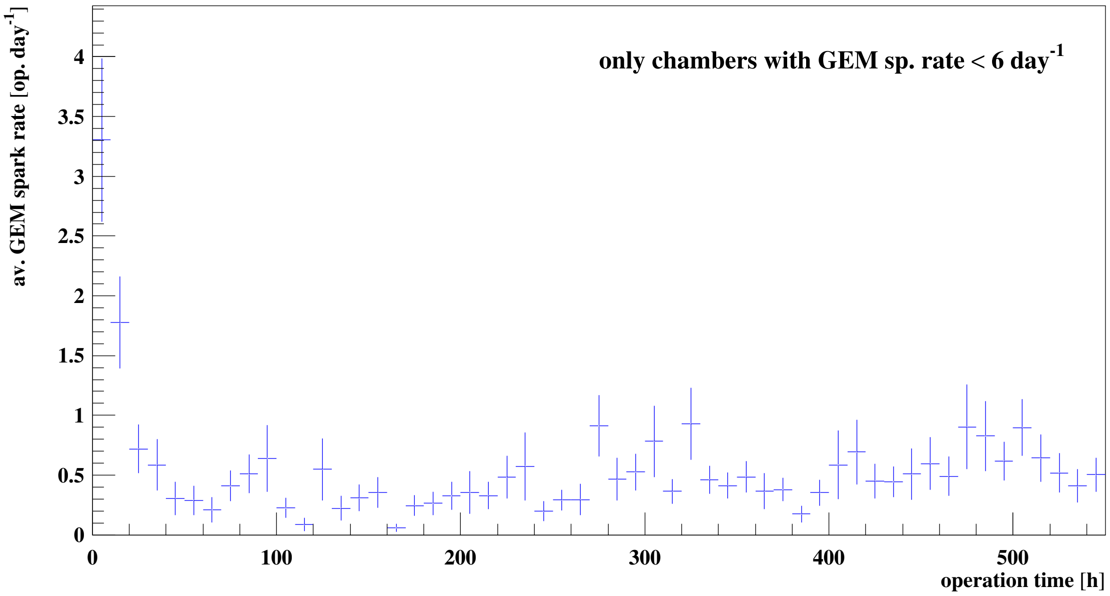

Figure 5.9: Development of the average GEM spark rate during the training progress. The spark rate decreases rapidly at the beginning of the training process. The error bars indicate the error of the average value.

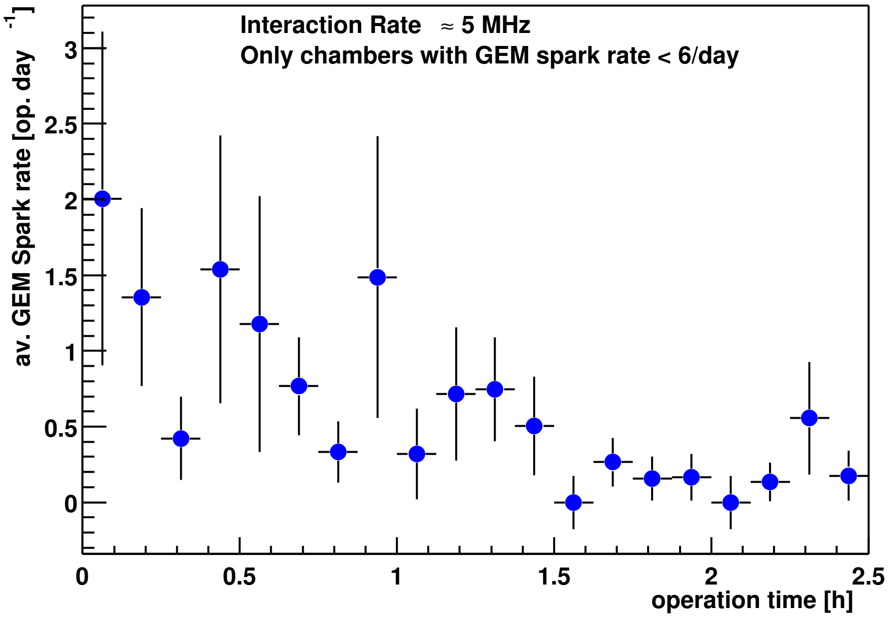

Figure 5.10: GEM spark rate depending on the operation time after the begin of a fill. Shown are the first 2.5 hours of operation. The errors bars show the error of the mean value of all chambers.

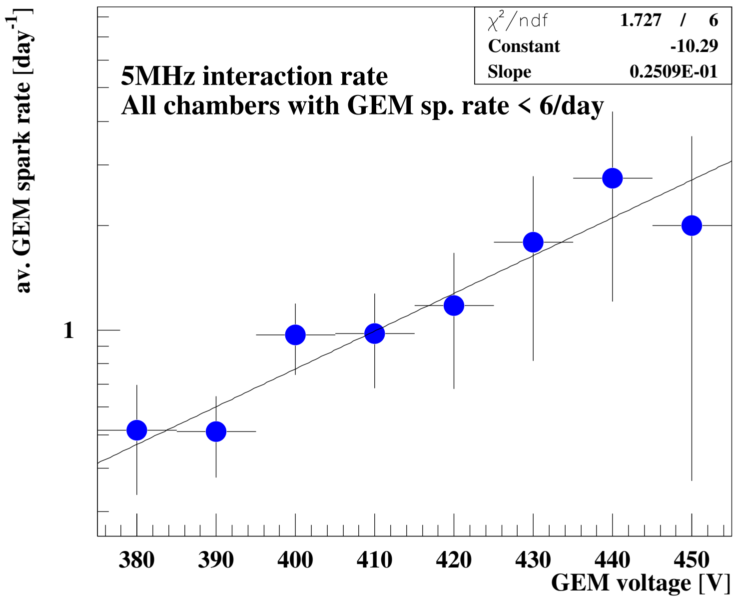

Figure 5.11: Spark rate against the GEM voltage.

which were done to understand the target function. During these rate-scans different target wire configurations were used in short succession at different interaction rates. Almost all high-rate running between June and August, when the final high voltage settings had been reached, was under rate-scan conditions. Many of these high interaction rate periods were very short. The effect caused by high rate running was therefore always combined with the observation that at the beginning of a run the GEM spark rate is also higher.

The increase of the spark rate (Fig. 5.12) with the interaction rate only suggests that the development of discharges in the chamber is caused by the particles going through the chamber.

The design rate of 40 MHz was not set for significant amounts of time, but already at 30 MHz the average spark rate is higher than in any other measurement of trained chambers presented here. Nevertheless this result is not very significant.

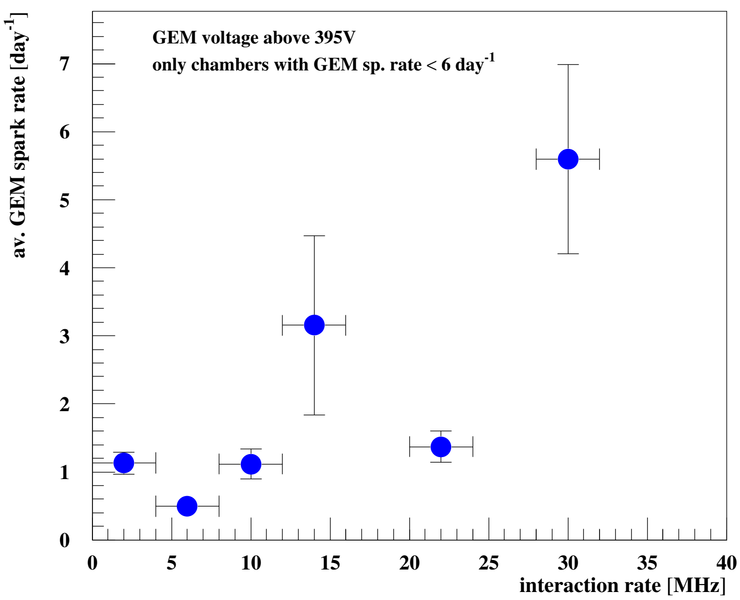

Figure 5.12: GEM spark rate against the set interaction rate. The experiment was mainly operated at rates between 3 and 8 MHz.

During the operation of the year 2000 we have learned that operation of GEM MSGCs in hadronic environment is possible. GEM sparks are unavoidable at operational conditions with high gas gain as needed for the GEM MSGCs at HERA-B. Although GEM sparks are unfavorable they seem to be no serious risk for the operation of our detector.

5.3 GEM Shorts

As mentioned in the section above, the most severe malfunction of a chamber is a short between the two sides of the GEM. A chamber with a short in the GEM produces no signal at all.

This was learned the hard way in 1999 when out of the first operated twelve chambers in MS14- four developed a GEM short and became unusable. Later, this could be avoided to a large extent by

- the protection system, switching the high voltage off at persistent GEM sparks,
- the training procedure, and
- the switching on-procedure.

However, in the course of the 2000 running four chambers in other stations developed GEM shorts. Two chambers were lost for the operation. In the other chambers the shorts could be removed during access days.

None of the chambers that developed a GEM short were fully trained at the time the short appeared.

Based on the experience gained in 2000 at most 0.053 GEM shorts for one year of operation can be expected at 95% confidence level in one chamber.

Some GEM shorts can be removed by applying a high voltage of ≈500 V for a short time, so that a high current goes into the GEM, bypassing the current-limiting resistors. It was observed that two different types of GEM shorts exist. They can be distinguished by the resistivity of the short. "Low-resistivity" shorts have a typical resistance of ≈1MΩ while "high-resistivity" shorts have a resistance of more than 20MΩ. With the small statistics from the experience in 2000 it was seen that only low-resistivity shorts can sometimes be removed.

5.4 Cathode Shorts

Less severe than the GEM shorts are shorts between cathode and anode strips. Such a short affects 16 adjacent strips. These 16 strips cannot any longer be put to high voltage and therefore produce no signal. This means that one cathode short produces a dead area of about 2% in a chamber of 752 strips. The short circuit in these 16 strips does not directly affect the other strips because each group of 16 strips is protected by a 10MΩ high voltage resistor and an additional protection diode. The shorted group draws a current typically $> 45\,\mu$A higher than before the short. The upper limit of the HV box of $204\,\mu$A per chamber is reached when more than three groups in one chamber develop shorts.

In the design of the high voltage system the occurrence of cathode shorts was included and the limit of three shorted groups per chamber seemed sufficient for long term operation.

In the course of the 2000 operation another kind of problem developed in the high voltage protection diodes. In some chambers with a cathode short the current was larger than $200\,\mu$A, even if only one short was seen. The characteristic curve (as in Fig. 5.13) of the current was no longer linear. Fig. 5.14 shows the wiring diagram of the cathode fan-in with HV resistors and protection diodes. After a chamber with such a problem was examined the problem could be assigned to the break down of a diode. To avoid this problem, it was decided to remove the HV diodes in the upgrade of the inner tracker, after it was established that stable operation is possible without the diodes.

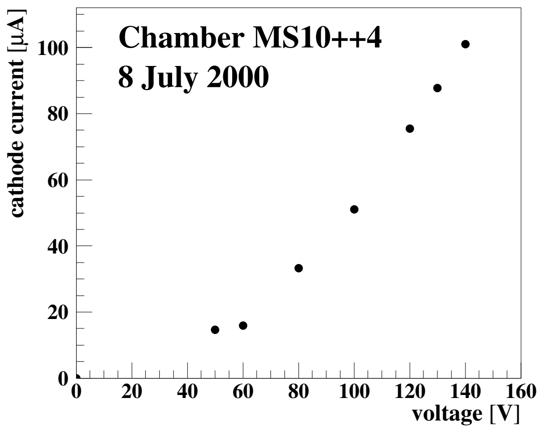

Figure 5.13: Characteristic curve for a chamber with a diode break-down.

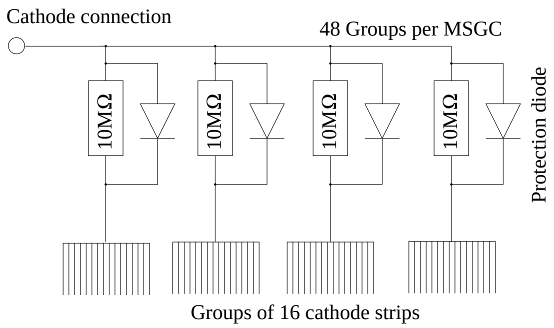

Figure 5.14: Schematic picture of the layout of the cathode fan-in. This circuit is realized on a Kapton carrier with copper structures.

The occurrence of cathode shorts could be studied with the slow control data of the 2000 operation. The appearance of cathode shorts can be seen in the cathode current immediately. In Fig. 5.15 the development of the cathode current in the course of operation is shown for chamber MS05--2. This chamber had one short in the beginning and developed two more anode-cathode shorts in succession, which is visible in the steps in the current. Despite the larger current needed for operation, this chamber was working to the end of the running without problems.

During the operation in 2000 the 150 inner tracker chambers developed 79 anode-cathode shorts. This is equivalent to a loss of 1.1% of the active strips. During the upgrade of the inner tracker for the year 2001 the lost cathode groups were recovered to a large extent (14-15 of the 16 lost strips of one cathode group). This recovery is done by cutting the anode wire with the short outside the chamber. A significant amount of the charge that would be collected in this wire is then seen by the neighboring strips so that a cut strip not necessarily means a loss in efficiency. The percentage of strips lost by cathode shorts is below 0.1% after the cutting.

Already during the production of the MSGC-wafers a significant (up to 2%) number of anode strips is faulty. These strips have an interruption of the gold layer at some place

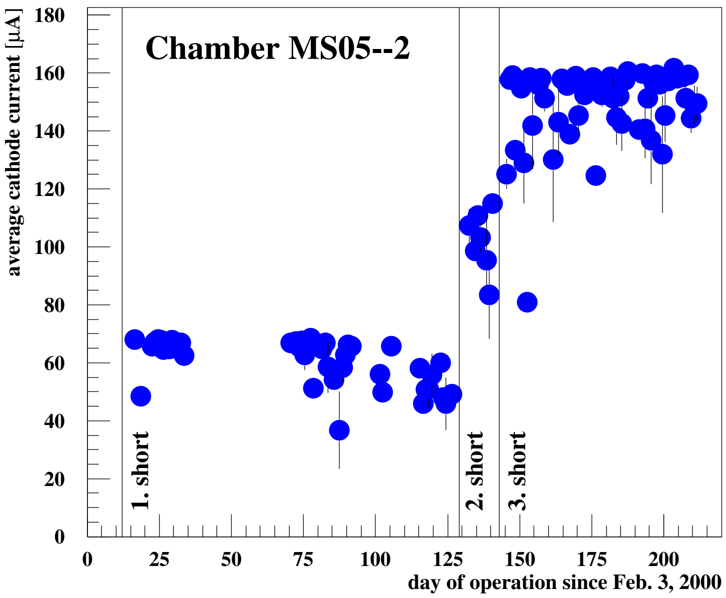

Figure 5.15: Development of the cathode current in chamber MS05--2. This chamber had one cathode group shorted in the beginning, around day 130 two more shorts appeared in succession.

on the strip. All wafers were tested in an automated procedure to identify these short strips. Details about the measurements of the wafers in Zürich can be found in [43].

During the repair and upgrade of the inner tracker in 2001 it was found that shorter strips have higher probability to develop a cathode short. Table 5.2 shows the numbers supporting this. Strips that have already been damaged during wafer production have a tenfold higher probability to develop an anode-cathode short during operation. These findings led to the decision to cut all anode strips which were interrupted during production, at the Kapton fan-in, based on the measurements done during production in Zürich. This will significantly reduce the probability to develop additional anode-cathode shorts in the future operation.

Table 5.2: Numbers on cathode short probabilities in shorter anode strips. Here not cathode shorts of groups are counted but individual strips with a short. A short in a group can have more than one shorted strip.

Number of chambers analyzed	61
Number of short strips identified during production	703
Number of cathode shorts in these chambers	106
Number of correlated shorts	17
Probability of cathode short in all strips	0.23%
Probability of cathode short in short strips	2.42%

Fig. 5.16 shows the occurrence of anode-cathode shorts as a function of the operation

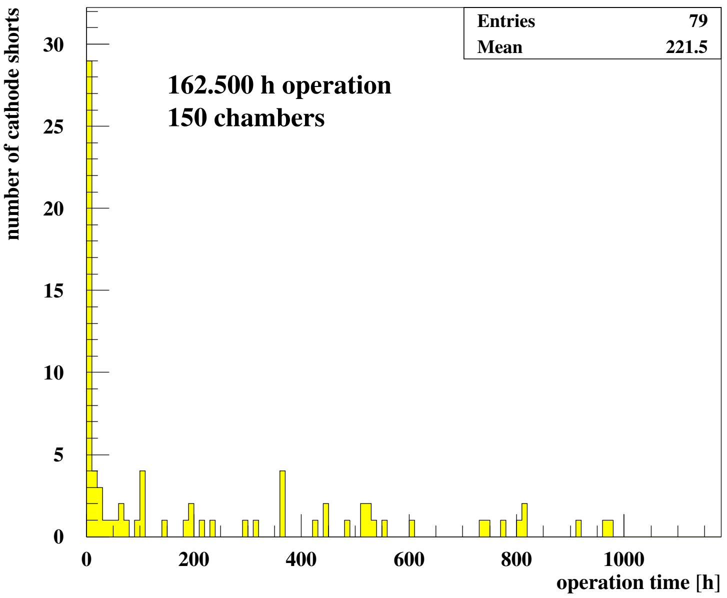

Figure 5.16: Operation times at which cathode shorts were seen in the inner tracker. During the operation in the year 2000 the operational conditions were changed several times. The chambers operated longest have accumulated 1180 operation hours.

time. A high number of shorts occurred during the initial switching-on or during the high voltage training. After an operation time of about 200h, the rate of new anode-cathode shorts seems to become stable. The rate of shorts after the end of the training amounts to 0.64 cathode shorts per chamber and operation year of 10^7s. That is equivalent to about two new cathode shorts per week in the full system if it is operated as intensively as in July and August 2000. This means it would take more than 4 years of operation at 5 MHz until 5% of the strips are lost because of cathode shorts.

This calculation may, however, be too pessimistic. A large fraction of the shorts that occurred late in Fig. 5.16 are correlated to increases in the high voltage of the chambers. Eight cathode shorts were observed in the days after June 16th, when the cathode voltage was raised to 510 V. Almost as many new shorts, seven, developed after July 31st, when the drift voltage was changed from 2.4 kV to 2.5 kV. If these 15 shorts that are correlated in time with changes in the high voltage settings are disregarded for the calculation of the rate of new cathode shorts during operation, the value is reduced to 0.31 cathode shorts per chamber and HERA-B year. This gives an estimate on the number of cathode shorts that have to expected in the future, assuming that the $\approx$1,000 h of operation in 2000 are representative.

This is the upper value which is expected after all "built in" weaknesses of the chambers have resulted in a short.

Table 5.3 summarizes the reasons for chamber losses in 2000. Most of the lost chambers, eleven, became unusable because of cathode related problems. The category of diode problems will be eliminated by the removal of the diodes for the 2002 running period.

The mechanical damage of one chamber was a singular incident caused by an accident during movement of the half-station.

Four chamber developed a GEM short during the running in the year 2000; two of these could be repaired.

Table 5.3: Reasons for chamber losses and number of affected chambers during the 2000 running.

Number of Lost Chamber	Reason for Chamber Losses
1	mechanical damage
2	GEM short
5	multiple anode-cathode shorts
6	(most likely) diode problems

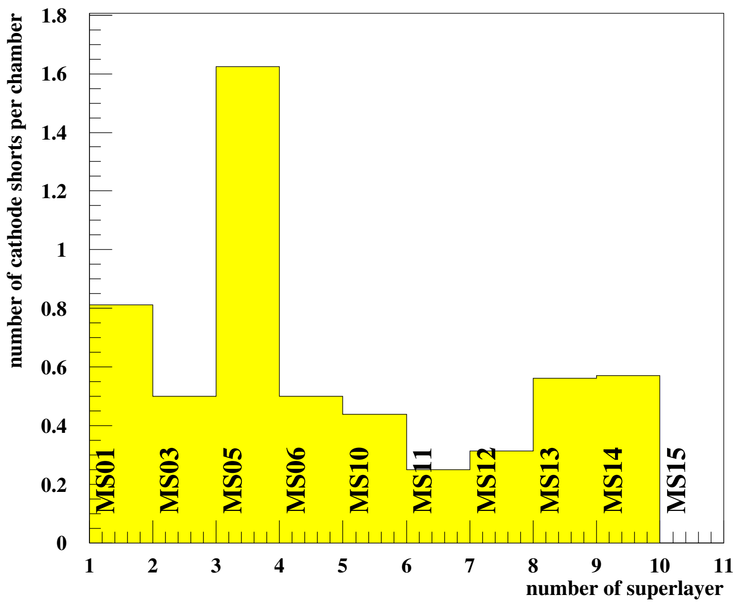

Figure 5.17: The number of anode-cathode shorts per chamber for all superlayers. The average number of anode-cathode shorts per chamber is 0.47.

The 79 anode-cathode shorts of the year 2000 are not evenly distributed among the stations, the distribution is shown in Fig. 5.17. The plot shows the average number of anode-cathode shorts in a superlayer. MS05 clearly takes the lead with more than 1.6 shorts per chamber. There seems to be a tendency that the superlayers MS11 and MS12, which were the last to be completed, also show a lower number of anode-cathode shorts per chamber. This can not only be explained by the shorter operation time of these stations as both superlayers were operated for roughly the same amount of time (see Fig. 4.11). A possible reason for this is that these stations were assembled and trained more carefully and with the experience of the previous stations. This is promising for the upgrade and restart of the inner tracker.

In the complete system 41% of the chambers developed at least one anode-cathode short. 14 chambers (of 61 with at least one short) showed more than one anode-cathode short.

Table 5.4: Probabilities for various kinds of cathode shorts in the chambers with high and low surface resistance.

	High resistance chambers in total 31 chambers		Low resistance chambers in total 114 chambers	
	Number	Fraction	Number	Fraction
anode-cathode short at first switching-on	2	6.5%	34	29.8%
anode-cathode short during operation	11	35.5%	32	28.1%
Sum	13	41.9%	66	57.9%

The inner tracker chambers are made with two different types of wafers with different surface resistivity, as reported in section 5.1. The difference in the treatment of the coating was introduced to improve the diamond aging behavior of the chambers [33]. Table 5.4 shows the number of cathode shorts and the probabilities of shorts in baked and untreated chambers. There is a significantly lower number of immediate shorts in chambers with high surface resistance. This can be explained by the fact that these chambers were installed later during the year 2000, when the training procedure was well established. However these chambers developed a significantly higher number of shorts during the operation. The sum of cathode shorts in these chambers is 12 in 28 chambers, and the overall probability of a cathode short in these chambers is 42%.

The chambers which were built early in the production phase all have wafers with low surface resistance. In these chambers the number of shorts is almost equally distributed to shorts appearing at the initial switching-on and shorts which were seen in the course of the operation. In 114 chambers a total of 66 shorts were recorded, giving a probability of 58% for a cathode short in these chambers.

The probability that a chamber develops a cathode short in the course of operation does not seem to be significantly affected by the surface resistivity. It rather seems that intrinsically existing weak points on the wafers develop into cathode shorts regardless of the surface treatment.

5.5 Readout Performance

The readout system of the inner tracker was commissioned in parallel with the high voltage operation of the inner tracker. The start of the commissioning was smooth because large parts were common to the VDS and ITR systems. However, some problems specific to the inner tracker readout were found and have been largely solved in the meantime.

A major part of problems seen in the data was related to the low voltage system. The power supplies were unreliable, which caused the front-end electronics to be switched off frequently, leading to large holes in the acceptance. Another problem arising in 2000 was a loss of synchronization for single stations. This was caused by the digital interfaces (IF6, see Fig. 4.15). Some analog thresholds on the IF6 were drifting with time. Changes in the design of the interfaces solved this problem.

It was also found that the parallel use of different HELIX versions caused some instabilities. These instabilities resulted in erratic end of data transmission in some chambers or even stations. This problem will be cured in the 2002 setup by feeding the two different HELIX versions individually adjusted control signals. Details about the inner tracker readout system and its performance are presented in [31].

5.6 Chamber Efficiency

The final goal to assess the chamber performance is the determination of the chamber efficiency. To do that not only the initial problems in the hardware had to be solved but the tracking software had to be understood in parallel. The fundamental problem in the assessment of the chamber performance of the inner tracker chambers is, that the gas gain can not be determined from the pulse height spectrum. The HERA-B tracking system is dominated by hits that are not coming from primary tracks but that originate from "soft" particles. The pulse height spectrum therefore does not show a separation of signal and noise necessary for the determination of the gas gain. The only way to determine a meaningful pulse height spectrum is therefore to look at hits on a reconstructed track.

It took a while to adjust the tracking software to the needs of a not yet understood tracking system. In 2000 it was only possible for the inner tracker to use the tracks in the first station MS01 during the running period by using the well defined tracks of the vertex detector as reference.

The gas amplification in the inner tracker chambers varies for identical high voltage settings, caused by the GEM geometry variations. To compensate for this, the high voltage at the GEM has to be individually adjusted on the basis of the measured pulse height spectrum for hits on tracks – or even better the hit efficiency of a chamber. The pulse height on tracks or the efficiency values were not available for all chambers during the 2000 running period. The adjustment of GEM settings was therefore done on the basis of the drift current alone.

The analysis of the data at a later stage showed that this was not sufficient to reach an efficiency above 95% in all chambers. The chambers in station MS01, for which the efficiency was determined during the running, reached an efficiency of $> 90\%$. In Fig. 5.18 the chamber efficiency as a function of the GEM voltage is shown for MS01. In 2002 the final operation point has to be determined again based on the efficiency measurement. The understanding of the tracking software is now much better, so that the working points can be fixed much faster.

The aim is to reach an efficiency of $> 90\%$ for all chambers in the 2002 running period.

5.7 Summary

The inner tracking system of HERA-B is a high resolution detector covering an active area of $17\,\mathrm{m}^2$ which was developed for an environment of high hadronic particle density.

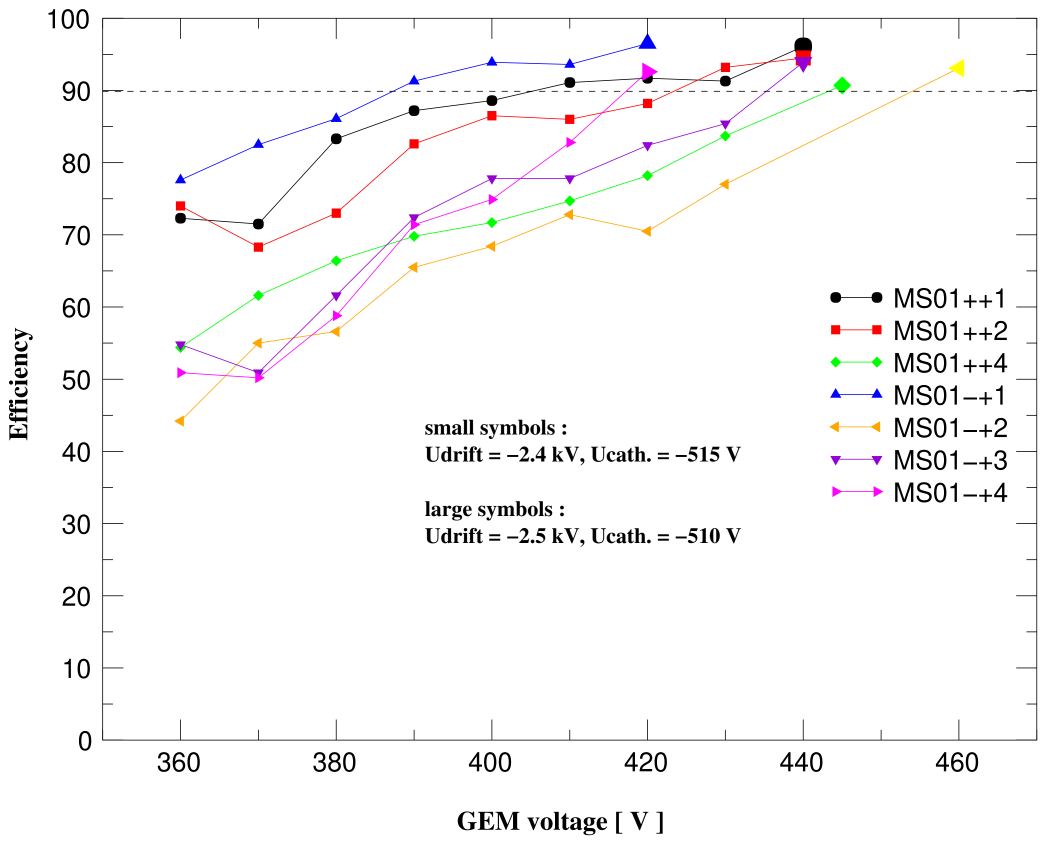

Figure 5.18: Chamber efficiency for the chambers of MS01 depending on the applied GEM voltage [35].

It was successfully commissioned and operated for $\approx 1,000$ hours of luminosity running in 2000.

During the running, several operational problems were seen: sparks in the GEM, shorts between neighboring anode and cathode strips – sometimes caused by multiple electrode sparks, and shorts within the GEM. Each of these problems is inherent to the operation of GEM MSGCs in an environment with heavily ionizing particles, and each of these operational problems can cause irreversible damage to the detector.

The operation of GEM MSGCs at HERA-B is therefore a critical task. It was, however, established that the inner tracker chambers can be operated under continuous monitoring and with special safety devices, as shown in this chapter. New GEM MSGCs have to be carefully trained to reach stable operation conditions. In addition the chambers have to be switched on in a well defined and careful way, to allow the chamber to slowly adjust to the operational conditions.

After the running period in 2000 the inner tracker system was completely reassembled to improve it and repair the faults that have developed during the running. The high probability of cathode shorts in faulty strips led to the decision to cut all strips, which could be identified as problematic. This will significantly lower the risk of new shorts and dead regions developing in the system during the 2002 running.

We have gained confidence that albeit all the observed problems the inner tracker will be able to contribute to the 2002 physics program as planned.

Chapter 6

A Study to Reconstruct χ_c Decays

This chapter presents results on an analysis of χ_c production, based on Monte Carlo studies and a set of data acquired in June and August 2000. The main emphasis of this analysis is to prepare for the coming run period of the years 2002 and 2003. Alternative studies have been performed earlier which led to a first publication of the rate of χ_c production to J/ψ production based on the complete data set of 2000 [20].

The intention of the search for χ_c states is to better understand the production and hadronization of $c\bar{c}$ states in nuclear matter. In the search for quark-gluon plasma the suppression of J/ψs is the most important indicator for the phase transition to the quark-gluon plasma phase. To trace the origin of J/ψs observed in heavy ion collisions, it is very important to know the fraction of $c\bar{c}$ pairs that form charmonium states and what fractions of J/ψ, ψ', and χ_c are produced in proton interactions with nuclear matter.

HERA-B can measure the ratio of χ_c to J/ψ production in different nuclear materials and in a so far unexplored range of phase space.

The principal aim of this study is to understand and optimize the signal and its significance so that a good and fast start of the analysis can be assured for the 2002 data. No complete systematic study was performed, which is due to lack of time.

6.1 Introduction

Table 6.1: Properties of the χ_c charmonium states [56].

	χ_{c0}	χ_{c1}	χ_{c2}
J^{PC}	0^{++}	1^{++}	2^{++}
Mass	3415.0±0.8 MeV	3510.5±0.12 MeV	3556.2±0.13 MeV
Mass difference to J/ψ	319.0±0.8 MeV	413.6±0.21 MeV	459.3±0.14 MeV
Width	$14.9^{+2.6}_{-2.3}$ MeV	0.88±0.14 MeV	2.00±0.18 MeV
BR ($\chi_{cx} \rightarrow J/\psi\gamma$)	$6.6\pm1.8\times10^{-3}$	27.3 ±1.6%	13.5 ±1.1 %

The decay channel which can be used to reconstruct χ_cs at HERA-B is the decay $\chi_{c1/2} \rightarrow J/\psi\ \gamma$.

The χ_{c0} has a branching ratio to this state that is too small to be observed at HERA-B. Therefore the χ_{c0} will not be further discussed here, and the symbol χ_c is used in the following chapters to denote both the χ_{c1} and the χ_{c2}. The branching ratios of these two χ_cs are large enough, so that reconstruction is possible.

6.1.1 Determination of R_{χ_c}

In order to determine the Ratio R_{χ_c}, the numbers of J/ψ and χ_c in a given sample have to be known and the efficiency of the photon reconstruction ϵ_γ has to be measured.

$$R_{\chi_c} = \frac{N_{\chi_c}}{N_{J/\psi}\epsilon_\gamma}$$

In this study the efficiency ϵ_γ is not determined and no value for R_{χ_c} stated.

6.2 The Samples

For the purposes of this study two Monte Carlo samples and a sub-set of the 2000 data were used. The data sample is a set of 33524 "slicer"-triggered events classified as $\mu\mu$ events in the most recent re-processing. To compare the data taken in 2000 with Monte Carlo a sample reconstructed with the detector geometry of 2000 without contribution of the inner tracker was used. The expectations for 2002 were studied with a Monte Carlo sample based on the complete HERA-B detector. Both Monte Carlo samples contain only charmonium decays into the $\mu^+\mu^-$ channel.

The HERA-B Monte Carlo generator uses the generators PYTHIA and FRITIOF to generate proton nucleon interactions [57]. PYTHIA is used to generate $c\bar{c}$ pairs in the proton nucleus interaction. Not all available energy is used in the hard interaction so the remaining energy is passed on to FRITIOF to generate additional "soft"particles. The output of this combination of event generators does not describe the data in some properties, such as the track multiplicity of the event. These have to be adjusted to data.

The charmonium fractions in the used Monte Carlo samples are not based on a solid production model, such as the ones discussed in Chapter 2. The charmonium fractions and properties of the produced particles may therefore differ from those found in data.

The effects of nuclear suppression can therefore not directly be studied with the standard HERA-B Monte Carlo.

6.2.1 Monte Carlo Sample 2000

The used sample of 10.000 events contains charmonium events with a fraction of prompt J/ψ (6119 events), χ_{c1} (1069), and χ_{c2}(2812). The sample was produced with the 2000 detector geometry (version 99.1015), and the generated events are re-weighted to adjust the particle multiplicity of the Monte Carlo to that of data [58].

The inner tracker did not significantly contribute to the 2000 data, therefore the ITR digitization was switched off for the Monte Carlo sample of 2000.

6.2.2 Monte Carlo Sample 2002

For the 2002 data taking period the geometry of the detector was changed in several ways: the magnet chambers of the trackers were removed and the nominal positions of the VDS were changed. In addition the target positions and materials were changed. The geometry file used has the index 01.1116.

The sample of 10.000 charmonium events uses the same multiplicity re-weighting as the 2000 sample. Of the 10.000 events 6201 are prompt J/ψ events, 1001 contain a χ_{c1} and 2798 a χ_{c2}. For the analysis ARTE-03-09-R7 and BEE-1-1 were used.

6.2.3 2000 Data Sample

The data sample used was reprocessed with the latest set of calibration and alignment constants (Repro 3). This sample contains events from runs with the SLT-based 'slicer' trigger taken between June and August 2000. Only events classified 'JPSIMM' by the event classification were included in the analysis. These event classes contain events with at least two muon tracks. The sample contains 33,524 events taken in runs 16000 to 17000.

Of the events only the *MINI-DST* files are used, which contain only reconstructed tracks and clusters. During the data taking for these samples the inner II carbon wire and the below I titanium wire were used.

The sample is divided into two subsets: one with interactions at the carbon wire, the other with interactions at the titanium wire. The sample with proton-carbon interactions contains 997 J/ψ events in single wire running and 507 events in runs taken together with the titanium wire. The titanium wire was not used in single wire running, but the multi-wire sample contains 663 events with a selected J/ψ.

6.3 Reconstruction of χ_c Events

The χ_c states are reconstructed in the channel $\chi_c \rightarrow J/\psi\ \gamma$. This is done in two steps: first finding a J/ψ, secondly finding and matching a photon to it.

The J/ψ decays into a pair of electrons of muons with a branching ratio of 6% each. In this analysis only the channel $J/\psi \rightarrow \mu^+\mu^-$ is studied. A lepton pair with a high invariant mass has a clean experimental signature in a hadronic environment.

When a J/ψ has been reconstructed, photons are reconstructed in the event and matched to it. The invariant mass spectrum of the three particle final state is then plotted, and the χ_c should become visible as a peak in the spectrum.

6.3.1 Reconstruction of the J/ψ

In the $J/\psi \rightarrow \mu^+\mu^-$ channel the main source of background are muons from hadron decays in flight. $K^\pm$ and $\pi^\pm$, which are produced in large numbers in HERA-B (the cross section is 5 orders of magnitude higher than the J/ψ cross section), can decay into muons in the detector. These muons are reconstructed in the muon system, adding muons to the sample which are not decay products of the charmonium state.

Another source of background is the production of Drell-Yan $\mu^+\mu^-$ pairs. However the cross section for Drell-Yan production is only 1.5% that of the J/ψ production and therefore negligible in the mass range of the J/ψ resonance.

The muons in the used data sample are identified already at the trigger level. The identification of a track as muon track is based on a likelihood calculated from the number

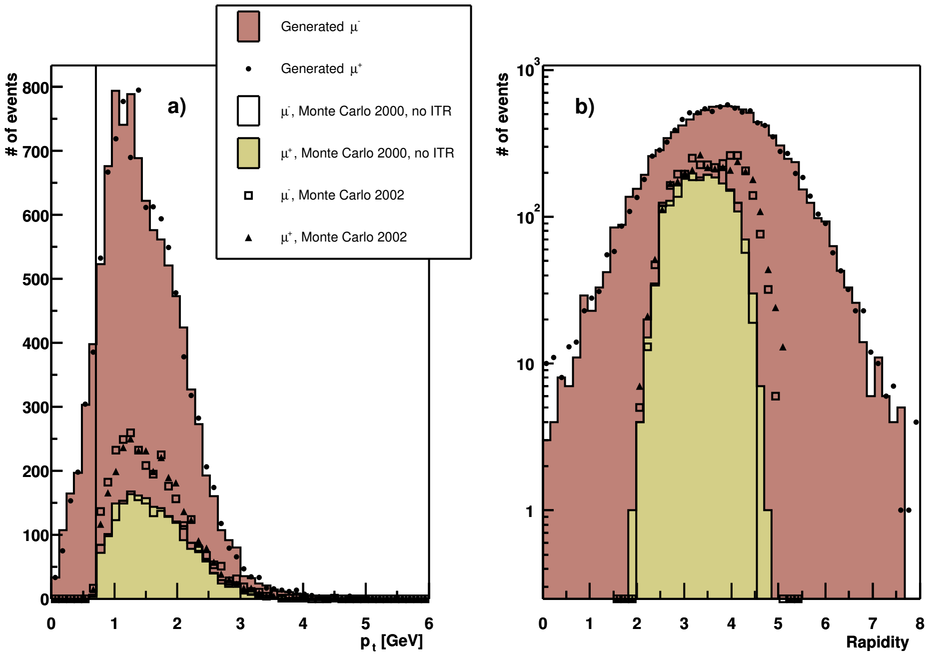

Figure 6.1: Kinematic properties of generated and reconstructed muons from the 2000 and 2002 Monte Carlo sample. a) Transverse momentum. The line shows the p_t cut used in the J/ψ reconstruction. b) Rapidity.

of hits associated to the track in the muon system. For this analysis a likelihood L_μ larger than 0.005 was required.

To reconstruct the J/ψ, two muon tracks with opposite charge are required. The tracks are selected by requiring a p_t larger than 0.7 GeV. To select events with a clean signature only events with exactly two muon tracks are accepted. The muon selection cuts are summarized in Tab. 6.2.

Table 6.2: Muon Cuts for the J/ψ reconstruction.

Cut Parameter	Value
Muon likelihood L_μ	> 0.005
Transverse momentum p_t	>0.7 GeV
Opposite charge $q_{\mu_1} \cdot q_{\mu_2}$	< 0
Number of muons in event $\#\mu$	$= 2$

The p_t spectrum of muons from J/ψ decays generated in the 2000 Monte Carlo sample is shown in Fig. 6.1 a). Muons are generated in the full rapidity range between 0 and 8, Fig. 6.1 b) shows this. In the reconstructed muons in Fig. 6.1 b) a rapidity cut can be seen which is introduced by the acceptance of the spectrometer. Without the inner tracker HERA-B covers only the rapidity interval $2.1 < \eta < 4.5$, with the inner tracker the range is extended up to a rapidity of 5. The reconstructed muons in Figure 6.1 were identified as muons by the muon likelihood cut and have a p_t >0.7 GeV.

The average generated momentum of muon tracks coming from a J/ψ is 42 GeV. The tracks selected with the described cuts have an average momentum of 28 GeV in reconstructed Monte Carlo events. The average transverse momentum of generated muons is 1.46 GeV while the reconstructed muons have a higher average p_t of 1.66 GeV, because of the cut p_t >0.7 GeV. The transverse momentum spectra of reconstructed muons in the 2000 and 2002 Monte Carlo samples are also shown in in Fig. 6.1.

The invariant mass of pairs of selected muon tracks from the Monte Carlo sample without contribution of the inner tracker is shown in Fig. 6.2.

For the J/ψ reconstruction two more cuts are applied. The vertex fit probability has to be larger than 0.5%, to increase the quality of the J/ψs in the sample. The distance in z of the target wire and the reconstructed vertex must be smaller than 1 cm for the event to be accepted. This cut is done to assign the J/ψ to one wire in multi-wire runs. The filled histogram in Figure 6.2 shows the J/ψs passing these cuts for the reconstruction of χ_cs. The J/ψs selected for the reconstruction of the χ_c are shown in the filled histogram of Fig. 6.2. The mass limits for the selection are set to 3.1 ± 0.1 GeV.

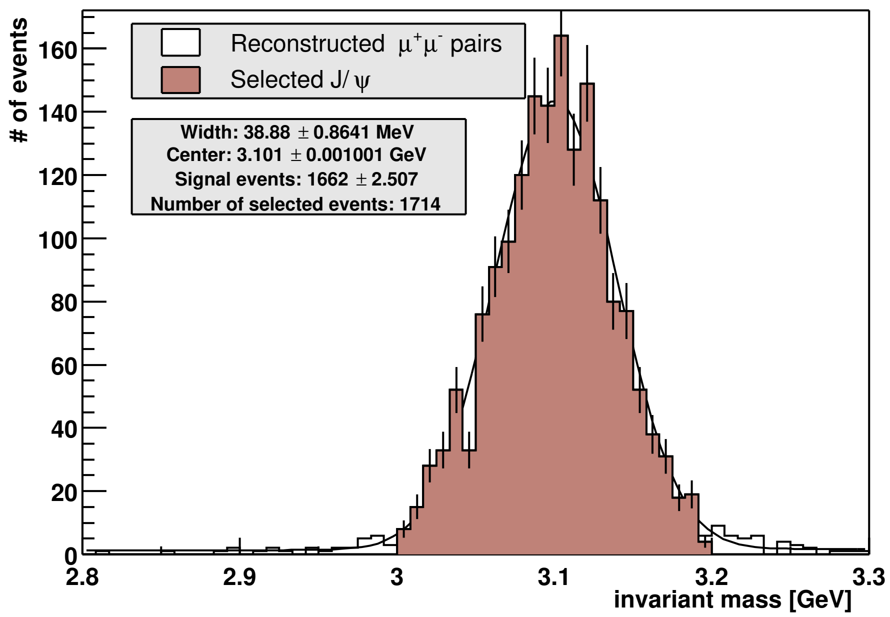

Figure 6.2: J/ψ reconstructed invariant mass in 2000 Monte Carlo. The filled Histogram shows the events within the mass range of 3.1 ± 0.1 GeV.

6.3.2 Selection of Photons

Photon finding starts with a reconstructed cluster in the ECAL. Every reconstructed cluster is a photon candidate. A cluster in the electromagnetic calorimeter is the sum of neighboring calorimeter cells. A center of gravity method is used to calculate the impact position of the particle which deposited the energy. At HERA-B clusters are reconstructed at energies starting at about 200 MeV. For the reconstruction in the data taken in 2000 only high energetic clusters are of interest, many of the others were caused by electronic noise in the system. For this study photons are selected with a hard energy cut requiring an energy deposition greater than 4 GeV and a soft cut of 0.05 GeV on the transverse energy of the cluster. In addition there is an isolation cut for ECAL clusters setting the minimal allowed distance to the closest reconstructed cluster in the calorimeter to 2 cm. For this isolation cut all clusters are taken into account, even if they have a low energy of 200 MeV.

In the HERA-B experiment many photons are detected in every event. The photon coming from the χ_c decay has to be selected and reconstructed with a high efficiency. In Fig. 6.3 the energy and transverse energy spectra of the photons from the χ_c are shown. Only a tiny fraction of 6.7% of the originally generated photons can be reconstructed correctly.

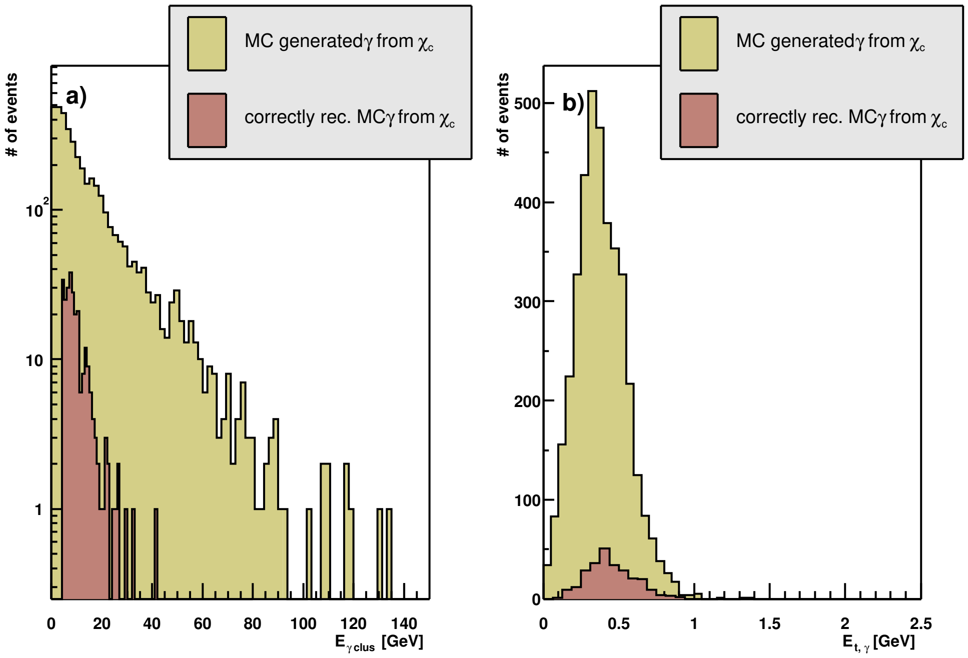

Figure 6.3: Monte Carlo generated photon spectrum coming from χ_c decays. a) Energy spectrum. b) Transverse Energy Spectrum. (2000 Monte Carlo sample)

A typical Monte Carlo charmonium event contains on average 6.5 neutral pions with more than 1.5 GeV energy which are produced in the vicinity of the primary vertex. These π^0s decay into two photons. The electromagnetic clusters produced in the calorimeter by these photons can not be distinguished from those of photons coming from a χ_c. The high number of candidates make it difficult to find the correct photon for the χ_c. Another source of background are calorimeter clusters which are produced by electrons and charged pions.

The photons from χ_{c1} and χ_{c2} events are most likely to hit the central region of the ECAL. Fig. 6.4 shows the impact positions in the ECAL for photons coming from χ_cs.

However, the inner part of the calorimeter is problematic, because the occupancy is very high. In a region with a too high occupancy, clusters can not be reliably separated,

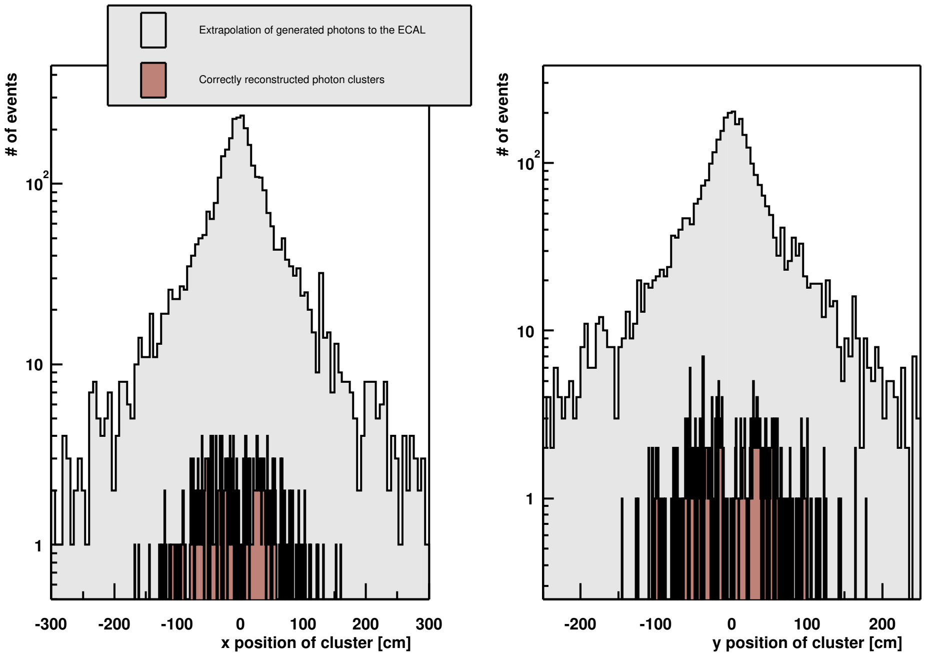

Figure 6.4: Impact points of generated Monte Carlo photons originating from χ_cs in the electromagnetic calorimeter (2000 Monte Carlo sample). In the dark histogram selected clusters that could be associated to a photon from a χ_c decay are shown.

causing the energy to be incorrectly measured. The inner part was therefore excluded by requiring $x^2/4 + y^2 > 150\,\mathrm{cm}^2$ for the x and y positions of the photon candidate. The reason for the elliptic shape of the cut is the dipole field of the HERA-B magnet. In this field the shape of the region with the largest particle density is shaped almost elliptical.

Table 6.3: Selection criteria for photon candidates.

Cluster Cuts	Value
Exclude inner region $(x^2/4 + y^2)$	$< 150\,\mathrm{cm}^2$
Transverse energy of cluster$E_{t,\gamma}$	$> 0.05\,\mathrm{GeV}$
Cluster energy E_γ	$> 4\,\mathrm{GeV}$
Isolation cut $d_{\mathrm{nearest}\gamma}$	$> 2\,\mathrm{cm}$

A "selected cluster" now means a cluster fulfilling the four cluster cuts given in Table 6.3.

Fig. 6.5 shows the distribution of all accepted clusters in the reconstructed Monte Carlo (2000 geometry) data. The region at x=0 cm and y=0 cm is affected by the acceptance hole in the detector, needed for the beam-pipe. In Fig. 6.6 the cluster positions of the same clusters can be seen in two dimensions.

An interesting feature of the kinematics of the $\chi_c \to J/\psi\gamma$ decay is the dependence of the ECAL cluster energy on the angle between the J/ψ and the γ. The anti-correlation

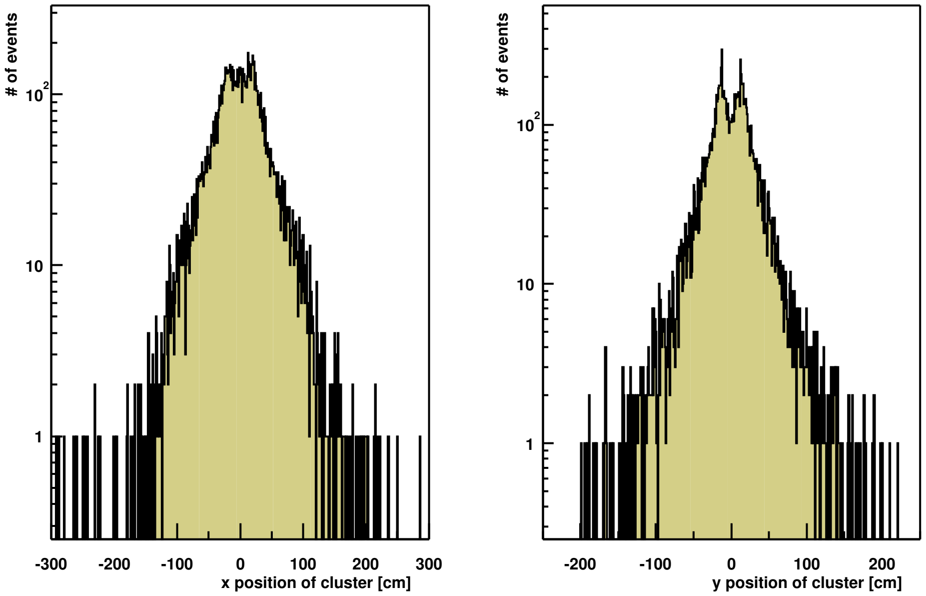

Figure 6.5: Distribution of selected clusters in x and y. All cluster cuts are applied (2000 Monte Carlo Sample).

between these two values is shown in Fig. 6.7a) for photons coming from a χ_c decay. The characteristic dependence seen in this figure is produced by the decay kinematics of the events. So there is unfortunately no way to use this for an enrichment of signal photons in the sample. This can be seen in Fig. 6.7b). In Figure b) only photon candidates are included which result in an invariant mass in the region of the χ_c when combined with the J/ψ.

In Fig. 6.8 the number of photon candidates in each event is shown. On average 7.5 photon candidates pass the cluster cuts given in Tab. 6.3.

With the high average number of 7.5 selected photons in each Monte Carlo event it is of course interesting to find out where these photons come from. In the Monte Carlo file it is known which particle produced a cluster in the ECAL. In the 2000 Monte Carlo sample these are mainly photons from π^0 decays. Fig. 6.9 shows the identity of particles causing electromagnetic clusters in the calorimeter.

The two photons from the decay of a π^0 are in 30% of all cases reconstructed as only one cluster in the electromagnetic calorimeter. These π^0 can not be reconstructed.

The surroundings of an ECAL cluster can influence the energy reconstruction of a cluster by a leakage of energy from one into the next cluster. To study if an influence of the next cluster can be seen, the distance to the next cluster was calculated for each selected photon candidate. Fig. 6.10 shows the distance between the selected clusters and their next neighbors.

A small increase in the significance of the χ_c signal was seen when a cut of $d_{cl} > 2\,\mathrm{cm}$ on the distance to the next cluster was introduced.

The energy and transverse energy of the selected cluster candidates after all selection

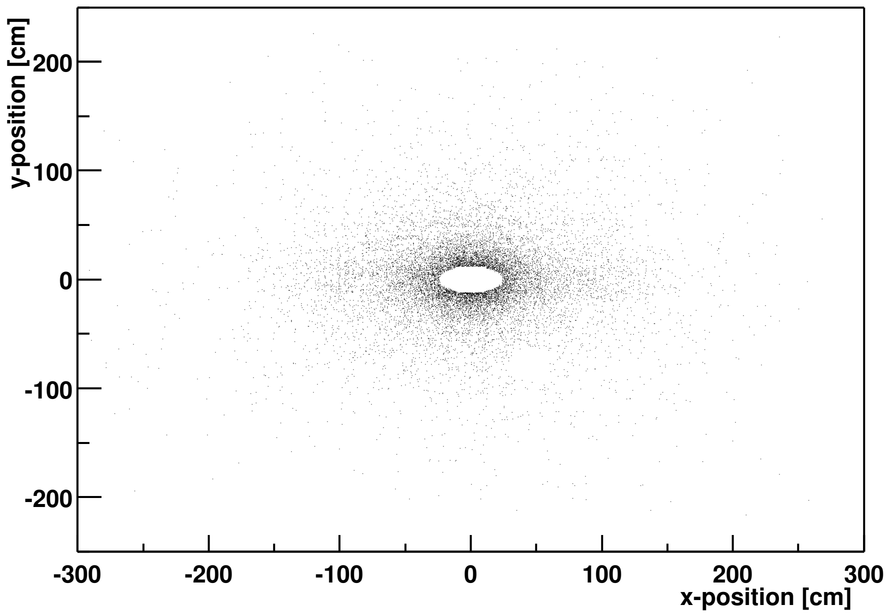

Figure 6.6: Two-dimensional plot of the selected photon candidates in Fig. 6.5. The recesses for the electron beam-pipe (at x=45 cm and y= -60 cm) and the elliptical cut on the inner region around the proton beam-pipes can be seen as holes (2000 Monte Carlo sample).

cuts are shown in Figure 6.11. In the left figure the energy of the selected clusters is shown together will all clusters with an energy above 1 GeV. Fig. 6.11b) shows the transverse energy spectra of the selected clusters and of all clusters (E>1 GeV).

6.3.3 Reconstruction of the χ_c

With the reconstructed J/ψ and the selected photon candidates χ_cs can be reconstructed. The invariant mass spectrum of the combined χ_c for the 2000 Monte Carlo sample are shown in Fig. 6.12. This spectrum shows very well the combinatoric background produced by the high number of photon candidates in the sample. With 1714 J/ψ events selected, 12,670 combinations are generated. Also drawn is the invariant mass of χ_{c1} and χ_{c2} events, which were correctly reconstructed. For a precise measurement of the χ_c properties the invariant mass spectrum is not a good choice, because the width of the J/ψ is intrinsically included in this picture. The mass difference $M_{\chi_c} - M_{J/\psi}$ provides a resolution which is better by a factor of 7. The mass difference plot is the best way to see the χ_c signal. In this plot the table value of the J/ψ mass is subtracted from the mass of the reconstructed χ_c. Figure 6.13 shows the mass difference plot for the 2000 Monte Carlo sample. This plot again shows the mass difference of the correctly reconstructed χ_cs in two histograms at the bottom at a mass difference of 414 MeV for the χ_{c1} and 449 MeV for the χ_{c2}.

The background below the χ_c peak is described by mixing reconstructed J/ψs with photon candidates from different events. The J/ψ is also mixed with clusters from events in which no charmonium was reconstructed. This is a valid approach since the numbers of

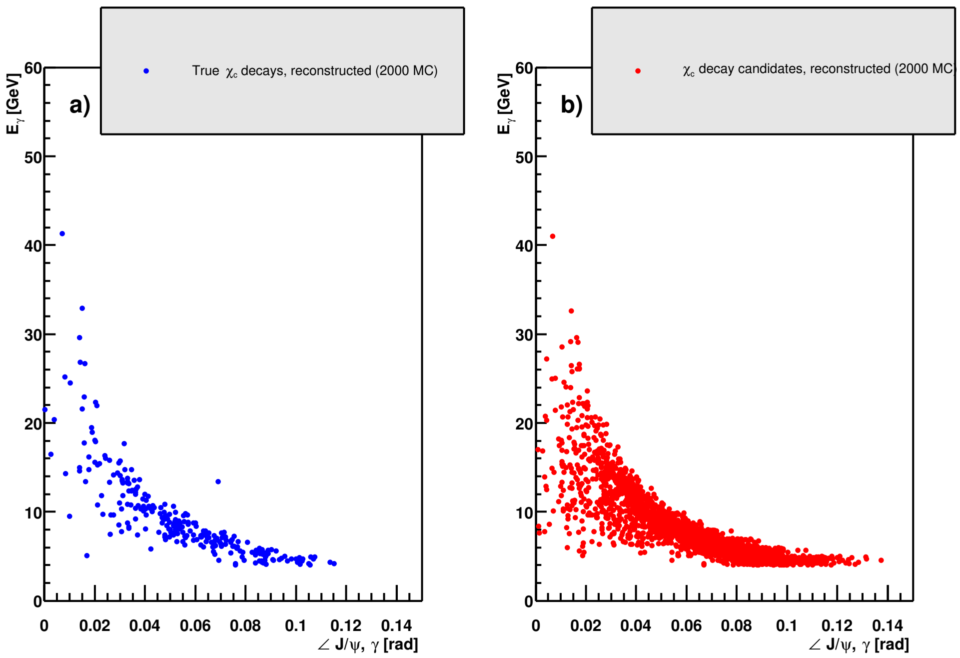

Figure 6.7: Correlation between ECAL cluster energy and angle between the cluster and the reconstructed J/ψ. a) Reconstructed Monte Carlo events from χ_c decays (2000 geometry). b) Reconstructed events from the same sample with 0.41 GeV$< |m_{\gamma,J/\psi} - m_{J/\psi}| <$ 0.51 GeV.

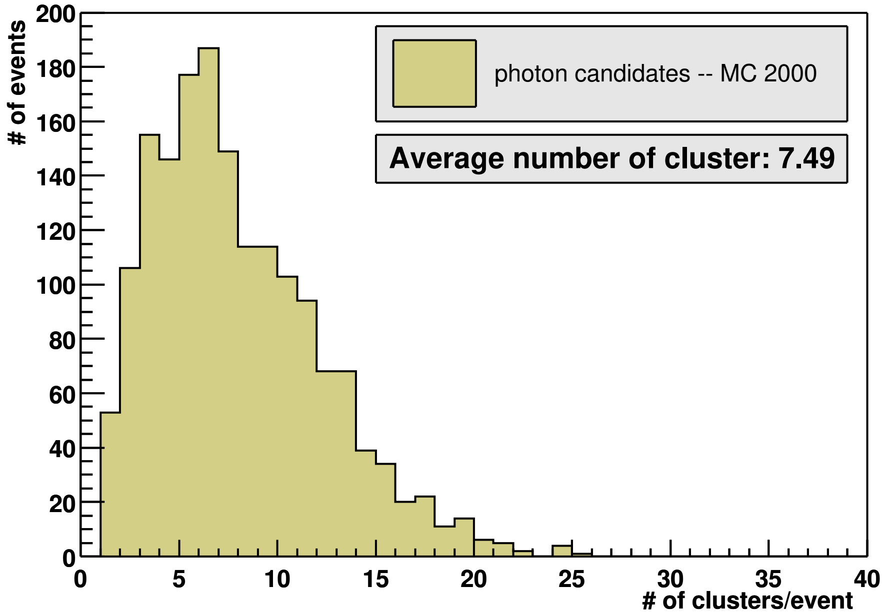

Figure 6.8: Number of clusters that pass the photon selection in a Monte Carlo Event.

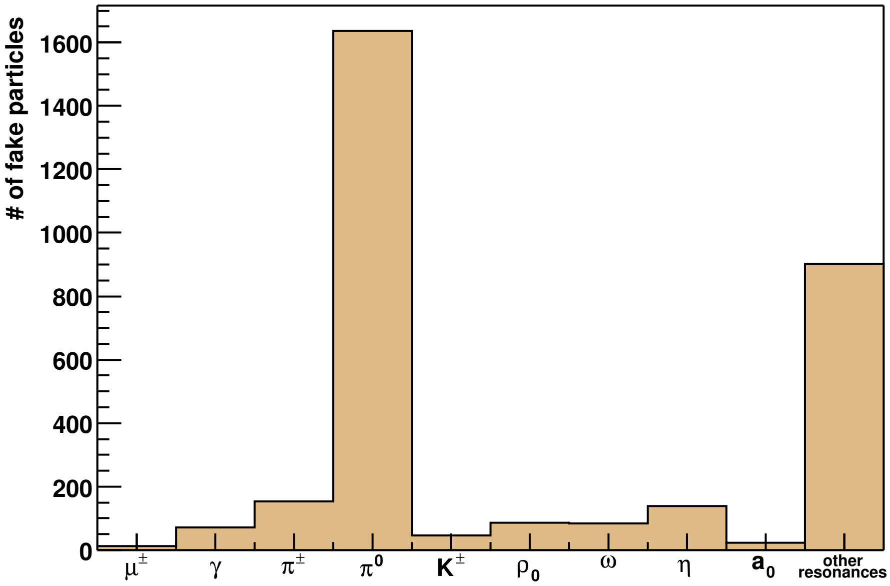

Figure 6.9: The clusters observed in the ECAL originate from these particles, which were produced close to the interaction point (2000 Monte Carlo sample).

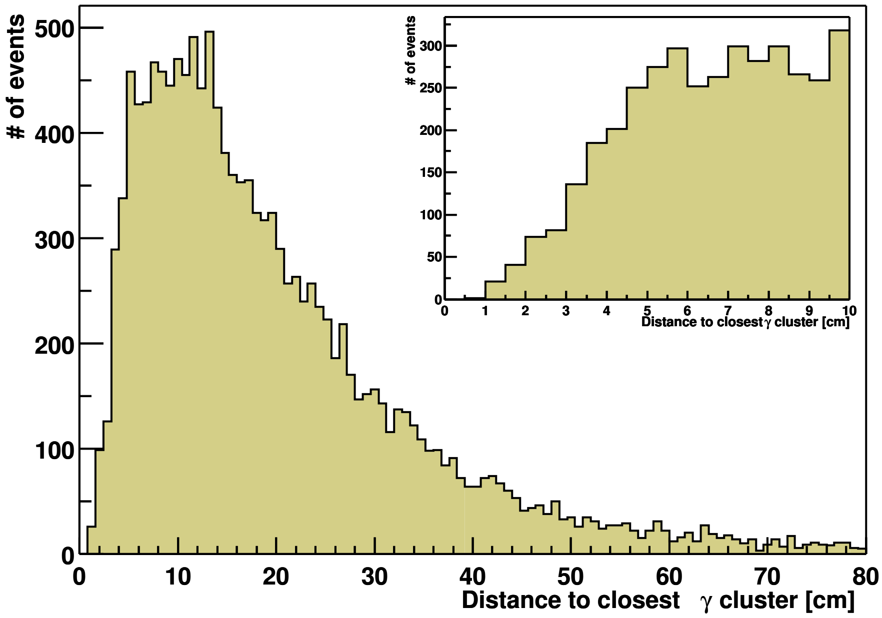

Figure 6.10: Distance between the selected clusters and closest neighboring cluster. The range between 0 and 10 cm is enlarged in the inset. (2000 Monte Carlo).

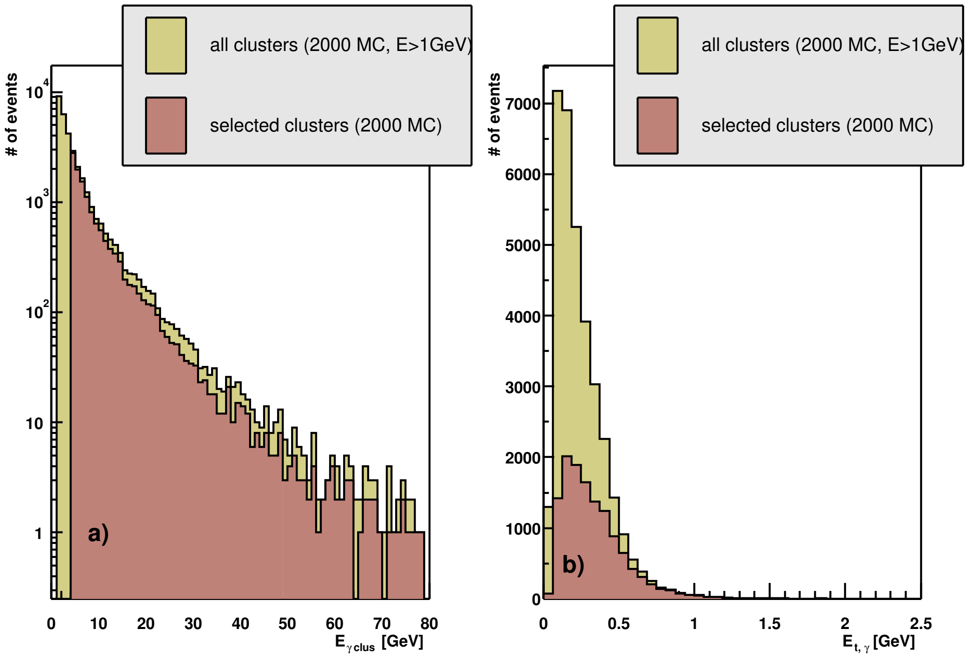

Figure 6.11: a) Energy of clusters with E>1 GeV and selected clusters. b) Transverse energy of clusters with E>1 GeV and selected clusters. Both in 2000 Monte Carlo.

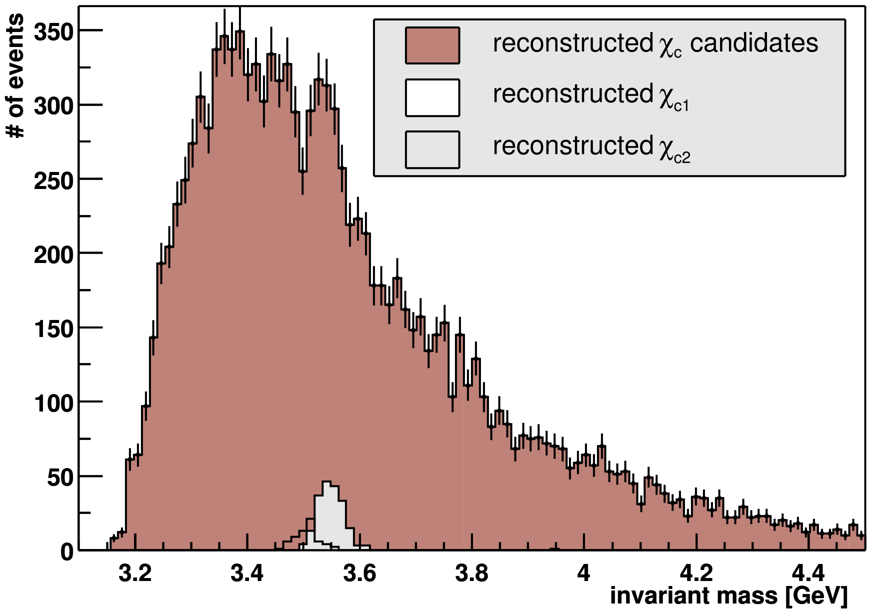

Figure 6.12: Reconstructed mass of all combinations of the photon cluster pairs from the sample of selected photons for the χ_c (Monte Carlo 2000). The correctly reconstructed χ_c events are superimposed.

ECAL clusters in these event is only slightly higher than in the events with a reconstructed J/ψ.

In Figure 6.13 both the χ_c sample and a sample of mixed events describing the background are shown.

Also in the mass difference plot the resolution is not sufficient to separate the χ_{c1} from the χ_{c2}. The precision needed to disentangle the two states is beyond the spectrometer in its present shape, because the photon can lose a lot of energy before reaching the calorimeter, reducing the precision of the energy measurement in the ECAL. The energy and momentum resolution for the reconstruction of converted photons should be much better, because additional momentum information for the electron and positron are added. Roughly 10% of the photons from a χ_c convert within the vertex detector vessel. This should be a high enough number to try this approach with the 2002 data.

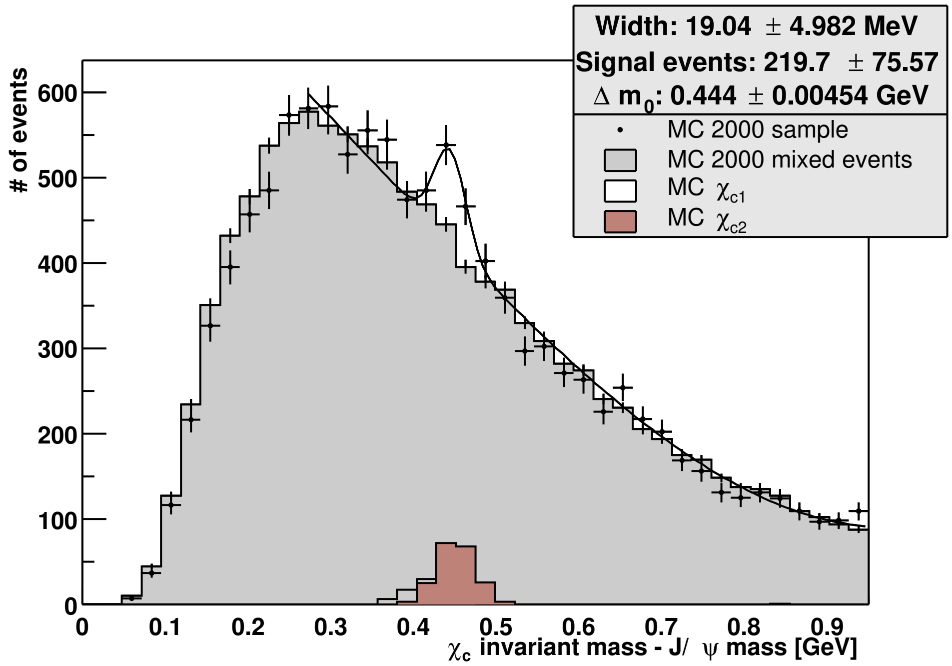

Figure 6.13: Mass difference of reconstructed χ_c and the J/ψ mass in 2000 Monte Carlo events. Superimposed are the generated χ_cs, that pass the reconstruction cuts.

The function fitted to the points in Figure 6.13 is the sum of a polynomial function which fits the background spectrum and a Gaussian. The three parameters of the Gaussian are free in the fit, the polynomial is fixed to the values obtained with the mixed events. The width of the peak is 19.0±5.0 MeV with 219±76 signal events. The center of the Gaussian is at 444±5 MeV, which fits well with the expected value 446 MeV for the weighted average of the mass difference in χ_{c1} and χ_{c2} events.

When the inner tracker is included in the reconstruction of the same data sample, the number of events increases to 389±90 with a width of 29.2±4.8 MeV.

With the Monte Carlo sample reconstructed for 2002, the significance is also higher than without ITR, the number of events found in the peak is 363±85 with a width of 27.2±4.6 MeV.

When the inner tracker resolution in the 2002 Monte Carlo is reduced to 200 μm the width of the peak increases to 29.2$\pm$5.3 MeV.

Chapter 7

Reconstruction of the χ_c in Data

The data taking period in 2000 was mainly devoted to detector commissioning. The data sample is therefore rather small and difficult to analyze, because many parameters were constantly changing during the data taking period. This study is therefore limited to a sample of "slicer" triggered events, which were taken with relatively stable running conditions. These events were taken in July and August of 2000. This "slicer" trigger simulates the functionality of the FLT two muon trigger in the second level trigger nodes. In addition, tracks are reconstructed at the SLT level, using wire information. In total 33524 events containing two reconstructed muons were taken with the slicer trigger.

7.1 Observed J/Ψ Signal

For the reconstruction of J/ψ events, two muon tracks with opposite charge are required. In this analysis only events which were identified as "JPSIMM" events during the reprocessing are used. Therefore no specific study on the selection and optimization of the reconstruction of J/ψs was done in this analysis, and a selection based on well tried selection cuts was used. They require a muon transverse momentum p_t larger 0.7 GeV and a muon identification likelihood $L_\mu > 0.005$.

The acceptance for muon tracks in 2000 was limited since the inner tracker was not regularly available. Nevertheless already in the data taken in 2000 a fraction of 60% of the muon tracks in the carbon sample had at least one hit in the inner tracker. In the sample taken with the titanium wire, the inner tracker even contributed hits to 65% of the tracks.

The 2000 data was reprocessed several times to include the improved calibration and alignment of the detector into the sample. The data of the third re-processing is used for this analysis. In this re-processing the best available alignment and calibration constants for all sub-detectors were used and the common mode noise in the ECAL was subtracted.

For the reconstruction of χ_c events the suppression of events with a very high number of hits is very important. If the few events with a very high number of hits in the detector are included in the analysis, the signal becomes much less significant because of the high combinatorial background in the χ_c reconstruction. As the multiplicity is not too well described in Monte Carlo events, the optimization of this cut was done for the data sample. In this analysis the number of hits was measured by the number of hits in the vertex detector. It was found that rejecting events with more than 800 hits in the

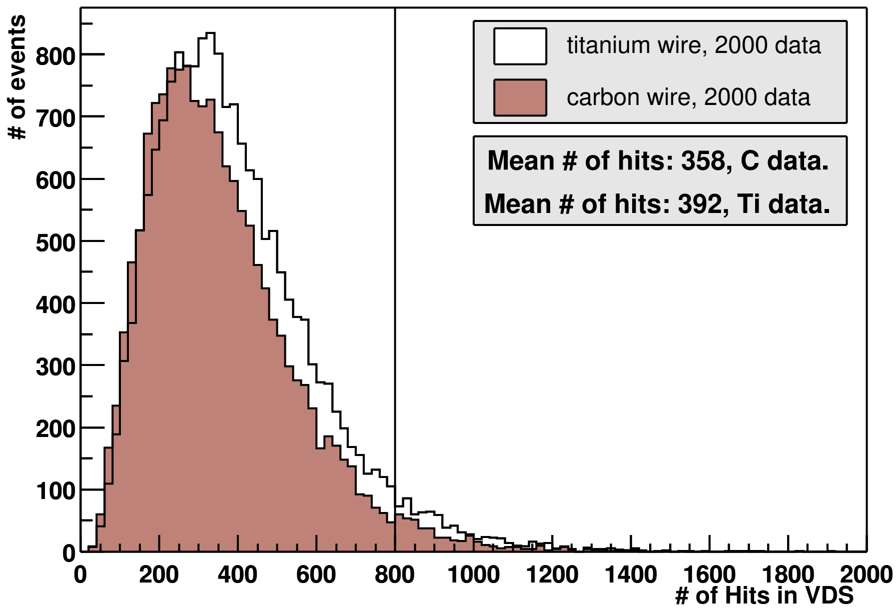

Figure 7.1: Number of hits in the 2000 carbon and titanium data sample.

vertex detector gives the most significant χ_c signal. The number of hits seen in the vertex detector data for both target wire materials is shown in Fig. 7.1.

The titanium wire was not used in single wire operation during the data taking period for the runs considered. To separate the contribution of the titanium and the carbon wire in multi-wire runs, the position of the J/ψ vertex has to be clearly associated with one wire. To do this the distance in z between the reconstructed vertex and the wire has to be less than 1 cm. The distribution of the z-position of the J/ψ vertices in the multi-wire runs is shown in Fig. 7.2. The figure also shows the distance of roughly 3.3 cm between the carbon and titanium wire. The distance of the vertex to the wire in z is compared for data and Monte Carlo in Fig. 7.3. The distribution for data is much broader, but still sufficient to separate the events produced at the carbon and titanium wire.

The p_t and rapidity of reconstructed muons are shown in Fig. 7.4. The mean p_t of reconstructed muons tracks in data is 1.27 GeV while the average p_t in Monte Carlo is 1.66 GeV. This is one property of the data which is not well described by the simulation. In data the positive muon tracks are a little more peaked at central rapidity than the negative tracks. This difference is not visible in Monte Carlo (Fig. 6.1).

The combination of two opposite sign muon tracks (see Fig. 7.5) shows a clear J/ψ peak. The probability of the vertex fit is required to be larger than 0.5%. The mass window for the selection of J/ψs for the χ_c search is 3.1±0.1 GeV, the same as used for the Monte Carlo sample in section 6.3.1.

The reconstructed mass peaks at 3.09 GeV with a width of 51.2±2.0 MeV. In the carbon sample 997 events are selected.

In the titanium sample the peak position is at 3.09 GeV with a width of 54.3±2.4 MeV. The sample contains 663 selected J/ψ events. Fig. 7.6 shows the invariant mass spectrum

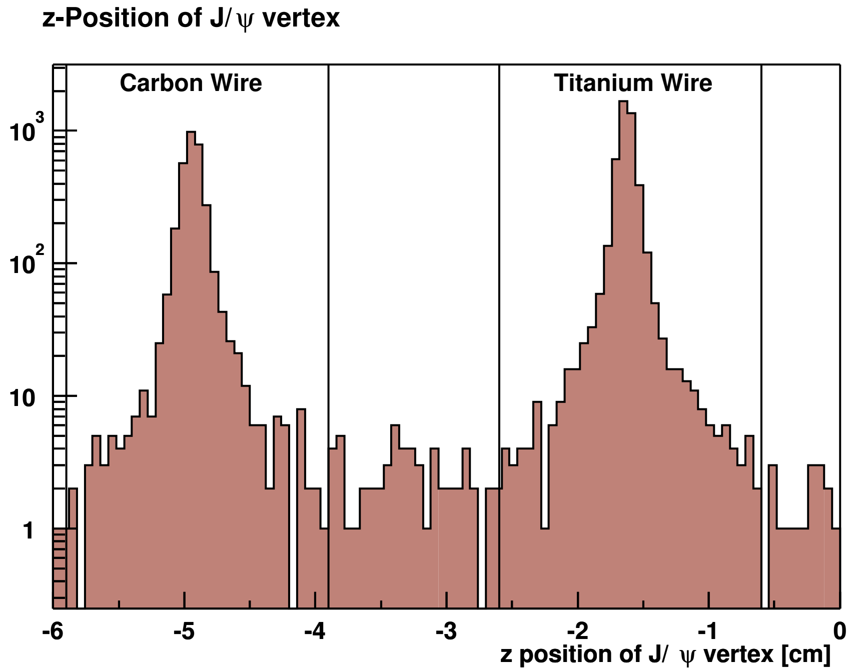

Figure 7.2: Z-position of the J/ψ vertex in the runs with both the carbon and the titanium wire in operation. The vertical lines indicate the regions in which a vertices are associated to each wire.

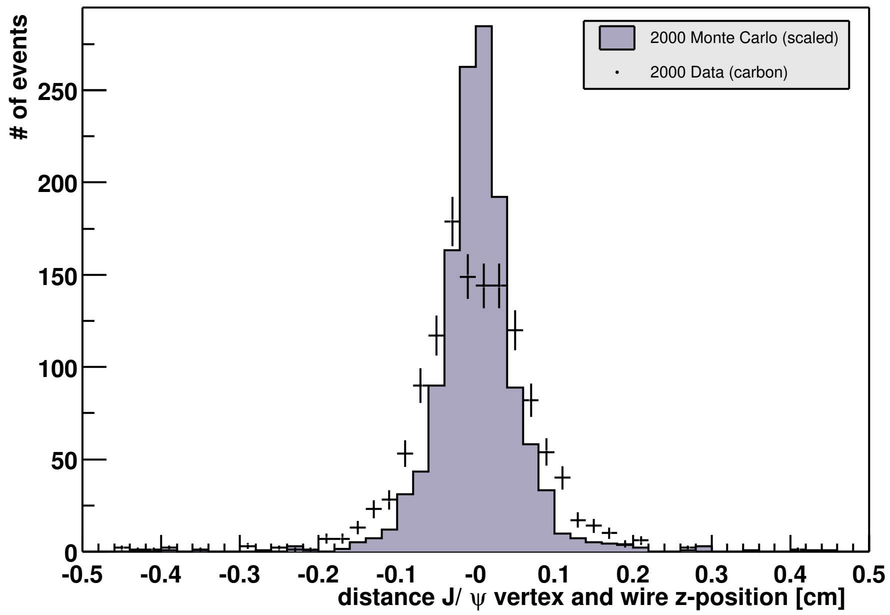

Figure 7.3: Distance between J/ψ vertex and the target wire.

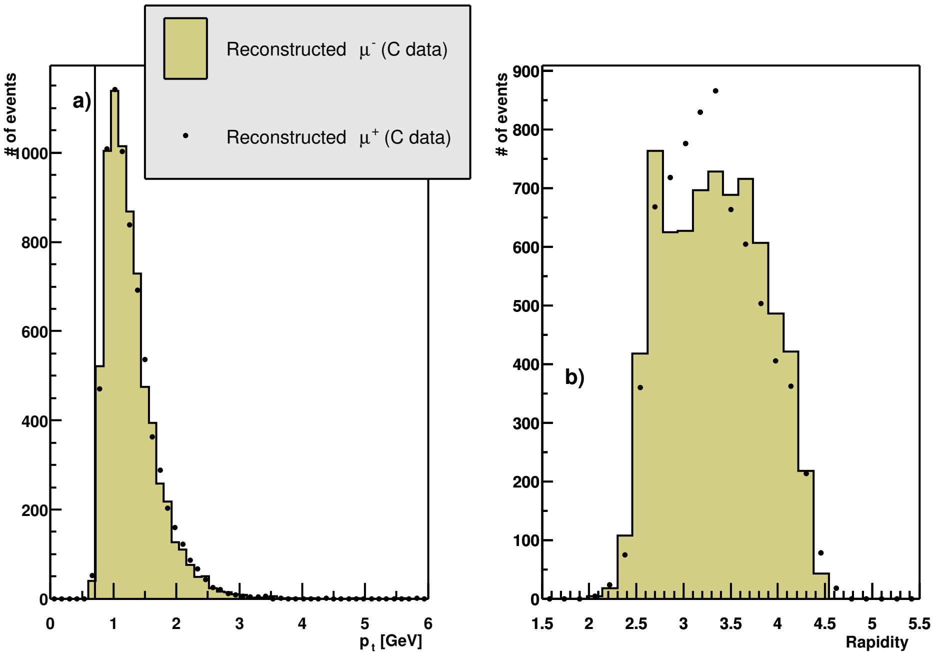

Figure 7.4: Kinematic properties of all reconstructed muons in the 2000 carbon data sample. a) Transverse momentum. The line shows the cut used in the J/ψ reconstruction. b) Rapidity.

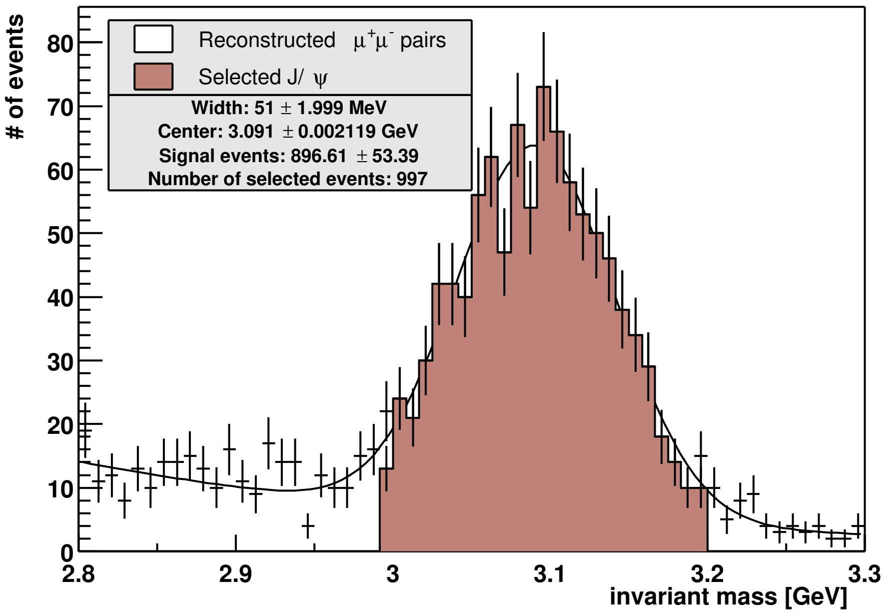

Figure 7.5: Reconstructed invariant mass in the 2000 data (carbon target).

of the reconstructed J/ψ in titanium data.

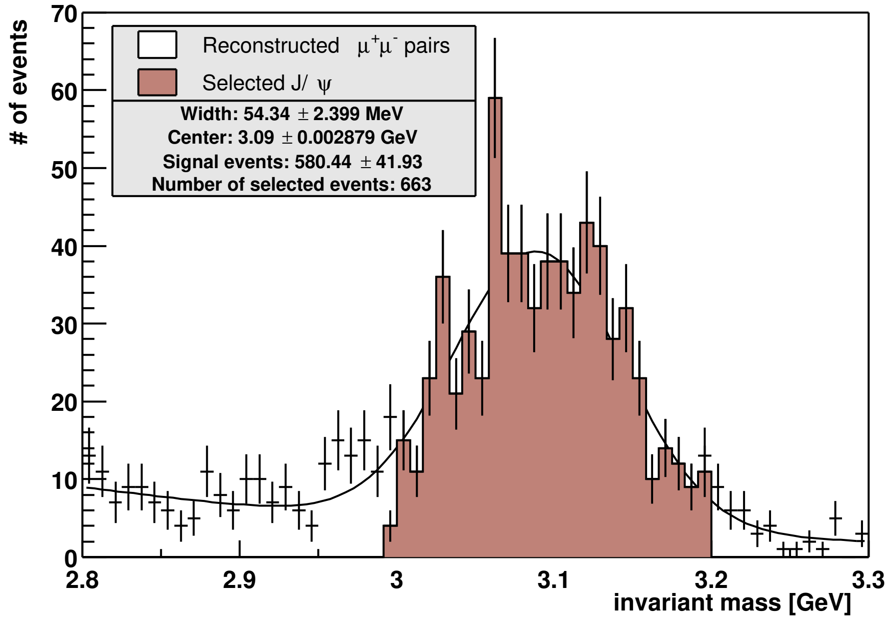

Figure 7.6: Invariant mass of the J/ψ in 2000 titanium data.

7.1.1 Photons in 2000 Data

The ECAL performance was limited by coherent noise in the readout channels during the 2000 running. In the latest re-processing the noise was corrected by calculating the common mode of the noise for groups of calorimeter cells and subtracting it from the data.

The clusters have to have an energy of at least 4 GeV and a transverse energy of more than 0.1 GeV to be selected. The radial cut from Table 6.3 and the isolation cut are also used. Fig. 7.7 shows the impact points of the clusters in the electromagnetic calorimeter. The hit distribution in data shows holes that are caused by inefficient regions in the ECAL.

Fig. 7.8 shows the cluster energy and the E_t of the selected photon candidates together with all clusters above 1 GeV energy. This has to be compared with Fig. 6.11. The shapes in data and Monte Carlo are very similar.

7.1.2 Reconstructed χ_c in 2000 Data

The invariant mass spectrum of the χ_c is shown in Fig. 7.9. It looks very similar to the one in Monte Carlo. The peak in the data at ≈3.5 GeV is, however, less pronounced.

In the mass difference plot of the single wire runs with the carbon wire (Fig 7.10), the peak can be seen much better above the combinatorial background from event mixing. The fit in Figure 7.10 describes the background from mixed events by a polynomial and

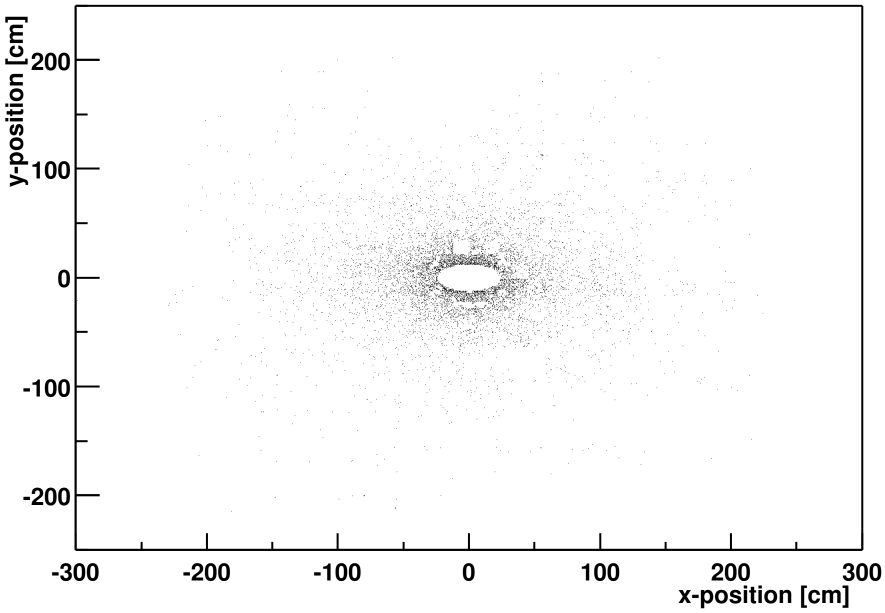

Figure 7.7: Distribution of the photon candidate clusters used for χ_c reconstruction in carbon data. The energy of these clusters is greater than 4 GeV.

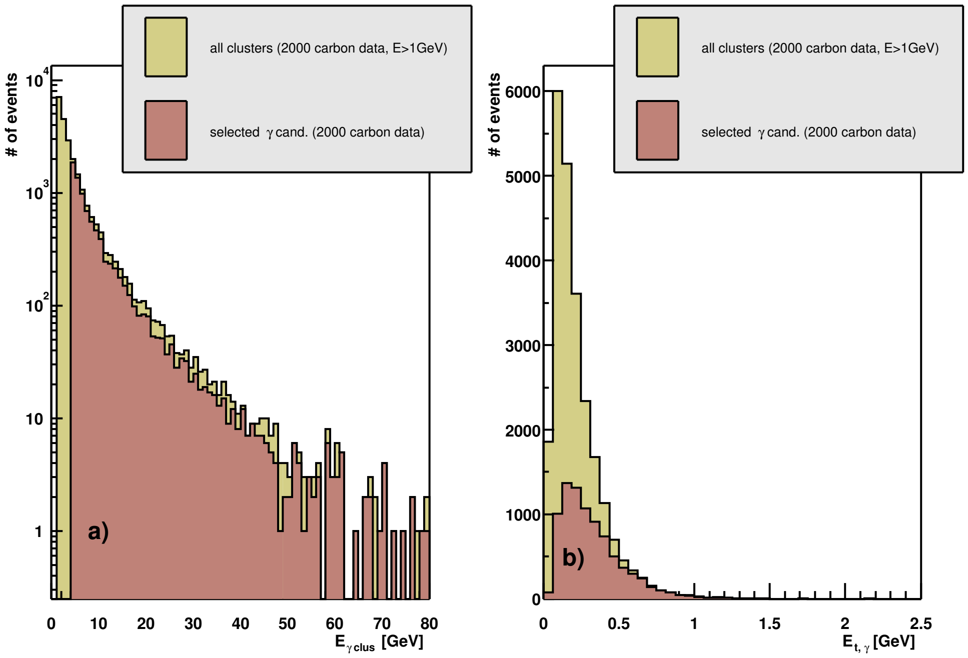

Figure 7.8: a) Energy of clusters with E>1 GeV and selected clusters. b) Transverse Energy of clusters with E>1 GeV and selected clusters. All in 2000 carbon data.

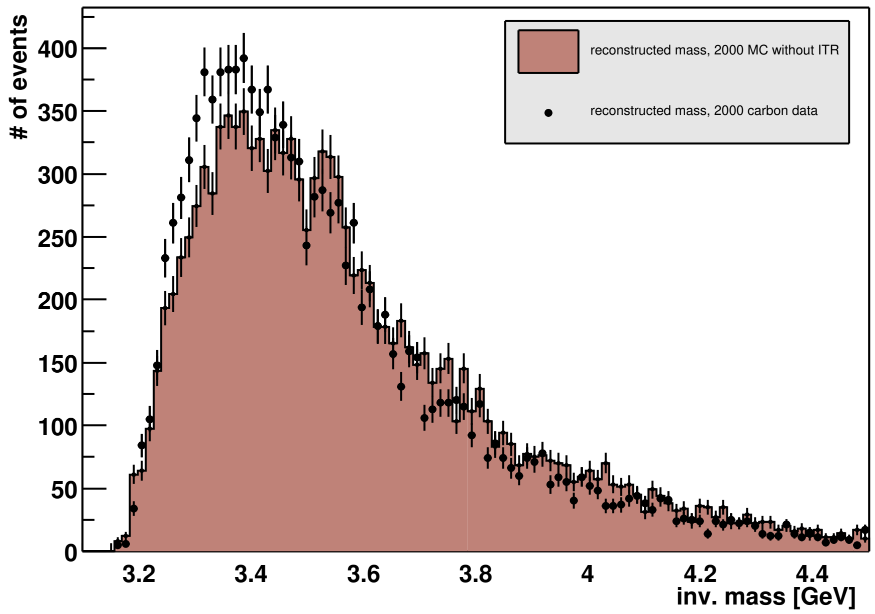

Figure 7.9: Invariant mass of the χ_c in data from the carbon target.

the signal with a Gaussian. In the fit the polynomial is fixed and the parameters of the Gaussian are free. The parameters of the fit give 123.5 $\pm$62.6 events. The position of the peak is at 462 $\pm$ 12 MeV with a width of 29.9$\pm$11.0 MeV. The position of the peak is within the expected value for χ_cs. To extract additional information about the composition of the χ_c states more Monte Carlo studies with different production ratios have to be made. With a width of 29 MeV the two χ_c states can not be resolved at a mass difference of just 46 MeV.

In Fig. 7.11 the mixed event background is subtracted from the mass difference spectrum. A Gaussian is fitted to the resulting points. This fit leads to 108$\pm$59 events with a width of 27.6$\pm$10.5 MeV.

Multi-wire operation with the carbon wire does not contain a visible χ_c signal. The reason is not fully understood. One contribution is the higher occupancy in these runs.

In the titanium multi-wire runs a signal peak is visible. The position of the peak is at 413$\pm$12 MeV with 77$\pm$50 events, see Fig. 7.12. The width is 23$\pm$11 MeV. This shift of the peak position was also observed in other analyses. It has not been explained so far.

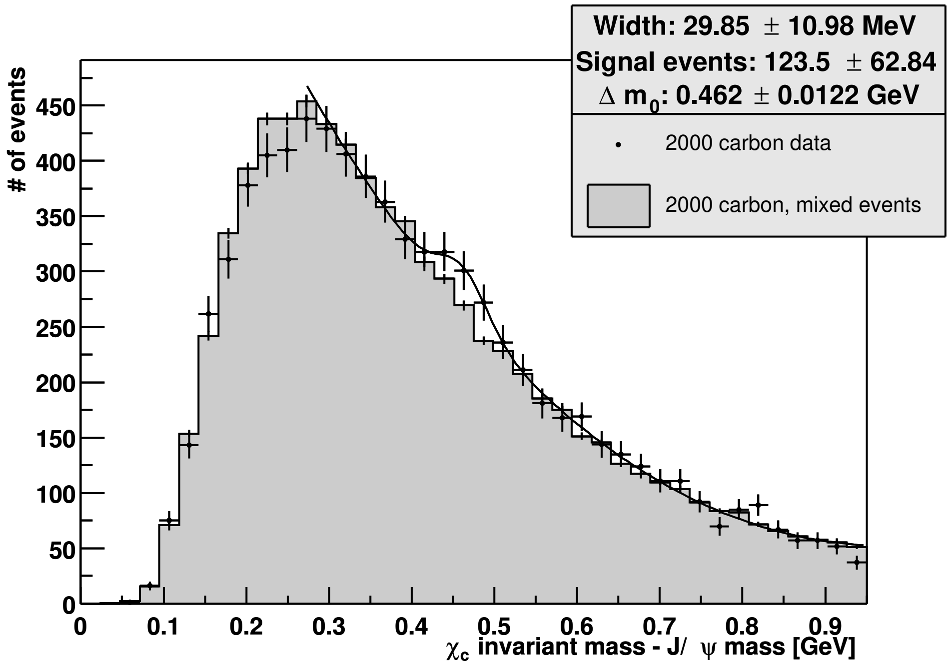

Figure 7.10: Mass difference of the χ_c to the J/ψ in data, from the 2000 carbon target data.

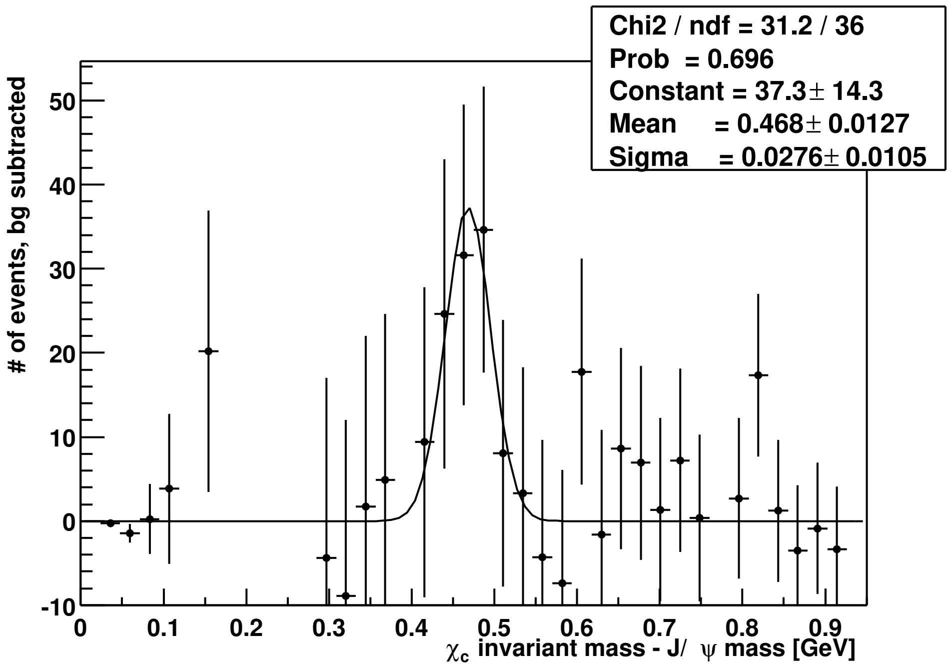

Figure 7.11: Background subtracted mass difference in data, from the 2000 carbon target data. Fitted is an unconstrained Gaussian.

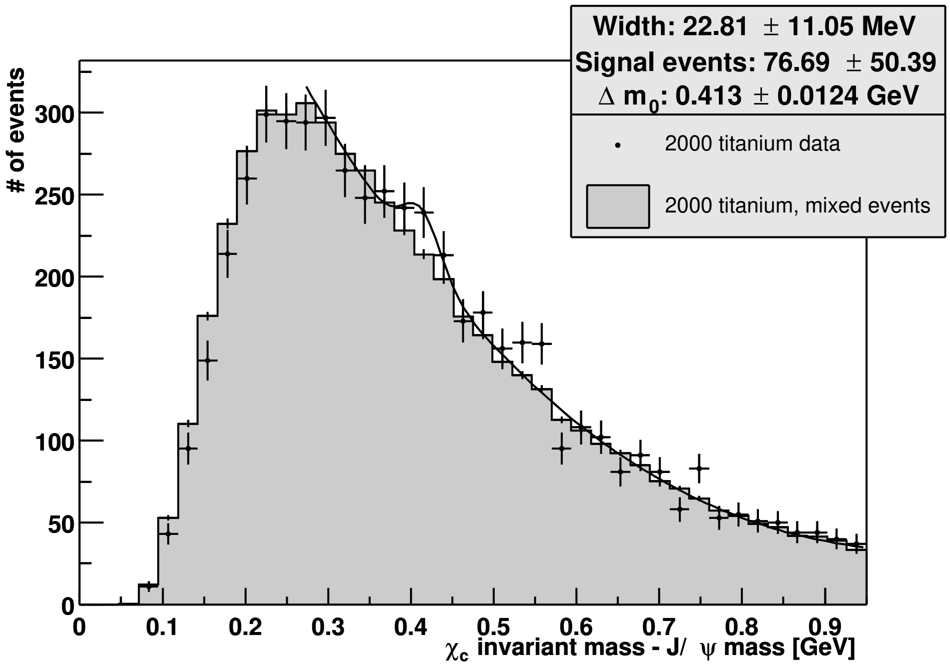

Figure 7.12: Mass of the χ_c to the J/ψ in data, from the 2000 titanium target data.

Chapter 8

Outlook for the χ_c Analysis

The analysis presented in the two previous chapters is a starting point for future data taking only. There are many details that should be studied in more detail. Some of the issues not thoroughly analyzed in this study are discussed here.

8.1 Reducing the Background

The objective for further studies is to decrease the combinatoric background by improving the selection of photon candidates. Several further studies are discussed here, which might improve the background rejection in the future.

8.1.1 Cluster Shape

A property of electromagnetic interactions in a calorimeter is the characteristic shape of the cluster. A typical property that can be studied in this context is the ratio $R_{\mathrm{cent\_cl}}$ between the energy deposited in the central cell of the cluster and the total cluster energy. An ECAL cluster is reconstructed by using the energy content of nine neighboring cells (for the cell geometry see Fig. 3.5). The central cell has a much larger energy than the surrounding cells, so the ratio between the energy of the central cell and the total energy can be used to determine the identity of the cluster. Hadrons produce clusters which are much broader than photon clusters, the $R_{\mathrm{cent\_cl}}$ therefore is smaller for hadronic clusters. The energy ratio between the central cell and the full cluster in the carbon data is shown in Fig. 8.1. The ratio $R_{\mathrm{cent\_cl}}$ peaks at 0.85, these are most likely photon clusters. The plot suggests a second peak containing hadrons, which can be suppressed when a cut on the energy ratio is introduced.

This analysis was also used as a test of the analysis software tool BEE [59], which is a convenient tool to perform an analysis based on reconstructed tracks and vertices. The BEE package was missing some parts needed for this study, which were added and are now available to the collaboration. In this study the $R_{\mathrm{cent\_cl}}$ was not used, but the possibility to use it within BEE has been added for the analysis of 2002 data.

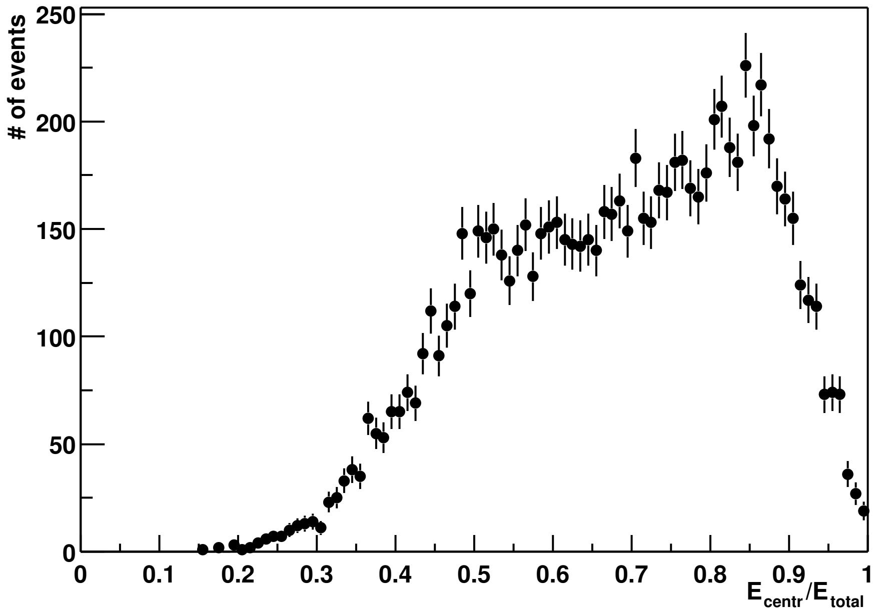

Figure 8.1: Distribution of the cluster shape parameter E_{cent}/E_{total} in carbon data.

8.1.2 Track requirement for Photon Reconstruction

One possibility to suppress fake photon clusters is to require that no reconstructed main tracker track points to the cluster position. This suppresses all charged particles that cause clusters in the calorimeter. But since photons can convert to e^+e^- pairs in the material of the detector in front of the ECAL, this also suppresses some photons.

The detailed study on photon reconstruction done by Olya Igonkina showed that the suppression with tracks is not efficient for data taken in 2000 as the track requirement actually suppresses the signal stronger than the background.

In the data that will be taken in 2002 this has to re-examined, because the tracking system in the magnet was removed to reduce the amount of dead material in front of the ECAL. The main reason for this was to reduce the probability of photons to convert in the magnet.

8.1.3 Reconstruction of π^0s

Having established that a large fraction of the reconstructed photon candidates are produced by neutral pions, it could be possible to reconstruct these pions and remove the candidates that can be reconstructed to the correct pion mass. The $\pi^0 \rightarrow \gamma\gamma$ is reconstructed by combining two photon candidates from the selected clusters (Table 6.3) and calculating the invariant mass of the two photon candidates. Fig. 8.2 shows the reconstructed invariant mass spectrum of ECAL cluster pairs, assuming a π^0 decay at the interaction point in Monte Carlo events. This is a starting point as a test of the feasibility of the approach. The rejection power of such a scenario has to be studied.

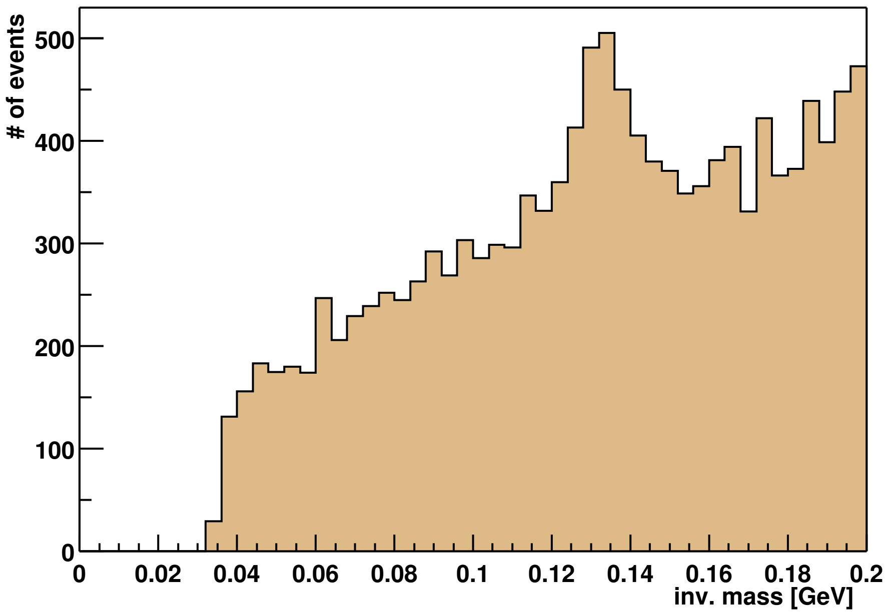

Figure 8.2: Reconstructed mass of all combinations of the photon cluster pairs from the sample of selected photons for the χ_c (MC 2000).

8.1.4 Radial Cluster Energy Dependence

When the average energy of photons from a χ_c decay is shown as a function of the radial distance from the beam (see Fig. 8.3) and compared with the same distribution for the selected clusters candidates, it is clearly visible that the clusters from χ_c have a higher energy near the center of the detector. The average energy also falls more rapidly in the generated Monte Carlo photon sample. The ratio between these samples of photons is shown in Fig. 8.4. Here the difference in behavior is clearly visible.

It has to be studied if this can be used in the future to find a more efficient cut scenario for the cluster energy. This cut will have to be dependent on the radial position of the cluster. Due to lack of time this option was not further studied for this analysis.

8.2 Electron channel

The reconstruction of $J/\psi \to e^+e^-$ is also possible with the HERA-B detector, but it is more difficult and was not included in this study. For the reconstruction of e^+e^- pairs the emission of bremsstrahlung photons by the electron has to be taken into account. The high probability of bremsstrahlung emission also decreases the trigger efficiency in this channel. In addition electrons are loosing a larger fraction of energy on their way through the detector by bremsstrahlung and multiple scattering. This makes the reconstruction more difficult, and the background higher. The electron channel is nevertheless very valuable because an independent measurement can be performed.

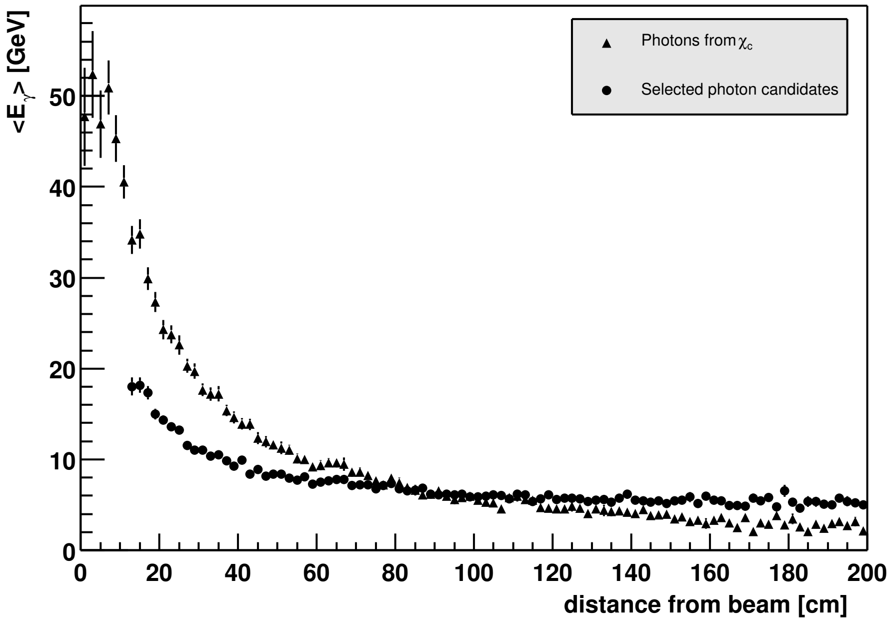

Figure 8.3: Comparison of the radial dependence of the average cluster energy in photons from χ_c and selected photon candidates.

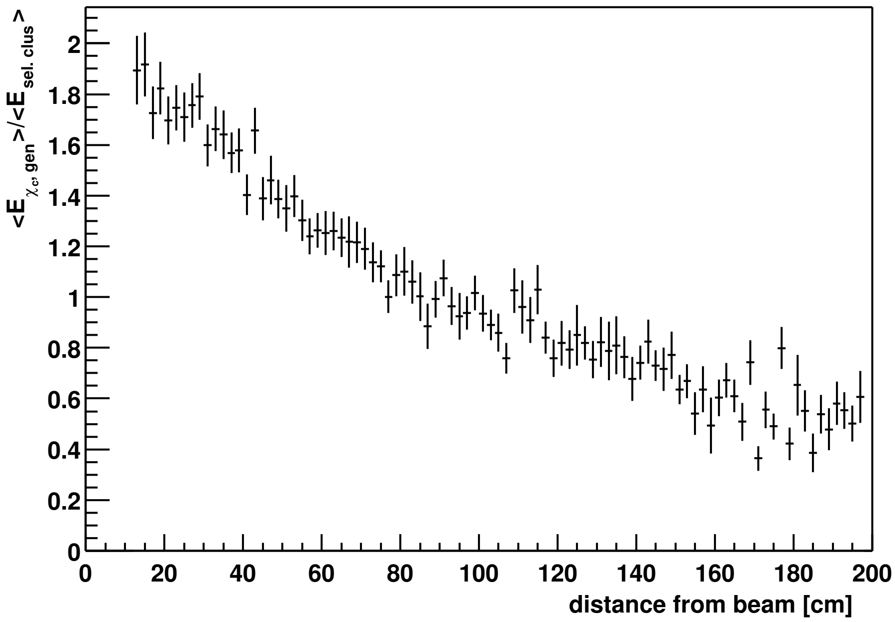

Figure 8.4: Ratio of average energies of clusters from generated χ_c and all selected clusters. The energy of the photons from χ_c is larger near the beam-pipe than that of the selected cluster candidates.

8.3 Summary

An analysis of χ_c production at HERA-B has been performed. The significance of the signal is still small, but the signal is firmly established now at HERA-B with three parallel independent analyses.

In this analysis 124 χ_c events were found in proton carbon interactions based on 997 selected J/ψ. In the titanium sample 77 χ_cs were found in 663 selected J/ψ events.

The systematic uncertainties of the analysis still have to be studied.

To determine a value for R_{χ_c} the dependence of the reconstruction efficiency on the production model will have to be studied in detail.

The reason for not finding a χ_c signal in the multi-wire carbon data is still unclear. This sample, however, is the smallest and it might well be that the number of events in it is simply not sufficient.

All the results are consistent with the other analyses, giving confidence, that HERA-B will be able to measure the charmonium production in 2002/2003.

Chapter 9

Conclusion

For the first time in a hadronic high rate environment a large system of micro pattern gaseous detectors was operated in 2000. The inner tracker of HERA-B was equipped with more than 136 GEM MSGCs which were successfully operated during the running period from February to August 2000.

The inner tracker research and development phase with its manyfold problems was brought to a conclusion during the running period in 2000. The inner tracker system achieved a stable operation with the required specifications. Hit efficiencies of above 90% were observed in some chambers and are expected to be achieved for the full system after the conclusion of the training procedure in 2002.

The detector technology has only a narrow operational safety margin. This is seen in the high number of sparks in the GEM, which can not be avoided and that are always a potential operational risk. The number of anode-cathode shorts in the system is the main reason for losses of active channels in the system. We expect losses not larger than 1% during the operation.

The experience gained with the inner tracker system has led to the conclusion that a MSGC based system is not an optimal solution for the environment at HERA-B. The experiments LHC-b and CMS have consequently chosen to equip their inner tracking systems with silicon strip detectors, which now have become affordable.

Nevertheless with the existing GEM MSGCs the inner tracker is well prepared for the coming data taking period. All necessary tools and procedures are in place and the system is ready to contribute to the physics program of 2002 and 2003.

In the data sample taken in 2000 a significant χ_c signal was seen both in proton-carbon and proton-titanium interactions. Several ideas to further improve the photon finding efficiency were discussed and can be studied in the coming run period by our working group. A measurement of the parameter R_{χ_c} with this data is also possible and is now being prepared for publication [20]. For a precise measurement more statistics is needed. There are also good prospects for a differential measurement with the data of the coming data taking period.

For the measurement of the A dependence of R_{χ_c}, further understanding of the event properties in multi wire configurations is needed. In a data sample with titanium and carbon target wires inserted simultaneously, the χ_c signal could only be established for the titanium wire. The reason for the lack of a signal from the carbon wire in multi-wire operation still has to be found.

In 2002 the acceptance of the spectrometer is improved by the repairs in the inner and outer trackers.

This study showed that χ_c events can be reliably reconstructed at HERA-B giving additional confidence that the physics program of 2002 can be fulfilled.

List of Tables

List of Figures

Bibliography

[1] H. Albrecht et. al., An Experiment To Study CP Violation in the B System Using an Internal Target at the HERA Proton Ring, Letter of Intent, DESY-PRC 92/04, 1992.

[2] The HERA-B Collaboration, HERA-B An Experiment To Study CP Violation in the B System Using an Internal Target at the HERA Proton Ring, Proposal, DESY-PRC 94/02, May 1994.

[3] The BaBar Collaboration, A study of time-dependent CP-violating asymmetries in $B^0 \to J/\psi K_S^0$ and $B^0 \to \psi(2S)K_s^0$ decays, Submitted to the XXXth ICHEP, Osaka, Japan, SLAC-PUB-850, 2000.

[4] Hiroaki Aihara for the Belle Collaboration, A measurement of CP Violation in the B^0 Meson Decays with Belle, Submitted to the XXXth ICHEP, Osaka, Japan, 2000.

[5] Christenson, Cronin, Fitch, Turley, Evidence for the 2π Decay of the K_2^0 Meson, Phys, Rev. Lett. **13**, 138, 1964

[6] G. Anzivino (NA48 Collaboration), Measurement of direct CP violation by NA48, hep-ph/0111383, Nov 2001.

[7] Zee Bob Hsiung for the KTeV Collaboration, $\epsilon`/\epsilon$ and Rare K_L Decays from KTeV experiment, FERMILAB-Conf-00/345-E KTeV, 2000.

[8] The BaBar Collaboration, The BaBar Detector, Submitted to Nucl. Instrum. Meth. hep-ex/0105044, Apr 2001.

[9] The Belle Collaboration, Technical Design Report, KEK-Report 94-2, April 1995.

[10] LHCb, A Large Hadron Collider Beauty Experiment for Precision Measurements of CP Violation and Rare Decays, Technical Proposal, CERN LHCC98-1, Feb 1998

[11] Proposal for an Experiment to measure Mixing, CP Violation and Rare Decays in Charm and Beauty Particle Decays at the Fermilab Collider - BTeV, May 2000

[12] B. Aubert et. al. (BaBar Collaboration), A Study of Time-Dependent CP-Violating Asymmetries and Flavor Oscillations in Neutral B Decays at the $\upsilon(4S)$, hep-ex/0201020, 10 Jan 2002.

[13] K. Abe et. al. (Belle Collaboration), Observation of Large CP Violation in the Neutral B Meson System, hep-ex/0107061v2, 1 Aug 2001.

[14] HERA-B Collaboration, Measurement of the $b\bar{b}$ cross section at HERA-B with the 2000 data sample, HERA-B note 02-005, 2002.

[15] D. M. Jansen et. al.(E771 Collaboration), Measurement of the Bottom-Quark Production Cross Section in 800 GeV/c Proton Gold Collisions, Phys. Rev. Lett. 74(16) 3118, 1995.

[16] T. Alexopoulos et. al. (E789 Collaboration), Measurement of the $b\bar{b}$ Cross Section in 800 GeV/c Proton-Silicon Interactions, Phys. Rev. Lett. 82(1) 41, 1998.

[17] M. C. Abreu et. al. (NA50 Collaboration), Observation of a threshold effect in the anomalous J/ψ suppression, Phys. Lett. B, 450, Issue 4, 456-466, 25 March 1999.

[18] M Leitch (NuSea Collaboration), Measurement of Differences Between J/ψ and ψ' Suppression in p-A Collisions, Phys. Rev. Lett. 84 3256, 2000.

[19] Ramona Vogt, Are the J/ψ and χ_c A Dependencies the Same?, hep-ph/0107045, 2001.

[20] Olya Igonkina, Determination of the Fraction of J/ψ Produced via Radiative Decays of χ_c, HERA-B internal note 02-028, February 2002

[21] Joachim Spengler, `http://www-hera-b.desy.de/subgroup/pictures/ detector_schematic_2002.eps`, 2002

[22] Selim Issever, Entwicklung des Target-Steuersystems für das HERA-B Experiment und Untersuchung der Eigenschaften des Targetbetriebs am HERA Speicherring, PhD thesis, Universität Dortmund, 2001.

[23] C. Krauss for the HERA-B Collaboration, Charged Particle Tracking with the HERA-B Detector, proceedings of the 7th International Conference on Advanced Technology and Particle Physics in Como, Italy, submitted to World Scientific, 2001.

[24] Sergey Shuvalov, The HERA-B Electromagnetic Calorimeter, presentation given at the VIII International Conference of Calorimetry in High Energy Physics, Lisbon, Portugal, 1999, `http://www-hera-b.desy.de/subgroup/detector/ecal/transpar/calor99/ calor99-over.ps`.

[25] S. Shuvalov for the HERA-B ECAL collaboration, HERA-B ECAL Status and Plans, IX int. Conference on Calorimetry in Part. Physics, Annecy, Oct 2000.

[26] Ranger – A Pattern Recognition Algorithm for the HERA-B Main Tracking System, HERA-B internal notes HERA-B 97-082, HERA-B 98-079, HERA-B 98-154, HERA-B 98-206 and HERA-B 99-111, 1997-1999.

[27] D. Emeliyanov, I. Gorbounov, I. Kisel, OTR/ITR CATS: Tracking based on Cellular Automaton and Kalman Filter, HERA-B internal note, HERA-B 01-137, 2001.

[28] Iris Abt, Evaluation of Pattern Recognition Packages for the HERA-B main tracking system, HERA-B internal note 01-070, June 2001.

[29] Martin Bräuer, Die Alignierung des HERA-B Vertexdetektors, PhD thesis, Universität Heidelberg, 2001.

[30] Torsten Zeuner, Entwicklung eines Spurdetektors für das Experiment HERA-B, PhD thesis, Universität Siegen, 1998.

[31] Wolfgang Gradl, The Readout System of the HERA-B Inner Tracker and Prospects of HERA-B in the Field of Drell-Yan Physics, PhD thesis, Physikalisches Institut Universität Heidelberg, July 2001.

[32] Stefan Keller, Aufbau eines Spurtriggers bei HERA-B mit GEM MSGC Detektoren, PhD thesis, Universität Siegen, 2001.

[33] Carola Richter, Development of Micro Pattern Gas Detectors for High Rate Experiments, PhD thesis, Physikalisches Institut Universität Heidelberg, 2000.

[34] Malte Hildebrandt, Entwickung und Bau der Detektoren für das Innere Spurkammersystem bei HERA-B, PhD thesis, Physikalisches Institut Universität Heidelberg, 1999.

[35] Y. Bagaturia et. al., Inner Tracker Performance in 2000, HERA-B internal note, HERA-B 01-060, 2001.

[36] Bagaturia et. al (HERA-B ITR collaboration), Studies of Aging and HV Break down Problems during Development of MSGC and GEM Detectors for the Inner Tracking System of HERA-B, submitted to Nuclear Instruments and Methods, Feb. 2002.

[37] A. Oed, Position Sensitive Detectors with Microstrip Anode for Electron Multiplication with Gases, NIM A 263, 351-359,1988.

[38] Bernhard Schmidt, Micro Strip Gas Chambers: Recent Developments, Radiation Damage and Longterm Behavior, NIM A 419, 230-238, 1998.

[39] F. Sauli, Nuclear Instruments and Methods A386, 531, 1997.

[40] CERN Surface Treatment Workshop, EST/SMCI, CH-1211 Geneva 23.

[41] Fraunhofer Institut für Schicht- und Oberflächentechnik IST, D 38108 Braunschweig.

[42] Malika Wilde, Die Slow-Control der Inneren Spurkammern bei HERA-B und Untersuchungen zu geeigneten Hochspannungs-Parametern der GEM-MSGCs, Diplomarbeit, Physikalisches Institut Universität Heidelberg, 2000, `http://www-hera-b.desy.de/general/thesis/diploma/diploma_malika_wilde.ps.gz`.

[43] Thomas Walter, Contributions to the Development of Micro Strip Gas Chambers (MSGC) for the HERA-B experiment, PhD thesis, Universität Zürich 2001.

[44] Peter von Walter, Manual for the high voltage current meter A339 Elektronikwerkstatt des Physikalischen Institutes der Universität Heidelberg, 2000, `http://www.physi.uni-heidelberg.de/~vwalter/Geraete/A339_Current_Meter/A339-6_Man.pdf`.

[45] Peter von Walter, Manual for the GEM voltage distribution box A344 Elektronikwerkstatt des Physikalischen Institutes der Universität Heidelberg, 2000, `http://www.physi.uni-heidelberg.de/~vwalter/Geraete/A344_GEM-Verteiler/A344-8_Man.pdf`.

[46] Carsten Heiß, Aufbau und Inbetriebnahme eines automatisierten Gasversorgungssystems für das innere Spurkammersystem des HERA-B Experimentes, Diplomarbeit, Physikalisches Institut Universität Heidelberg, 1999,

[47] Graphical Control of the Inner Tracker Gas System, Florian Gmeiner, DESY Summer Student report, 2001.

[48] Andreas Köster, Plein & Baus GmbH, Müllersbaum 20, Burscheid, private communication, April 2000 - June 2001

[49] Jens Kovar, DESY MKK1, private communication, June 2001

[50] Alexei Jelezov, Ulrich Uwer, The HERA-B Slow Control Software, HERA-B Documentation, April 1998

[51] C. Richter, A. Lange, C. Werner , PSI-beam-test results (26.3.-14.4.99) GEM-MSGCs for the HERA-B experiment, HERA-B note 99-170, August 1999.

[52] Sebastian Hausmann, Das Auslesesystem der inneren Spurkammern bei HERA-B, PhD thesis, Universität Heidelberg, 1999.

[53] W. Fallot-Burghardt et al., Helix128-x User Manual, HD-ASIC-33-0697, http://wwwasic.kip.uni-heidelberg.de/~feuersta/projects/Helix/helix/helix.html, 1999

[54] Torsten Zeuner, private communication, 2001.

[55] U. Straumann et al., Operation of a large GEM-MSGC detector in a high intensity hadronic test beam using fully pipelined readout electronics, HERA-B note 99-149, Oct 1998.

[56] Review of Particle Physics, The European Physical Journal C, Volume 15, 2000.

[57] Jenny Ivarsson, Peter Kreuzer, Thomas Lohse, PYTHIA and FRITIOF: Event Generator for HERA-B, HERA-B internal note 99-067, 1999

[58] Ulrich Husemann, first Results of Monte Carlo Multiplicity Tuning, Presented at the HERA-B meeting August 22, 2001, available as HERA-B note 01-108

[59] Torsten Glebe, The BEE/Clue Analysis Framework, documented in various HERA-B internal notes, for example 01-110, 01-136, 01-138, 02-001

Acknowledgments

I am very grateful to my supervisor Prof. Franz Eisele, who gave me the wonderful opportunity to work in his group. My thanks also extends to Prof. Karl-Tasso Knöpfle who took the duty as second referee.

It was a pleasure to work in this group of motivated collaborators and friends, who helped a lot during my time as PhD student. I want to thank them all: Sonja Gradl, Malika Wilde, Thomas Hott, Hans-Bernd Dreis, Stefan Keller, Torsten Zeuner and Peter Robmann.

A special thanks is in place for those who took the duty of helping me with the manuscript of this thesis: Wolfgang Gradl, Hartmut Rick and Carlo Duprel. Not to forget my brother Philipp Krauss who helped me to remember long forgotten English grammar rules (not enough of them, I fear).

My parents deserve more than just a thank you, as they always gave the support needed.